D I S S E R T A T I O N

Einfluss von Wüstenstaub auf die PM Konzentration und Deposition in Österreich

Influence of desert dust on PM concentrations and deposition in Austria

ausgeführt zum Zwecke der Erlangung des akademischen Grades einer Doktorin der Naturwissenschaften unter der Leitung von

Ao. Prof. Dr. Anne Kasper-Giebl
Institut für Chemische Technologien und Analytik (E164)
Technische Universität Wien

eingereicht an der Technischen Universität Wien
Fakultät für Technische Chemie

von

Ing[in]. Mag[a]. Marion Greilinger
0747027

Wien, am 15.11.2019

_____
eigenhändige Unterschrift

Contents

Abstract

Natural mineral dust from arid regions, also referred to as desert dust, is the second largest natural source of PM in the atmosphere, right after sea spray, with the deserts in the Saharan-Sahel region as the main emitters. Large quantities are known to be regularly transported over the North Atlantic Ocean or across the Mediterranean to Southern Europe via synoptic wind patterns. Still, demonstrations of the impact of desert dust on PM concentrations or deposition in Austria on a long-term base are missing. This thesis investigates the quantitative influence of desert dust on PM concentrations and deposition in Austria, as such an analysis is missing until now.

The long-term influence of desert dust on the ion concentration in wet deposition is explored to reveal that desert dust deposition is a constant factor influencing the ecosystem in the Alps. Based on a snow pack of the winter accumulation period 2015/2016 situated close to the Sonnblick Observatory in the National Park Hohe Tauern in the Austrian Alps, featuring two Saharan dust events visible by a reddish colour of the snow, thresholds of a $pH > 5.6$ together with a Ca^{2+} concentration > 10 µeq/l were defined to identify desert dust affected snow layers. This approach was extended to the accumulation periods 2014/2015 and 2016/2017 and the performance was validated together with trajectories and on-line aerosol measurements at the Sonnblick Observatory. Subsequently the whole data set of the 31-year long snow chemistry data set (1987–2017) was investigated regarding the contribution of desert dust to ion deposition loads. Results show that especially Mg^{2+} and Ca^{2+} depositions are strongly affected by desert dust input while the long-term decreasing trends of other ions, such as sulfate or Nitrate, are not affected.

The influence of mineral dust on PM_{10} concentrations was investigated to draw conclusions on its impact on PM_{10} limit value exceedance in Austria. The applicability of the approach proposed in the European Air Quality Directive (2008/50/EC), for the subtraction of desert dust contributions, is investigated for two stations in the region of Graz, Styria, over a time period of six years (2013 to 2018). Different stations and different statistical parameters were evaluated to determine the regional background load and subsequently the net dust load (NDL) which might be subtracted. Results suggest an adapted approach to the methodology described in the directive, using the +/− 15-day mean average of the PM_{10} at the regional background station Masenberg, together with threshold criteria to identify only desert dust affected days. The results of calculated NDLs were in good agreement with crustal loads determined on filter samples during two desert dust events in 2016. In contrast to regions in southern Europe or the Mediterranean, the impact of desert dust to a daily PM_{10} limit value exceedance in Austria is neglectable, although, considering the legal maximum amount of days exceeding the daily PM_{10} limit value as given in the EU directive, the scales might be tipped in favour of a transgression of that very maximum.

Based on the need for an easy and fast quantification method of mineral dust on filters sampled within the air quality monitoring networks methodological developments were started. While, in a first step, analysis was limited to elemental carbon, the approach may serve as a step for further refinement into mineral dust also.

Kurzfassung

Mineralstaub aus natürlichen Quellen, wie bspw. aus Wüstenregionen, stellt global gesehen, nach Meersalzaerosolen, die zweitgrößte Aerosolquelle dar. Hauptemittenten sind dabei die Wüsten der Sahara-Sahel-Region. Große Mengen an Wüstenstaub aus der Sahara werden regelmäßig über den Nordatlantik aber auch über das Mittelmeer bis nach Europa transportiert. Trotzdem ist der Einfluss von Wüstenstaub auf die Partikelkonzentration und Deposition sowie der Einfluss auf die Luftqualität in Österreich, im Hinblick auf den Langzeiteinfluss, kaum erforscht. Im Rahmen dieser Arbeit wird der Einfluss von Wüstenstaub auf die Partikelkonzentration und -deposition sowie auf die Luftqualität in Österreich quantitativ erfasst.

Die Untersuchung des Langzeiteinflusses von Wüstenstaub auf die hochalpine, nasse Deposition zeigt einen regelmäßigen Einfluss. Basierend auf Proben der Winterschneedecke 2015/2016 gesammelt im hochalpinen Raum in der Nähe des Sonnblick Observatoriums im Nationalpark Hohe Tauern, welche 2 orange-braune Saharastaubschichten enthielt, wurde, basierend auf pH-Werten > 5.6 und $Ca2+$- Konzentrationen > 10 µeq/l eine Methode zur Identifikation von Saharastaubschichten etabliert. Dieser Ansatz wurde für die Akkumulationsperioden 2014/15 und 2016/17 erweitert und zusammen mit Rückwärtstrajektorien und on-line Aerosolmessungen validiert. Anschließend wurde der Ansatz auf die gesamte 31-jährige Zeitreihe (1987-2017) angewandt um den Langzeiteinfluss von Wüstenstaub auf die Ionendeposition zu untersuchen. Die Auswertungen zeigten, dass vor allem die Depositionen von Mg^{2+} und Ca^{2+} von Wüstenstaubeintrag stark beeinflusst werden. Im Gegensatz dazu spielen sie keine Rolle für die abnehmenden Langzeittrends der anderen Ionen wie, bspw. Sulfat oder Nitrat.

Der Einfluss von Wüstenstaub auf die PM_{10} Konzentrationen sowie deren Einfluss auf die Überschreitungen der PM_{10} Grenzwerte in Österreich wurde anhand zweier Stationen in Graz, Steiermark, über einen Zeitraum von 6 Jahren (2013 bis 2018) untersucht, da es besonders in diesem Gebiet aufgrund der geographischen Lage immer wieder zu Überschreitungen der Grenzwerte kommt. Dabei wurde die Anwendbarkeit der EU-Richtlinie 2008/50/EC zum Abzug des Beitrages von natürlichen Feinstaubquellen im Hinblick auf Wüstenstaubeintrag evaluiert. Unterschiedliche statistische Parameter sowie unterschiedliche Stationen wurden dabei berücksichtigt um einen repräsentativen ,Net Dust Load (NDL)' zu ermitteln, welcher dann von den Tagesmittelwerten der PM_{10} Konzentrationen abgezogen werden darf. Ergebnisse zeigen, dass ein adaptierter Ansatz der EU-Richtlinie unter Verwendung des Mittelwertes der PM_{10} Konzentration, der 15 Tage vor und nach dem zu untersuchenden Tag an der Station Masenberg ermittelt wird, sowie weitere Schwellwerte herangezogen werden können um Wüstenstaubtage zu identifizieren. Die so ermittelten NDLs stimmen sehr gut mit den ,crustal loads' überein, welche durch chemische Messungen der Filter ermittelt wurden. Es zeigte sich jedoch, dass der Einfluss von Wüstenstaub auf Grenzwertüberschreitungen der PM_{10} Konzentrationen in Österreich, im Gegensatz zu Stationen in Südeuropa oder im Mittelmeerraum, eher vernachlässigbar ist. Allerdings besteht dennoch die Möglichkeit, betrachtet man das in der EU-Richtlinie festgesetzte Maximum jener Tage die das tägliche PM_{10} Limit überschreiten, dass Wüstenstaubereignisse ggf. als das Zünglein an der Waage fungieren und zu einer Überschreitung von eben jenem Maximum führen können.

Basierend auf der Notwendigkeit Wüstenstaub auf Filtern der Immissionsmessnetze quantifizieren zu können wurde versucht eine einfache und rasche Analysenmethode zu entwickeln. Der methodische Ansatz über Durchlichtmessungen der Filter konnte jedoch bisher nur für ,Black Carbon' realisiert werden. Diese Ergebnisse stellen aber eine wichtige Grundlage für weiterführende Arbeiten hinsichtlich der Quantifizierung von Mineral- oder Wüstenstaub dar.

Acknowledgements

First and foremost, I would like to thank my supervisor Ao. Prof. Dr. Anne Kasper-Giebl for her scientific and personal guidance. In every sense she acts as a reliable supporter, earning the name 'Doktormutter' for good reason. Her scientific expertise and innovative ideas were very inspiring and I am grateful having had the opportunity to work with her.

I would also like to thank Univ. Prof. Dr. Wolfgang Schöner for attracting me to join ZAMG and helping me to find my ways in the institute. He spawned the idea for the project behind this thesis and was the driving force in the process of applying for funding. Without him this thesis could not have been put together. Of course the support of both the Austrian Research Promotion Agency (FFG) as well as ZAMG, by financing the project "DUSTFALL" (project ID: 848858) on which this thesis is based upon, is greatly acknowledged and appreciated as a crucial factor in realizing this very study.

Next I would like to thank all current and former colleagues at ZAMG as well as at TU, especially Toni. He is my long-time companion both at the office and working in the field and is always helpful and supporting in every sense. I am very sorry that until now he just made it to the acknowledgements of all my works and is not yet being referenced as a co-author, although this will hopefully change in the near future. Thanks to all the others as well, I am very grateful meeting such warm-hearted and humorous people, providing a friendly and supportive environment in the workplace.

Apart from the scientific world I would like to thank my parents and my family, always supporting me and believing in what I am doing. As well as my close friends, distracting me from strenuous work by playing Tarock, gardening together or just having an occasional after-work drink.

Last but of course not least thanks to my husband Michi for his persistent support, buffering a lot of tasks and to-dos to have time for work, field trips and writing the thesis but also for all the proof-reading, the conceptual ideas and most of all for all the inspiring conversations we have, science related or not. Thanks also to my little mouse Lea for being such a cheerful, pleasant and happy person, cheering up the revision process during my maternity leave. I love both of you from the bottom of my heart!

"The saddest aspect of life right now is that science gathers knowledge faster than society gathers wisdom."

Isaac Asimov

Chapter 1
General Introduction

Atmospheric aerosols are technically defined as a disperse system consisting of solid or liquid particles suspended in air. Commonly the term 'aerosol' is often referred to the particle phase only, but also the more precise term of particulate matter (PM) is widely used. The aerosol properties are highly dependent on the size and the chemical composition of the PM, which itself are a result of the different sources. In the following an overview of the aerosol properties as well as the chemical composition of the PM will be given. Furthermore the lifetime of PM as well as the impact on climate and health will be discussed, all in the light of the importance of natural mineral dust as one of the main contributors to atmospheric PM. PM can be found in the troposphere as well as in the stratosphere, but for the purpose of the thesis only tropospheric PM is regarded, based on the fundamentals given in Finlayson-Pitts and Pitts Jr. (1999), Seinfeld and Pandis (2006) and additional references given therein.

Physical and chemical properties of ambient aerosols

The size of PM in the atmosphere ranges from a few nanometers to hundreds of micrometers. Due to the irregular shape of the particles, the size of the particles is often presented via the aerodynamic diameter. This diameter refers to a sphere particle with a density of 1 g/cm³ featuring the same aerodynamic properties as the irregular shaped particle. Within this work all given diameters refer to the aerodynamic diameter unless explicitly mentioned otherwise.

The most important terms describing the PM include the total suspended particle number (TSP) as well as size specific mass fractions of it such as PM_{10} (all particles up to a diameter of 10 μm), $PM_{2.5}$ (all particles up to a diameter of 2.5 μm) and PM_1 (all particles up to a diameter of 1 μm). Generally, particles with less than 2.5 μm in diameter are referred to as 'fine' and those larger than 2.5 μm as 'coarse' fraction. These two size fractions in general originate separately, are transformed separately, are removed by different mechanisms, have different chemical and optical properties and significantly differ in their deposition patterns in the human respiratory system. Therefore, the size distribution is fundamental for any discussion on physics, chemistry, climate or health effects of aerosols.

Due to the high importance and different impact of the size of the aerosol or, precisely the size of the PM suspended in air, there exists the necessity to mathematically describe aerosol size distributions in detail. A common way is to plot the logarithm of the aerodynamic particle diameter against the particle number, the particle surface or the particle volume (which is highly related to particle mass) to receive the respective number, surface or volume distributions. An idealistic scheme of the phenomena influencing the particle sizes is shown in Figure 1, highlighting the different modes, sources, and formation and removal mechanisms of atmospheric particles. The different modes can be classified as the *nucleation mode* with particles up to 10 nm in diameter, the *Aitken mode* with the size range of 10 nm to 0.1 μm, the *accumulation mode* extending from 0.1 μm to about 2.5 μm and the *coarse mode,* comprising particles greater than 2.5 μm. According to the classification mentioned before particles in the nucleation, Aitken and accumulation modes are often summarized as 'fine' particles with the 'ultrafine' particles with diameters smaller than 0.1 μm as a subset.
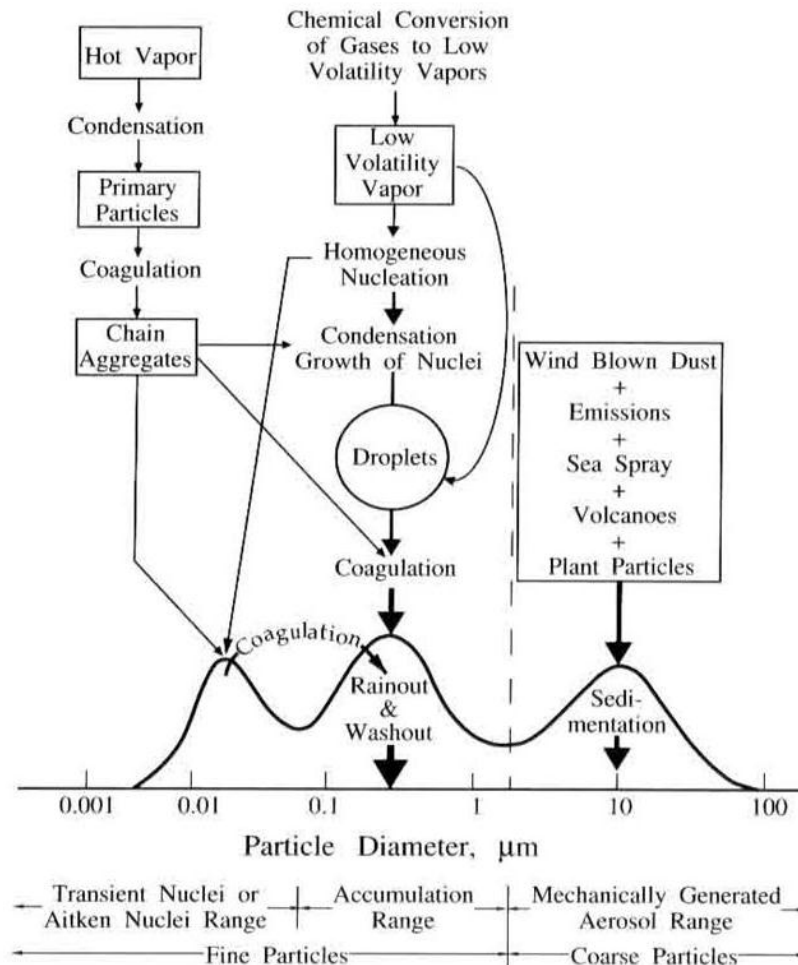
Figure 1: Idealistic scheme of the particle distribution of the atmospheric aerosol as given in Whitby and Cantrell (1976), figure taken from Seinfeld and Pandis (2006). The principal modes, sources, formation processes and removal processes are displayed.

The predominant occurrence of PM within different size ranges is related to the particle formation and removal processes and hence also reflects the chemical composition. Particles in the nucleation mode are formed by condensation of hot vapours during combustion processes and from nucleation from the gas phase of atmospheric gaseous species. This process is often referred to as 'gas-to-particle conversion'. The particles grow relatively fast through coagulation and further condensation of gases and water vapour and reach the Aitken mode. The major sink of these particles is the condensation of low-volatile vapours as well as coagulation and coalescence with equally sized or larger particles, thus conveying these particles to the accumulation mode. The nucleation and Aitken mode represent the prevalence of particles by number and, due to their rapid growth, their atmospheric lifetime is relatively short, sometimes in the order of minutes. Particles in the accumulation mode are too small to settle out, hence they tend to accumulate in this size range. Correspondingly these particles tend to have considerably longer atmospheric residence times than those in the other modes, even up to several weeks. The major removal process for the particles in the accumulation mode is by incorporation into cloud droplets followed by rainout, or by washout during precipitation. The linkage of the removal process to precipitation can thereby shorten their lifetime significantly. Alternatively, the particles may be carried to the surface of coarse particles, thereby forming a so called 'coating layer' and can thus be removed via dry deposition due to gravitational settling. The nucleation, Aitken and accumulation modes are highly related to each other due to the respective formation and removal processes, also highlighted in Figure 1. The coarse mode fraction is decoupled from the formation and removal processes described above. These particles are generally directly emitted and formed by mechanical processes and are thus often referred to as 'primary particles'. A major removal process involved is sedimentation due to the relatively large settling velocities as a result of their large

particle size, hence the atmospheric lifetime of these particles is rather small. Still, these particles can also be removed by rain- or washout and thus shortening their lifetime. Compared to air pollution gases, residence times of aerosols are rather long if the removal via rainout or washout is not considered as the amount of particles removed by dry deposition is quite small except for the coarse particle fraction.

Contradictory to size distribution, the nucleation and Aitken modes account only for a few percent of the total aerosol mass because of their small size, although they represent the majority of the particles by number. Vice versa the coarse mode dominates the particle mass distribution but is almost neglectable in terms of particle number.

The main constituents of the ambient aerosol are inorganic species (sulfates, nitrates, ammonium and sea salt), organic species (secondary organic aerosol SOA, primary organics), other carbonaceous species (i.e. elemental carbon, EC), mineral species (mostly from desert dust) and biological aerosol particles (such as pollen, spores or plant debris). Mineral dust, sea salt, primary organics, EC and biological aerosol particles are directly emitted into the atmosphere and hence account for 'primary particles', whereas Sulfate, Nitrate, Ammonium and SOA predominantly represent the 'secondary particle' fraction. The pattern of the different chemical composition of the primary and secondary particle fraction is also reflected in the chemical composition of the different size fractions. Sulfate, Ammonium as well as organics and EC are predominantly found in the fine fraction while human-made or natural crustal materials, including silicon, calcium, magnesium, aluminium and iron as well as biological aerosol particles dominate the coarse fraction. Nitrate can be found in both fractions since fine nitrate is usually the result of the formation of ammonium nitrate, while coarse nitrate is the product of the reaction of coarse particles with nitric acid. A comparison of the ambient fine and coarse particles is given in Table 1 and the key aerosol properties of the main aerosol species are summarized in Table 2.

Table 1: Comparison of ambient fine and coarse particles including their formation, composition and sources as well as their atmospheric lifetime. Table taken from Lippmann and Schlesinger (2000) adapted from Seinfeld and Pandis (2006)

Aspect	Fine mode	Coarse mode
Formed from:	Gases	Large solids/droplets
Formed by:	Chemical reaction, nucleation, condensation, coagulation, evaporation of fog and cloud droplets in which gases have dissolved and reacted	Mechanical disruption (e.g. crushing, grinding, abrasion of surfaces); evaporation of sprays; suspension of dusts
Composed of:	Sulfate, $SO_4^=$; nitrate, NO_3^-; ammonium, NH_4^+; hydrogen ion, H^+; elemental carbon; organic compounds (e.g. PAHs, PNAs); metals (e.g. Pb, Cd, V, Ni, Cu, Zn, Mn, Fe); particle-bound water	Resuspended dusts (e.g. soil dust, street dust); coal and oil fly ash; metal oxides of crustal elements (Si, Al, Ti, Fe); $CaCO_3$, NaCl, sea salt; pollen, mold spores; plant/animal fragments; tire wear debris
Solubility:	Largely soluble, hygroscopic, and deliquescent	Largely insoluble and nonhygroscopic
Sources:	Combustion of coal, oil, gasoline, diesel, wood; atmospheric transformation products of NO_x, SO_2, and organic compounds, including biogenic species (e.g. terpenes); high-temperature processes, smelters, steel mills, etc.	Resuspension of industrial dust and soil tracked onto roads; suspension from disturbed soil (e.g. farming, mining, unpaved roads); biological sources; construction and demolition; coal and oil combustion; ocean spray
Lifetimes:	Days to weeks	Minutes to hours
Travel distance:	100s to 1000s of kilometers	<1 to 10s of kilometers

Table 2: Key aerosol properties of the main aerosol species as presented in the 5th assessment report of the Intergovernmental Panel on Climate Change IPCC (Boucher et al., 2013).

Aerosol Species	Size Distribution	Main Sources	Main Sinks	Tropospheric Lifetime	Key Climate Relevant Properties
Sulphate	Primary: Aitken, accumulation and coarse modes Secondary: Nucleation, Aitken, and accumulation modes	Primary: marine and volcanic emissions. Secondary: oxidation of SO_2 and other S gases from natural and anthropogenic sources	Wet deposition Dry deposition	~ 1 week	Light scattering. Very hygroscopic. Enhances absorption when deposited as a coating on black carbon. Cloud condensation nuclei (CCN) active.
Nitrate	Accumulation and coarse modes	Oxidation of NO_x	Wet deposition Dry deposition	~ 1 week	Light scattering. Hygroscopic. CCN active.
Black carbon	Freshly emitted: <100 nm Aged: accumulation mode	Combustion of fossil fuels, biofuels and biomass	Wet deposition Dry deposition	1 week to 10 days	Large mass absorption efficiency in the shortwave. CCN active when coated. May be ice nuclei (IN) active.
Organic aerosol	POA: Aitken and accumulation modes. SOA: nucleation, Aitken and mostly accumulation modes. Aged OA: accumulation mode	Combustion of fossil fuel, biofuel and biomass. Continental and marine ecosystems. Some anthropogenic and biogenic non-combustion sources	Wet deposition Dry deposition	~ 1 week	Light scattering. Enhances absorption when deposited as a coating on black carbon. CCN active (depending on aging time and size).
... of which brown carbon	Freshly emitted: 100–400 nm Aged: accumulation mode	Combustion of biofuels and biomass. Natural humic-like substances from the biosphere	Wet deposition Dry deposition	~ 1 week	Medium mass absorption efficiency in the UV and visible. Light scattering.
... of which terrestrial PBAP	Mostly coarse mode	Terrestrial ecosystems	Sedimentation Wet deposition Dry deposition	1 day to 1 week depending on size	May be IN active. May form giant CCN
Mineral dust	Coarse and super-coarse modes, with a small accumulation mode	Wind erosion, soil resuspension. Some agricultural practices and industrial activities (cement)	Sedimentation Dry deposition Wet deposition	1 day to 1 week depending on size	IN active. Light scattering and absorption. Greenhouse effect.
Sea spray	Coarse and accumulation modes	Breaking of air bubbles induced e.g., by wave breaking. Wind erosion.	Sedimentation Wet deposition Dry deposition	1 day to 1 week depending on size	Light scattering. Very hygroscopic. CCN active. Can include primary organic compounds in smaller size range
... of which marine POA	Preferentially Aitken and accumulation modes	Emitted with sea spray in biologically active oceanic regions	Sedimentation Wet deposition Dry deposition	~ 1 week	CCN active.

Supplementary to the classification based on the size distribution (fine vs. coarse aerosol) or the different formation processes (primary vs. secondary aerosols), the ambient aerosol can also be classified based on its origin and can hence be separated in natural or anthropogenic aerosols. Natural sources include mineral dust erosion from arid regions, volcanoes, sea spray, biomass burning from natural fires and secondary inorganic aerosols from natural gaseous emissions. Anthropogenic emissions arise primarily from fuel combustion, industrial processes, transportation and anthropogenic related mineral dust sources (e.g. unpaved roads, cropland, construction sites, etc.), thus the majority of sulfate, nitrate, ammonium and BC are of anthropogenic origin. The classification based on the origin of the aerosol is overlapping with the classification based on the formation (primary vs. secondary) or the size (fine vs. coarse). While the latter ones are highly correlated to each other, meaning that primary particles correspond predominately to the coarse fraction and vice versa, the sources are not. According to Seinfeld and Pandis (2006) and references therein the global estimates for the major PM classes can be given as listed in Table 3. It is obvious that e.g. the carbonaceous fraction together with industrial dust form a substantial part of the anthropogenic fraction, but are of primary origin.

According to Table 3 natural sources clearly dominate the mass emissions of PM on a global scale covering 97% of the total emissions (see also Griffin, 2013). Sea salt is with 87% the main source of natural particulate matter followed by mineral dust as second largest source with a contribution of 13%. Of course it is very likely that local inventories may show a different pattern compared to the presented global emission estimates. Especially on a regional or local scale dominated by urban influence the anthropogenic contribution must not be ignored. There the contribution of natural sources might be negligible. A study of the Austrian Environmental Agency (Umweltbundesamt, UBA) on suspended dust in Austria suggests elemental carbon, organic matter and secondary inorganic aerosols such ammonium sulfate and ammonium nitrate as the main contributors to the PM fraction. Depending on the station type, the local emissions and seasonality the respective contributions range between 6-20% for EC, 16-31% for organic matter, 20-46% for secondary inorganic aerosols. The contribution of

mineral dust is with 3-5% relatively small (Umweltbundesamt, 2006).

Table 3: Global emission estimates in Tg per year for the major PM classes as given in Seinfeld and Pandis (2006) and references therein.

	Natural [Tg/year]			Anthropogenic [Tg/year]		
Primary		Secondary		Primary		Secondary
Mineral dust	1490	Sulfates from DMS	12.4	Industrial dust	100	Sulfate-S from SO2 a	48.6
Sea salt	10 100	Sulfates from volcanic SO2	20	C from Black Carbon	12	Nitrate-N from NOx	21.3
Volcanic dust	30	Organic aerosol from biogenic VOC	11.2	C from Organic aerosol	81		
Biological debris	50						
Total	*11 670 (97%)*		*44 (0.4%)*		*193 (2%)*		*70 (0.6%)*

As a consequence of the different formation and removal processes as well as of the chemical composition, the concentration of atmospheric aerosols varies considerably in space and time. The variability is determined mainly by the geographic distribution of the sources for the direct emission of the primary aerosol or the emission of their precursors for secondary particle formation as well as the meteorological conditions. Thus, for example, the sunshine duration, the temperature or residential heating influence aerosol concentrations on a seasonal scale whereas precipitation, advection or vertical mixing affect the aerosol concentrations on an hourly scale.

Figure 2 shows the typical number and volume distribution of atmospheric particles, which is highly correlated to the mass distribution. There the volume distribution is clearly dominated by the accumulation mode and the coarse mode. Particles in the accumulation mode are the result of primary emissions, condensation of secondary sulfates, nitrates and organics from the gas-phase (gas-to-particle conversion) and coagulation of smaller particles. Coarse particles are usually primarily emitted by mechanical processes but also include some secondary sulfates and nitrates. If the number distribution of the ambient aerosol is investigated, the nucleation and Aitken mode are clearly dominant, usually fresh aerosols created in situ from the gas-phase by nucleation.
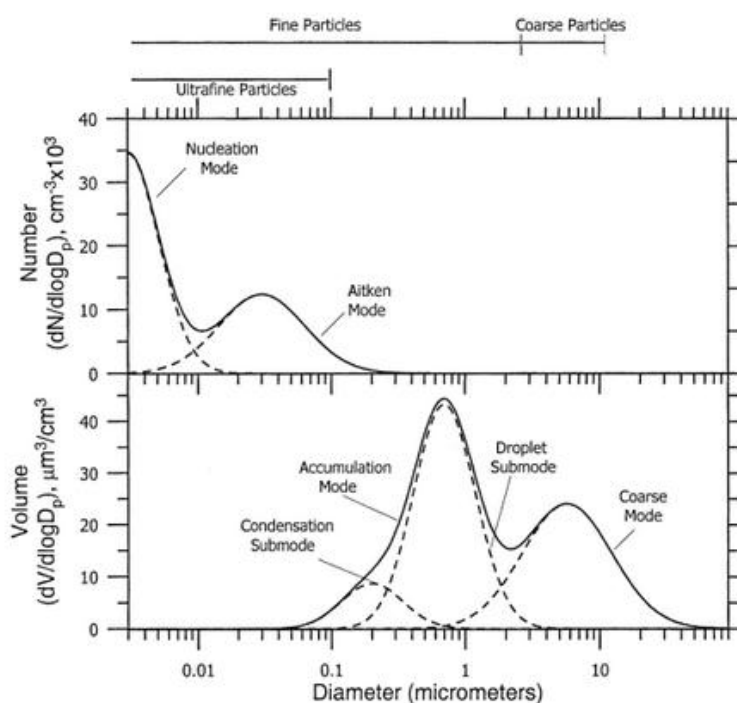

Figure 2: Typical number and volume distribution of atmospheric particles taken from Seinfeld and Pandis (2006)

The role of the main aerosol species in different environments is obvious when the aerosol size distributions are displayed for different aerosol types.

The number, surface and volume distribution of an urban aerosol, a mixture of primary and secondary particles highly influenced by anthropogenic activities, is exemplarily shown in the left panel of Figure 3. The number distribution is dominated by the nucleation and Aitken mode, the surface distribution by the accumulation mode and the volume distribution almost equally by the accumulation mode as well as the coarse mode, although the latter two modes being highly distinct, as already described earlier. In rural areas the aerosol is mainly of natural origin with moderate anthropogenic influence. The shape of the number distribution is comparable to the urban aerosol although with a much smaller value. The volume distribution has a small accumulation mode and is clearly dominated by the coarse fraction. For remote continental aerosols the Aitken and accumulation modes clearly dominate the number distribution, contradictory to the urban or rural aerosol where the nucleation and Aitken modes dominate. The volume distribution is dominated by the accumulation mode with only a small fraction in the coarse mode. In contrast, the number distribution of desert aerosol exhibits three overlapping modes at 0.1 μm, 0.5 μm and 10 μm according to (Jaenicke, 1993) and spanning a wide range of particle sizes in the right panel of Figure 3. Distinct to the before mentioned volume distributions of the different aerosol species the volume distribution of desert aerosol is almost solely represented by the coarse fraction and particles greater than 10 μm in diameter. Contradictory to urban and rural aerosols, the desert aerosol is almost solely of natural origin and thus primarily emitted.
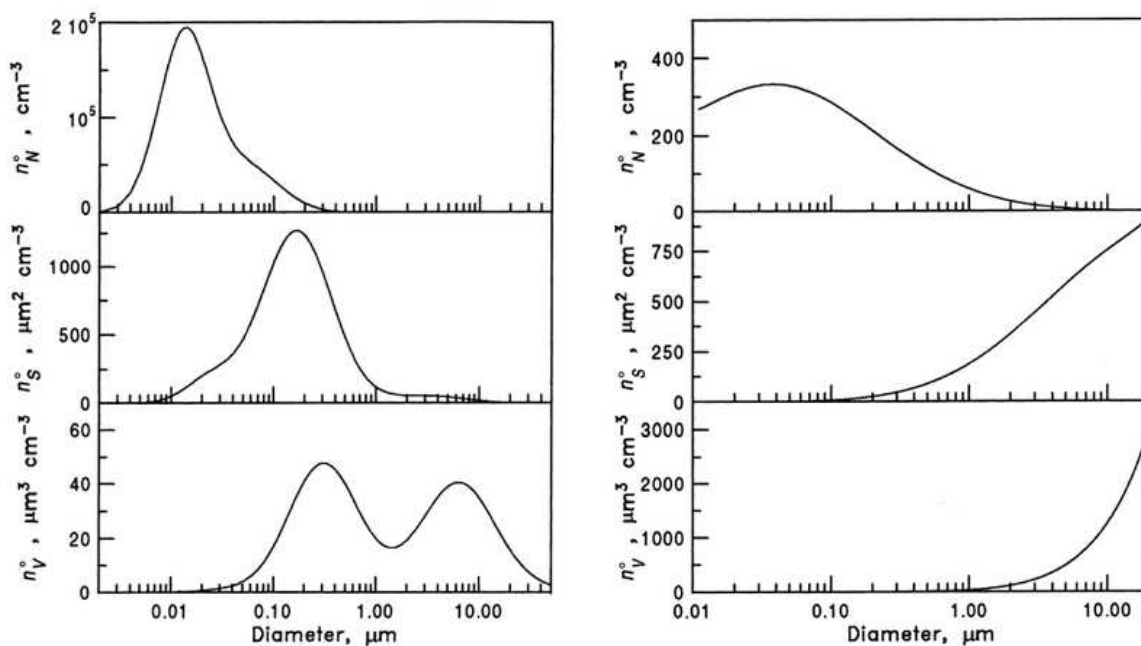

Figure 3: Typical urban (left panel) and desert (right panel) aerosol number, surface and volume distributions (to-down), figures take from Seinfeld and Pandis (2006). Note the different scales of the y-axis.

Impact of ambient aerosols on climate

Aerosols affect climate due to their impact on radiative forcing either directly via absorption or scattering of radiation or indirectly due to their influence on cloud formation and their life time. Thereby the size distribution and chemical composition are the most critical properties for the climate impact of aerosols. A schematic diagram of the various radiative mechanisms is given in Figure 4 and will subsequently be discussed in further detail based on the 5th assessment report of the International Panel on Climate Change IPCC (Boucher et al., 2013). An overview of the key climate relevant properties of the respective aerosol species is also given in Table 2.
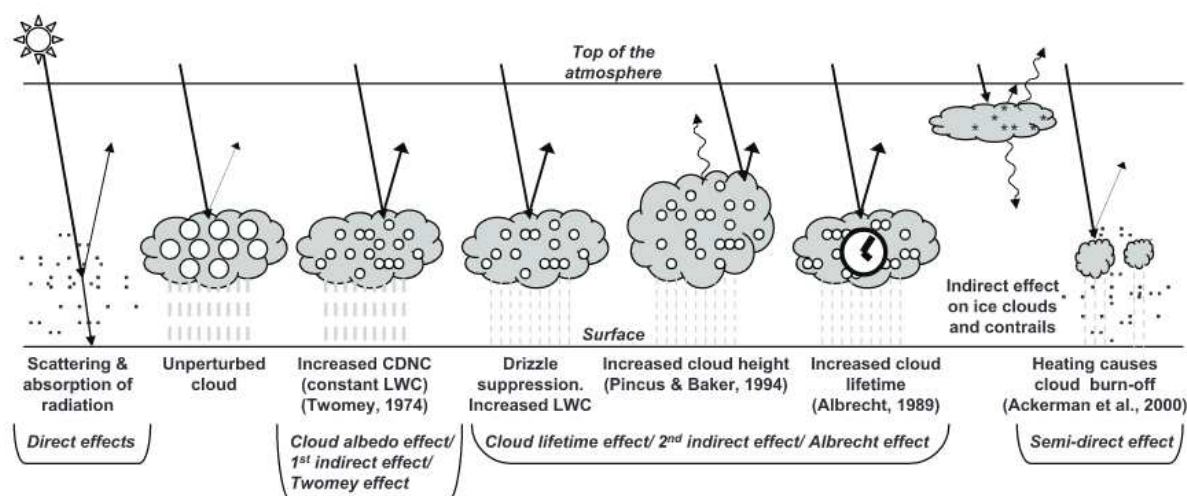
Figure 4: Schematic diagram of the various radiative mechanisms of aerosols. Figure taken from the 3rd assessment report of the IPCC (Andreae et al., 2001). The small black dots represent aerosol particles; the larger open circles cloud droplets.

The direct effect implies the mechanism where aerosols scatter and absorb solar and infrared radiation, thereby altering the radiative balance of the atmosphere. The optical properties of the aerosol, the atmospheric loading and the geographical distribution are the key parameters involved. The main agents of this mechanism in respect to the chemical composition are sulfates, organic carbon (OC) and black carbon (BC) from fossil fuel combustion, biomass burning aerosol as well as mineral dust since these components are known to be highly light absorbing, with BC and brown carbon (BrC) leading the way. The size properties mainly influence the scattering process since fine particles scatter more light per unit mass and have longer lifetimes than coarse particles.

The indirect effect includes the mechanisms where aerosols modify the microphysical and hence the radiative properties, the amount and the lifetime of clouds. An unperturbed cloud contains larger cloud droplets while clouds perturbed with more aerosol particles contain a higher number of smaller cloud droplets due to the increased availability of cloud condensation nuclei (CCNs). Such clouds will rain out less easily and thus have a longer residence time, also cloud heights might be influenced ('cloud lifetime effect'). Besides such clouds appear much whiter and reflect sunlight more efficiently ('cloud albedo effect'). The effectiveness of aerosol particles as a CCN depend on its size and its response to water, thereby the chemical composition of the aerosol is the most crucial point. Water-insoluble particles may feature hydrophilic sites and activate at higher supersaturations or have some water-soluble components and will activate at lower supersaturations. Especially sulfates, sodium chloride, originating mainly from sea salt, as well as inorganic acids are common CCN precursors. Organic aerosols may be important sources for CCN under some circumstances, e.g. aerosols from biomass burning often also due to inorganic coatings.

The droplet formation on CCN is the most relevant process to generate precipitation in warm clouds, i.e. clouds that are only in the liquid phase. These are responsible for the precipitation in the tropics. Aerosols decrease the precipitation efficiency of warm clouds and thereby cause an indirect radiative forcing associated with changes of cloud properties. Besides, aerosols can serve as ice nuclei (IN), allowing ice formations at higher temperatures, i.e. closer to zero, than would be needed without the presence of IN. This is a process highly relevant for the formation and lifetime of ice clouds and contrails. The formation of ice crystals is especially relevant for precipitation formation outside the tropics, the so-called cold cloud precipitation formation process. Especially mineral dust is known to be a very effective IN but also volcanic ash and primary bioaerosols like bacteria, fungal spores and pollen are typically known as good IN.

Besides the described direct and indirect effects, a semi direct effect on the lifetime of clouds exist due to aerosols in the atmosphere. Thereby the absorption of short wave radiation by aerosols lead to heating of the troposphere and thus a change in the relative humidity and the

thermal stability of the atmosphere. According to the wording in Figure 4 this causes a 'cloud burn off', thereby shortening the lifetime of clouds.

Impact of ambient aerosols on health

According to the report on health effects of particulate matter released by the World Health Organization in 2013 especially particles smaller than 10 µm aerodynamic diameter are small enough to penetrate the thoracic region of the respiratory system including respiratory and cardiovascular morbidity, such as aggravation of asthma, respiratory symptoms and an increase in hospital admissions as well as mortality from cardiovascular and respiratory diseases and lung cancer (Pope, 2000).

The effective health impacts of PM are again strongly related to the particle size and the chemical composition. Depending on their size they penetrate deep into the lower respiratory tract and potentially enter the blood stream via resorption of the alveoli (compare Figure 5). Especially ultrafine insoluble particles can be found in blood vessels and can thus be transported throughout the body.
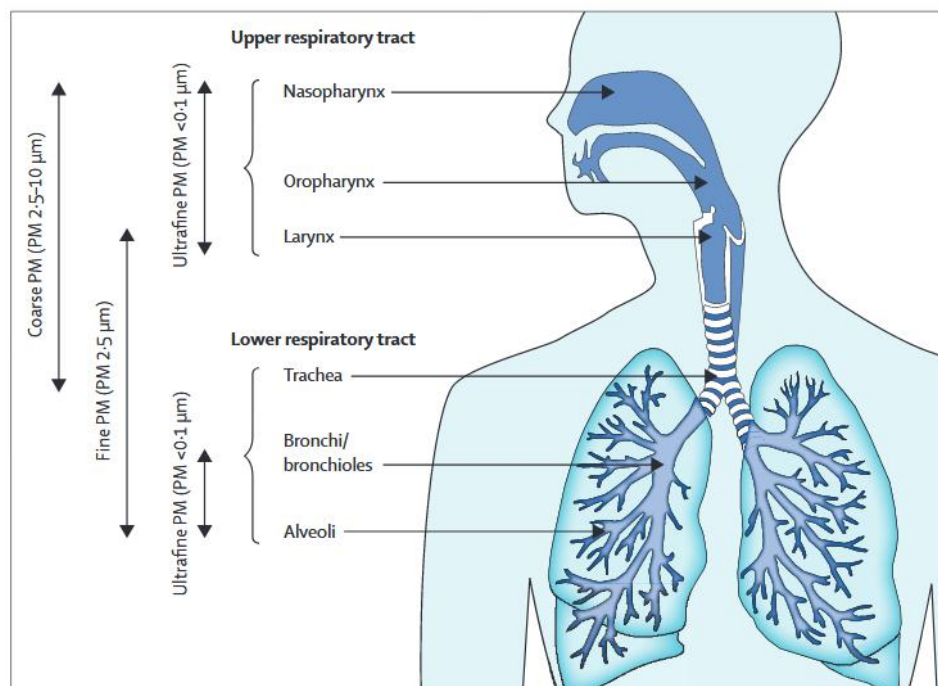

Figure 5: Scheme of the compartmental deposition of aerosols within the respiratory tract. Figure taken from Guarnieri and Balmes (2014)

Based on the health aspects of air pollution, with aerosols or particulate matter as part of this, many countries set up air quality monitoring networks to monitor and control air pollution, the basis for an effective air quality management system. Reasons to implement an air quality management system include the assessment of the extent of the pollution and to provide the data to the general public in a timely manner, to support or implement air quality goals or standards, to evaluate the effectiveness of emissions control strategies, to investigate air quality trend and provide data for the evaluation of air quality models and to support research regarding e.g. long-term studies of health effects of air pollution. Most of the ambient air monitoring networks supporting air quality management are designed and operated by the state or the local governments.

Air quality monitoring in Austria, including greenhouse gases, aerosols and PM, is operated by the local regional governments which have to report the data annually to the Austrian Environmental Agency (Umweltbundesamt, UBA) who in turn have to report the results of the national air quality monitoring to the European Commission (EC) through the European Environment Agency (EEA). Limit values are nationally regulated within the

'Immissionsschutzgesetz Luft (IG-L)' and on a European level within the actual European Air Quality Directive 2008/50/EC. Limit values for PM, as can be found in the respective directives as well as from the World Health Organization (WHO) are listed in Table 4.

Table 4: Limit values given in the IG-L and in the European Air Quality Directive 2008/50/EC. *) 35 days until 2004, 30 days between 2005 and 2009

	Daily mean value [µg/m³]	Annual mean value [µg/m³]	Amount of days where a daily mean value exceedance is permitted
PM_{10} IG-L	50	40	25*)
$PM_{2.5}$ IG-L		25	
PM_{10} EC	50	40	35
$PM_{2.5}$ EC		25	
PM_{10} WHO	50	20	
$PM_{2.5}$ WHO	25	10	

The air quality situation in Austria is documented in the annual reports of the UBA including results of the measurements from the air quality networks of the local regional governments as well as results from the background monitoring network of the UBA itself. Therein the annual situation as well as the long-term evolution of the air quality situation is displayed. Due to the relevance for this work, results from the monitoring of the particulate matter only will be presented in detail.

Within the latest report for 2018 (Spangl and Nagl, 2019), 127 PM10 monitoring sites of which 125 are registered as IG-L station where operated. 34 stations measured the PM_{10} concentration via the gravimetrical methods via weighting of filters before and after sampling according to the European standard reference method EN12341:2014, and 93 stations via continuous measurements. At 53 stations the continuous aerosol mass measurements are performed using the beta attenuation technology (MetOne beta attenuation monitor or the FH62I-R TRS beta gauge particulate sampler), sometimes combined with light-scattering nephelometry (Sharp Monitor). At 22 stations the aerosol mass is calculated based on the particle counts using a Grimm optical particle counter and 18 stations use the Tapered Element Oscillating Microbalance (TEOM) technology.

In 2018 only 3 of these stations exceed the 25-day limit with measured PM_{10} concentrations higher than 50µg/m³ as set by the IG-L whereas the 35-day limit as set by the EC was exceeded only at 1 station. All stations exceeding the daily limits are located in Graz, Styria. The annual mean value of 40 µg/m³ was not exceeded at any of the 125 stations with a maximum value of 30 µg/m³. Still, 55 stations exceeded the annual mean value limit of 20 µg/m³ as set by the WHO. Long-term trends of the PM_{10} pollution in Austria can be retrieved from 73 stations which continuously monitored the PM_{10} concentration since 2004. The amount of days exceeding the 50µg/m³ limit as well as the annual mean value significantly decreased but trends are overlaid by annual variations. 10 years ago many stations regularly measured concentrations higher than 50 µg/m³, thus exceeding the 35-day limit. Within the last years only stations in Graz exceed the 35-day limit on a regular base, mainly due to the specific orographic situation (Lazar and Podesser, 1999), whereas almost all other stations are below the IG-L criteria of 25 days. Still, also in Graz a strong decreasing trend from more than 100 days exceeding 50 µg/m³ especially in the years before 2005 to about 40 days in the last years could be observed.

In order to establish policies for PM emission reductions a detailed understanding of the source contribution is necessary. Based on results from Caseiro et al. (2009) and Puxbaum et al. (2004) the main contributors to PM_{10} are found to be Secondary Inorganic Aerosols (SIA) with Sulfate leading the way, OC and BC. Thereby wood burning aerosol was found to be the major contributor to OC, especially during winter in smaller cities and the rural background. Indicators for mineral aerosol were found as well, especially in the coarse fraction defined as

the difference of PM_{10} and $PM_{2.5}$.

Although mineral dust is only a minor contributor to the common PM composition, its impact on PM is undoubted. Regularly newspapers, not only in Austria, report on the impact of mineral dust or Saharan dust on air quality, and furthermore also on the influence of such events by disturbing the unadulterated sky thus reducing visibility, colouring snowy landscapes or the sky orange or by getting cars covered in dust (see Figure 6). According to a EU Commission working staff paper (European Commission, 2011), the contribution of natural sources to the PM_{10} load can be subtracted implying the necessity for a characterization of the sources of PM.

Figure 6: Phenomena caused by mineral dust, regularly making a great stir in the media and the society, Sources from top left to bottom right: https://www.diepresse.com/4959869/wetter-saharastaub-trubt-fernsicht-und-farbt-gletscher (c) imago/Roland Mühlanger; https://kurier.at/chronik/weltchronik/wie-auf-dem-mars-saharastaub-faerbt-schnee-orange/400011144 (c) Instagramm; https://www.express.de/ratgeber/wie-gefaehrlich-ist-der-sand-fuer-mein-auto-3769822 (c) dpa; https://www.wetter.at/wetter/oesterreich-wetter/Sahara-Staub-Oesterreich-sieht-bis-Dienstag-rot/330137058 (c) APA/Robert Parigger

Thus, based on the influence of mineral dust in the atmosphere on PM loads as well as the property of being an active ice nuclei involved in the process of cloud and precipitation formation, a detailed investigation of this atmospheric phenomena is justified not only in the sense of fundamental research but also for applied research regarding the implementation of air quality guidelines and will hence be elucidated within the next section.

Mineral dust in the atmosphere

As was shown in the previous section mineral dust, and as such desert dust, serves as a major aerosol source and hence is a key factor in the determination of the impact of aerosols on radiative forcing and has the potential to contribute to observed PM loads even in Austria, affecting air quality.

Mineral dust is introduced into the atmosphere primarily through wind erosion or different saltation related processes (compare Figure 7). As a function of wind speed mineral dust particles of about 100µm diameter are lifted and 'dance' along the surface, the so called saltation process. These leaping particles can mobilize additional particles of a wide range of sizes which are ejected into the air. Depending on the particle size the particles stay suspended in the air for short-term (20-70µm diameter) or long-term (<20 µm diameter) periods.

Especially long-term suspended mineral dust can remain in the atmosphere up to several weeks and can thus be transported thousands of kilometers from the source region. (Kok et al., 2012). While particles larger than 100 µm in diameter are found in the source regions, only particles smaller than 10 µm are transported over long distances (Seinfeld and Pandis, 2006).

Estimates of the mineral dust emission source strength vary strongly between 500-5000 Tg/year because of the different model assumptions regarding erosion, transport and scavenging of the particles (Goudie and Middleton, 2001). Independently, the main emitters of mineral dust to the atmosphere are the arid and semiarid regions of the world with the Saharan-Sahel region leading the way followed by Central Asia (Goudie and Middleton, 2001; Seinfeld and Pandis, 2006). According to Washington et al. (2009) half of the mineral aerosol emitted from the Sahara comes from the Bodélé depression in Chad whereas Salvador et al. (2014) report that the Saharan dust mainly originates from the Western Sahara, Morocco, Algeria and Tunisia.
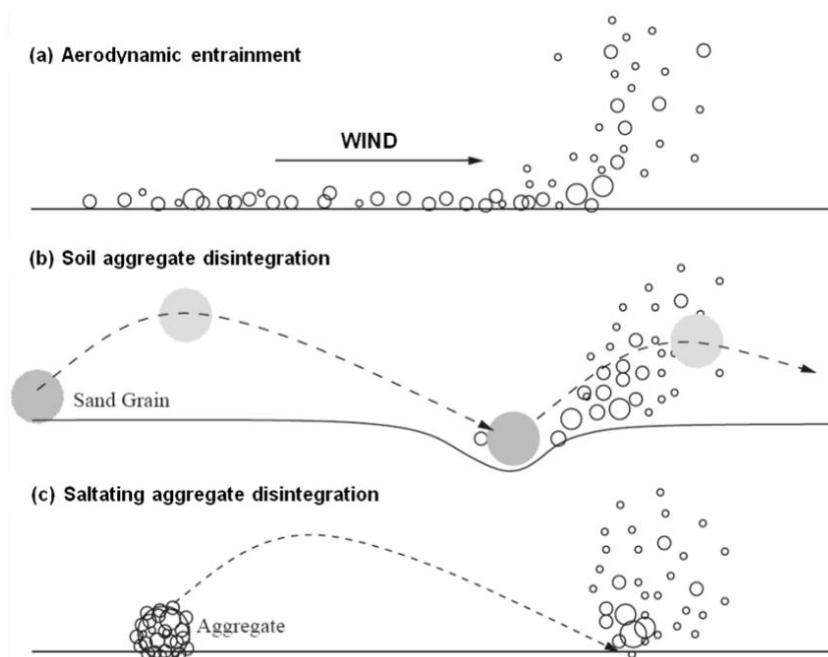

Figure 7: The three different dust emission mechanisms: (a) wind erosion, (b) ejection of dust by saltation of particles and (c) ejection of dust due to saltation of soil aggregates. Figure taken from Kok et al. (2012), adapted from Shao (2008).

Saharan dust, regularly released to the atmosphere via the processes described above, is mainly transported westwards over the North Atlantic Ocean towards the Caribbean as well as North and South America (e.g. Prospero, 1996), serving an important input of ions and nutrients to the Atlantic Ocean (e.g. Field et al., 2010; Schulz et al., 2012) and the Amazon (e.g. Rizzolo et al., 2017; Swap et al., 1992). However, large quantities are also regularly transported via synoptic wind patterns across the Mediterranean to Southern Europe, sometimes reaching as far north as Scandinavia, and towards east to the Middle East (Goudie and Middleton, 2001 and references therein). Estimated Saharan dust deposition amounts exist from various studies with a tendency toward decreasing impact with increasing distance to the source region, still providing a significant event based contribution to PM loads further North. A summary of dust deposition amounts from various studies is given in Goudie and Middleton (2001) with annual values ranging between 0.2 g/m² in the French Alps to 181 g/m² in Northern Algeria. Also for northern Scandinavia Saharan dust depositions of up to 0.16 g/m² were reported, although such events are very exceptional (Barkan and Alpert, 2010; Franzén et al., 1995). Due to the prominence of Saharan dust deposition far up to the North and not only in Southern Europe closer to the source region, the investigation of the influence of Saharan dust in middle Europe is of great importance. While most of the studies focus on the impact of Saharan dust only, contributions from the Arabian Peninsula should not be neglected as well (Tanaka and Chiba, 2006). Thus the more general terms 'desert dust' or 'mineral dust' are preferred.

Several studies investigate the influence of desert dust transport to middle Europe and the alpine region. Thereby the studies focus on the influence on snow chemistry on an event base or cover short time periods of only a few years, on the impact on high alpine ecosystems such as the nutrient input of alpine lakes or the impact on the bacterial community. Still, demonstrations of the impact of desert dust on PM concentrations or deposition in Austria on a long-term base, as well as their impact on air quality issues, are missing. For the first time the qualitative impact of mineral dust deposition on a long-term base of more than 30 years was highlighted in preliminary work to this thesis (Greilinger et al., 2016) while quantitative studies are still lacking.

Aim of this thesis

Based on the importance of desert dust aerosols in the atmosphere and the periodical long-range transport towards Europe and hence also towards Austria, the overall aim of this thesis is to **assess the quantitative influence of desert dust on PM concentrations and deposition in Austria**. Besides these quantitative studies a methodological approach was addressed to improve the routine determination of light absorbing compounds within air quality networks.

Following this general aim of the thesis, three subsidiary research questions are addressed and discussed in the subsequent chapters:

1. **Is there an ongoing influence of desert dust on ionic concentrations in wet deposition?**

In chapter 2, the long-term influence of desert dust on the ionic concentration in wet deposition is explored to reveal that desert dust deposition is a constant factor influencing terrestrial and aquatic ecosystems in the Alps.

2. **What is the influence of mineral dust on measured PM_{10} concentrations?**

For chapter 3 the influence of mineral dust on PM_{10} concentrations was investigated to draw conclusions on its impact on the PM_{10} limit value exceedance in Austria.

Based on the need to expand the set of available data in order to expand future evaluations, methodological developments were started to better and more widely access atmospheric concentration data of mineral dust. This led to investigate:

3. **How can light absorbing particles, and as such also desert dust, be measured on offline filters from air quality monitoring networks?**

In chapter 4 a methodological approach for the quantitative assessment of light absorbing particles sampled on filters within the air quality monitoring networks was investigated. While, as a first step, analysis was limited to black carbon, the approach may serve as a step for further refinement into mineral dust also.

The specific aims and backgrounds of the respective research questions are addressed in a short introduction in every chapter including the underlying methodology.

Literature

Andreae, M.O., Annegarn, H., Barrie, L., Feichter, J., Hegg, D., Jayaraman, A., Leaitch, R., Murphy, D., Nganga, J., Pitari, G., 2001. Aerosols, their Direct and Indirect effects in Climate change 2001: The Scientific Basis. Contribution of Working Group I tothe Third Assessment Report of the Intergovernmental Panel on Climate Change[Houghton, J.T., Y. Ding, D.J. Griggs, M. Noguer,P.J. van der Linden, X. Dai, K. Maskell, and C.A. Johnson (eds.)]. Cambridge University Press, Cambridge, United Kingdom and New York, NY, USA.

Barkan, J., Alpert, P., 2010. Synoptic analysis of a rare event of Saharan dust reaching the Arctic region. Weather 65, 208–211. https://doi.org/10.1002/wea.503

Boucher, O., Randall, D., Artaxo, P., Bretherton, C., Feingold, G., Forster, P., Kerminen, V.-M., Kondo, Y., Liao, H., Lohmann, U., Rasch, P., Satheesh, S.K., Sherwood, S., Stevens, B., Zhang, X.Y., 2013. Clouds and Aerosols in: Climate Change 2013: The Physical Science Basis. Contribution of Working Group I to the Fifth Assessment Report of the Intergovernmental Panel on Climate Change [Stocker, T.F., D. Qin, G.-K. Plattner, M. Tignor, S.K. Allen, J. Boschung, A. Nauels, Y. Xia, V. Bex and P.M. Midgley (eds.)]. Cambridge University Press, Cambridge, United Kingdom and New York, NY, USA.

Caseiro, A., Bauer, H., Schmidl, C., Pio, C.A., Puxbaum, H., 2009. Wood burning impact on PM10 in three Austrian regions. Atmospheric Environment 43, 2186–2195. https://doi.org/10.1016/j.atmosenv.2009.01.012

European Union: European Comission, 2011. Comission Staff Working Paper establishing guidelines for demonstration and substraction of exceedances attributable to natural sources under the Directive 2008/50/EC on ambient air quality and cleaner air for Europe. SEC(2011) 208 final.

Field, J.P., Belnap, J., Breshears, D.D., Neff, J.C., Okin, G.S., Whicker, J.J., Painter, T.H., Ravi, S., Reheis, M.C., Reynolds, R.L., 2010. The ecology of dust. Frontiers in Ecology and the Environment 8, 423–430. https://doi.org/10.1890/090050

Finlayson-Pitts, B.J., Pitts Jr., Ja.N., 1999. Chemistry of the upper and lower atmosphere: theory, experiments, and applications. Elsevier.

Franzén, L.G., Hjelmroos, M., Kållberg, P., Rapp, A., Mattsson, J.O., Brorström-Lundén, E., 1995. The Saharan dust episode of south and central Europe, and northern Scandinavia, March 1991. Weather 50, 313–318. https://doi.org/10.1002/j.1477-8696.1995.tb06139.x

Goudie, A.S., Middleton, N.J., 2001. Saharan dust storms: nature and consequences. Earth-Science Reviews 56, 179–204.

Greilinger, M., Schöner, W., Winiwarter, W., Kasper-Giebl, A., 2016. Temporal changes of inorganic ion deposition in the seasonal snow cover for the Austrian Alps (1983–2014). Atmospheric Environment 132, 141–152. https://doi.org/10.1016/j.atmosenv.2016.02.040

Griffin, R.J., 2013. The Sources and Impacts of Tropospheric Particulate Matter. Nature Education Knowledge 4, 1.

Guarnieri, M., Balmes, J.R., 2014. Outdoor air pollution and asthma. The Lancet 383, 1581–1592. https://doi.org/10.1016/S0140-6736(14)60617-6

Jaenicke, R., 1993. Chapter 1 Tropospheric Aerosols, in: International Geophysics. Elsevier, pp. 1–31. https://doi.org/10.1016/S0074-6142(08)60210-7

Kok, J.F., Parteli, E.J.R., Michaels, T.I., Karam, D.B., 2012. The physics of wind-blown sand and dust. Rep. Prog. Phys. 75, 106901. https://doi.org/10.1088/0034-4885/75/10/106901

Lazar, R., Podesser, A., 1999. An urban climate analysis of Graz and its significance for urban planning in the tributary valleys east of Graz (Austria). Atmospheric Environment 15.

Lippmann, M., Schlesinger, R.B., 2000. Toxicological Bases for the Setting of Health-Related Air Pollution Standards. Annu. Rev. Public Health 21, 309–333. https://doi.org/10.1146/annurev.publhealth.21.1.309

Pope, C.A., 2000. What Do Epidemiologic Findings Tell Us about Health Effects of Environmental Aerosols? Journal of Aerosol Medicine 13, 335–354. https://doi.org/10.1089/jam.2000.13.335

Prospero, J.M., 1996. Saharan dust transport over the North Atlantic Ocean and Mediterranean: An overview. The impact of Desert Dust Across the Mediterranean edited by S.Guerzoni and R.Chester, 133–151.

Puxbaum, H., Gomiscek, B., Kalina, M., Bauer, H., Salam, A., Stopper, S., Preining, O., Hauck, H., 2004. A dual site study of PM2.5 and PM10 aerosol chemistry in the larger region of Vienna, Austria. Atmospheric Environment 38, 3949–3958. https://doi.org/10.1016/j.atmosenv.2003.12.043

Rizzolo, J.A., Barbosa, C.G.G., Borillo, G.C., Godoi, A.F.L., Souza, R.A.F., Andreoli, R.V., Manzi, A.O., Sá, M.O., Alves, E.G., Pöhlker, C., Angelis, I.H., Ditas, F., Saturno, J., Moran-Zuloaga, D., Rizzo, L.V., Rosário, N.E., Pauliquevis, T., Santos, R.M.N., Yamamoto, C.I., Andreae, M.O., Artaxo, P., Taylor, P.E., Godoi, R.H.M., 2017. Soluble iron nutrients in Saharan dust over the central Amazon rainforest. Atmospheric Chemistry and Physics 17, 2673–2687. https://doi.org/10.5194/acp-17-2673-2017

Salvador, P., Alonso-Pérez, S., Pey, J., Artíñano, B., de Bustos, J.J., Alastuey, A., Querol, X., 2014. African dust outbreaks over the western Mediterranean Basin: 11-year characterization of atmospheric circulation patterns and dust source areas. Atmos. Chem. Phys. 14, 6759–6775. https://doi.org/10.5194/acp-14-6759-2014

Schulz, M., Prospero, J.M., Baker, A.R., Dentener, F., Ickes, L., Liss, P.S., Mahowald, N.M., Nickovic, S., García-Pando, C.P., Rodríguez, S., Sarin, M., Tegen, I., Duce, R.A., 2012. Atmospheric Transport and Deposition of Mineral Dust to the Ocean: Implications for Research Needs. Environmental Science & Technology 46, 10390–10404. https://doi.org/10.1021/es300073u

Seinfeld, J.H., Pandis, S.N., 2006. Atmospheric Chemistry and Physics: From Air Pollution to Climate Change, 2nd ed. Wiley, New Jersey.

Shao, Y., 2008. Physics and modelling of wind erosion, Vol. 37. Springer Science & Business Media.

Spangl, W., Nagl, C., 2019. Jahresbericht der Luftgütemessung in Österreich 2018. REP-0675.

Swap, R., Garstang, M., Greco, S., Talbot, R., Kållberg, P., 1992. Saharan dust in the Amazon Basin. Tellus B 44, 133–149. https://doi.org/10.1034/j.1600-0889.1992.t01-1-00005.x

Tanaka, T.Y., Chiba, M., 2006. A numerical study of the contributions of dust source regions to the global dust budget. Global and Planetary Change 52, 88–104. https://doi.org/10.1016/j.gloplacha.2006.02.002

Umweltbundesamt, 2006. Schwebestaub in Österreich (No. BE-277). Wien.

Washington, R., Bouet, C., Cautenet, G., Mackenzie, E., Ashpole, I., Engelstaedter, S., Lizcano, G., Henderson, G.M., Schepanski, K., Tegen, I., 2009. Dust as a tipping element: The Bodele Depression, Chad. Proceedings of the National Academy of Sciences 106, 20564–20571. https://doi.org/10.1073/pnas.0711850106

Whitby, K.T., Cantrell, B., 1976. Atmospheric aerosols- Characteristics and measurement, in: International Conference on Environmental Sensing and Assessment. Las Vegas, Nevada, p. 1.

World Health organization, 2013. Health effects of particulate matter.

Chapter 2
Long-term influence of desert dust on ion concentrations in wet deposition

Background and aim

At a number of sites the monitoring of ionic concentrations in wet deposition was initiated in the early 1980s to monitor the development of acid rain, originating mainly from anthropogenic emissions of gaseous pollutants with sulfur dioxide leading the way. Many research groups and national agencies throughout Europe and North America established extensive monitoring programs to examine the extent of the acid rain problem (Aherne and Farrell, 2002; Avila, 1996; Lehmann et al., 2007; Puxbaum et al., 2002). Also in Asia precipitation chemistry studies were initiated in the 1980s and gained more and more importance (Huang et al., 2008; Okuda et al., 2005). All of these quantitative long-term studies report that the anthropogenic influence of the sulfur emissions shows a negative trend, mainly associated to successive abatement regulations for sulfur dioxide by various countries worldwide. A global assessment of precipitation chemistry and deposition was performed by (Vet et al., 2014) using measurement data and modelling results to generate global and regional maps of major ion concentrations in precipitation and deposition. The results that in North America and Europe wet deposition levels of sulfur have decreased significantly since 1990, and particularly between 2000-2002 and 2005-2007, is in line with results from the other studies.

In Austria the investigation of the composition and impact of wet deposition started in 1957 at the station 'Retz' within the European Air Chemistry Network (EACN) and within the WMO Background Air Pollution Monitoring Network BAPMON. Sampling was performed on a monthly basis using bulk-collectors. The measurements showed that before 1960 concentrations of sulfate, nitrate and ammonium strongly increased which lasted until the mid (sulfate and nitrate) or end (ammonium) of the 70s (Cehak and Chalupa, 1985). The pattern of increasing sulfate depositions was recognized in the whole of Middle Europe between the 1950s and the early 1970s with an increase of 40-60% (Rodhe and Granat, 1984). In 1982 guidelines for the development and implementation of a national precipitation and wet deposition network in Austria, based on daily sampling using wet-only samplers, were prepared. On the basis of these guidelines the first stations within the monitoring networks of the respective environmental authorities of the local governments were activated. The first stations were activated in 1983 in Tyrol and Salzburg, 1984 in Upper Austria, 1986 in Vienna, 1989 in Carinthia and Lower Austria and 1990 in Styria. Thus, in the 1990s the wet deposition monitoring network in Austria comprised more than 30 stations, 5 of these stations were also part of the EMEP network, a 'Co-operative programme for monitoring and evaluation of the long-range transmission of air pollutants in Europe' and were operated by the Austrian Environmental Agency (Umweltbundesamt, UBA). The stations contributing to the EMEP network are Illmitz (117 m a.s.l.), Sankt Koloman (848 m a.s.l.), Zöbelboden (899 m a.s.l.), Vorhegg (1010 m a.s.l.) and Sonnblick (3106 m a.s.l.).

Approximately 20 years later first long-term trend evaluation studies (Puxbaum et al., 2002; Tsakovski et al., 2000, SIMEONOV 1999), investigated the concentration and deposition of major ions measured at 11 sites within the Austrian wet deposition network in the period from 1984 to 1999 and revealed a serious decrease of sulfate concentration and deposition, reflecting the effective emission reduction measures of the precursor gas sulfur dioxide, as well as for the hydrogen ion associated with acidity. The nitrogen containing ions nitrate and ammonia, base cations as well as chloride showed only a slight concentration and deposition decrease with some sites being exceptional by showing no trend at all. Thus, some local authorities reduced the amount of stations because the necessity for an extensive and dense network was not needed as much as at the beginning of the measurements, where acid rain was still a big issue.

15

Presently (status 2018) the wet deposition network in Austria comprises 18 stations in Tyrol, Salzburg, Lower Austria, Upper Austria and Styria. Respective annual reports of the local authorities, which are available online for Styria (e.g. Pongratz, 2018)and Tyrol (e.g. Egger, 2019), still document a significant decrease in sulfate concentration and deposition for the already more than 30-year long time series of some of these stations. This decrease is also documented in the master's thesis of Schreiner (2017). Within this study also nitrate and ammonium concentrations showed a decreasing trend for most of the stations, for the respective depositions the trend was not as pronounced.

Source classification analyses of the wet deposition data from Austria, e.g. via principal component analysis, reveals a factor including the afore discussed anthropogenic or acidifying ions like sulfate and nitrate in relation with ammonium from traffic and fossil fuel combustion, but also a factor related to crustal sources including mainly calcium and magnesium and one 'mixed salt' factor with sodium, chloride and potassium mainly attributed to manure and sea spray (compare Rogora et al., 2006; Simeonov et al., 1999; Tsakovski et al., 2000). For the 'crustal' factor not only mineral dust intrusion from long-range transport but also sporadic local events, like construction sites or agricultural activities, were found as potential sources (Rogora et al., 2006; Tsakovski et al., 2000). A recent thesis of Firmkranz (2019) also mentions gritting in winter and the resuspension of road dust to contribute to an increase of the ions loaded in the 'crustal' factor. Thus, besides the topic of acid rain in relation to the acidifying components, also the deposition of the base cations Na^+, Ca^{2+}, Mg^{2+} and K^+ should be investigated in more detail to draw conclusions on e.g., the influence of sea salt and mineral dust on precipitation acidity or the role of deposition on the biogeochemical cycling of Aeolian dust. It is well known that mineral dust, especially Saharan dust, serves as an important input of ions and nutrients to the Atlantic Ocean (e.g. Field et al., 2010; Schulz et al., 2012), the Amazon (e.g. Rizzolo et al., 2017; Swap et al., 1992) and alpine lakes (Psenner, 1999). Also the impact on the bacterial community due to desert dust intrusion, especially in remote areas (e.g. Chuvochina et al., 2011; Peter et al., 2014; Weil et al., 2017) can be altered.

Globally, wet deposition sums of the base cation Na^+, Ca^{2+}, Mg^{2+} and K^+ are investigated and were found to range from 0.01 to 11.7 keq ha^{-1} a^{-1} measured from 2000 to 2002 and from 0.01 to 8.5 from 2005 to 2007. Most of the high deposition sites (i.e. >1 keq ha^{-1} a^{-1}) are located in coastal zones or islands reflecting the importance of sea salt Na^+ to the sum of the base cations(Vet et al., 2014). The influence of land-based sources of base cations increases with distance inland from the coast, mainly attributed to the influence of aeolian soil dust, road dust or biomass burning. According to Vet et al. (2014)and references therein in Europe spatial and temporal analyses of base cations and sea salt in precipitation and wet deposition are presented in a few regional studies only, based on measurements and model estimates. The level of the deposition of sea salt ions was found to be, to a large extent, determined by the distance from the sea and the significance of sea salt episodes. Highest deposition amounts are seen at coastal sites in Norway, Island, Ireland, UK, France and Spain. In most areas of Europe, the anthropogenic contribution of mineral base cations was found to be small as well and that Saharan dust outbreak events have a large impact on levels of base cation wet deposition especially in the south of Europe, but occasionally, when atmospheric transport conditions are favourable, lead to observable further North as well (e.g. Barkan and Alpert, 2010; Franzén et al., 1995).

Several studies from Europe on the influence of mineral dust on wet deposition exist, mostly investigating this effect on either an event basis or short time spans of a few years at the most whereas long-term studies are very scarce. Avila et al. (1998) analysed the contribution of North African dust in rainwater samples collected weekly in the Montseny Mountains in NE Spain for the period of 1983 to 1994. Results from the same site but from subsequent years (1996-2002) were summarized in Escudero et al. (2005). The more recent study of Kutuzov et al. (2013) examined a four year record (2009-2012) of dust deposition events on Mt. Elbrus in the Northern Caucasus, Russia, using data from one snow pit dug in June 2009 featuring four visible yellow-brown layers of deposited mineral dust and from a firn core extracted in June 2012 featuring 13 visible dust layers. Maupetit and Delmas (1994) collected snow samples in the accumulation zone of four high altitude glaciers in the French Alps during three

consecutive years from 1989 to 1991 and investigated the acid and alkaline input. Rogora et al. (2004) investigated the rainwater chemistry from 1975 to 2002 at the Pallanza station in Northwestern Italy including event based samples and weekly rain water samples. Existing long-term dust records were obtained predominantly from ice cores and not from wet deposition measurements, characterizing dust events on a millennial time scale (De Angelis and Gaudichet, 1991; Gabbi et al., 2015; Schwikowski et al., 1999).

While the sampling of ice cores via deep drilling is much more laborious compared to event or annual based sampling, the chemical analysis is much more consistent since all samples, covering a time span of millennia, are analysed at the same time and in the same way. For event based or annual wet deposition sampling over a long-term period of several centuries the situation is different. Not only might the technological progress in the measurement techniques and the corresponding limits of detection have changed but also the person performing the measurements. This introduces an uncertainty to the data which has to be considered. Furthermore, event or annual based sampling may be easier compared to deep drilling, whereas the retrospective characterization or identification of mineral dust and its impact on long-term wet deposition data sets is not as straightforward. Thus, a uniform methodology for the investigation and quantification of the influence of mineral dust from long-term wet deposition data at a specific moment in time is appreciated to provide a possibility also for retrospective evaluations.

As in ice cores the identification of mineral dust events in wet deposition samples of rain or snow can be separated into two approaches. On the one hand, mineral dust affected samples are optically identified by their reddish, brownish or yellowish colour of either the snow sample itself, a visible turbidity of rain samples or by a colouring of the filters used for filtering the precipitation or snow samples (Avila et al., 1998; Kutuzov et al., 2013). On the other hand, they might be identified using the 'chemical footprint' of mineral dust affected samples such as their ability to increase the alkalinity and the concentrations of dust related cations such as Ca^{2+} and Mg^2 (e.g. Maupetit and Delmas, 1994; Rogora et al., 2004).

Within this study a methodology for the retrospective quantification of the influence of mineral dust to deposition samples collected in Austria was developed and applied to the most suitable data set, i.e. the snow pit samples collected at Sonnblick. The sampling site and the snow pit samples were chosen for several reasons. (1) The site is in the close vicinity to the Sonnblick Observatory, a remote station listed as global background station in the GAW (global atmosphere watch) program of the World Meteorological Organization (WMO). Thus, no anthropogenic related intrusion of mineral dust, as is the case at urban and rural site allows the determination of the dry deposition as well, a benefit compared to wet deposition measurements only, although this was not regarded within the presented study. (3) Due to the sampling within a snow pit, a stratigraphic evaluation is possible and a visual investigation based on the colour of the snow layers can be included. Due to a reliable reporting over the whole sampling period, this information is also available for retrospective evaluations.

The data set of these snow pit samples covers a time period from 1987 onwards and long-term records of inorganic ion concentrations of these wet and dry deposition samples were already published in a previous work from Greilinger et al. (2016). These snow chemistry measurements are performed annually within the Global Cryosphere Watch (GCW) Program of the WMO, financed by the Austrian federal ministry for tourism and sustainability. Figure 8 gives an impression of the snow sampling procedure as well as a picture of the snow pit from 2014 where two distinct orange-coloured Saharan dust layers are visible.
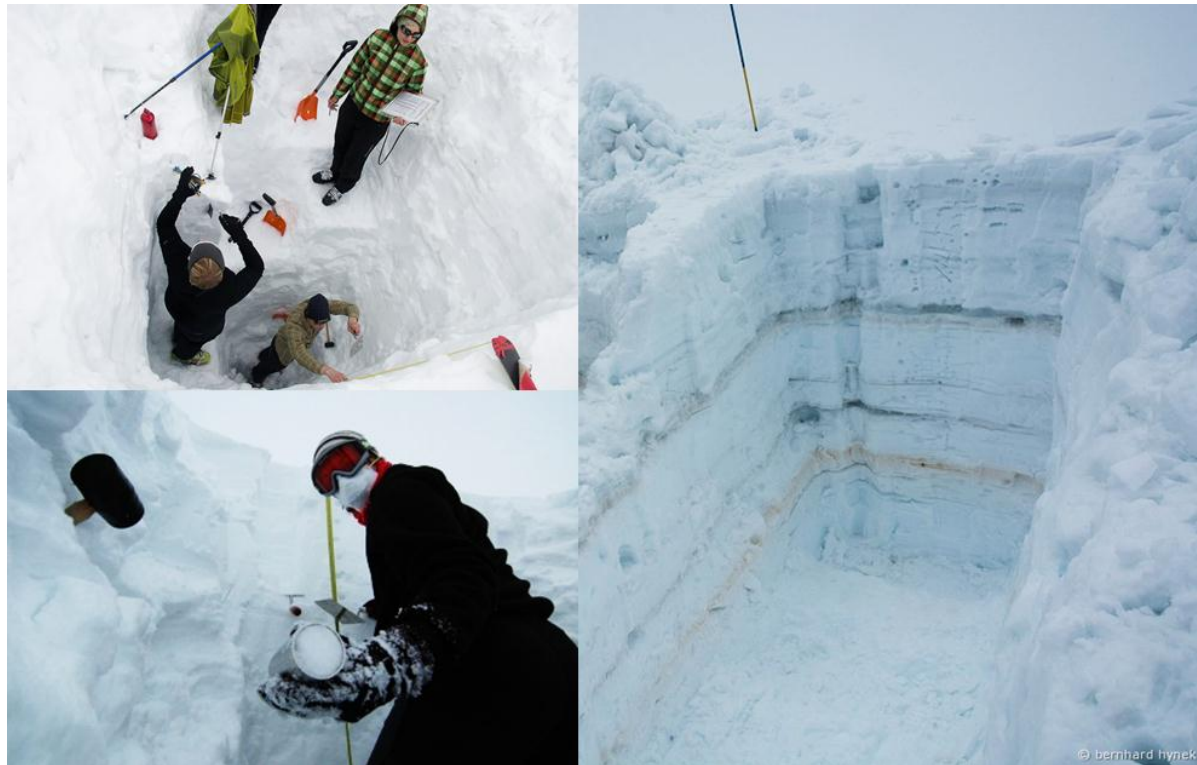
Figure 8: Pictures from the snow sampling, annually performed at the end of the winter accumulation period to perform ion deposition measurements. In the snow pit sampled at the end of April 2014 two distinct Saharan dust layers, representative for the events observed in February and April 2014.

The qualitative source assignments of the ions of the snow pit samples using principal component analysis (PCA) was investigated and a factor related to Ca^{2+}, Mg^{2+} and the pH, being indicative for a marked contribution of desert dust, could be identified (Greilinger et al., 2016). This result shows the presence of a significant 'chemical footprint' related to mineral dust in snow pack samples in Austria and provides a starting point for a retrospective analysis of the impact of mineral dust, or to be more specific the impact of Saharan dust deposition on the high alpine snow packs. The 'chemical footprint' together with documentations on a visible presence of coloured mineral dust layers in snow packs (compare Figure 8) were used to establish a method to distinguish mineral dust affected and non-affected samples according to the approach of Rogora et al. (2004) using the thresholds of the pH and the calcium concentration. Once the affected samples were identified, the intensity and frequency of mineral dust deposited in the high alpine snow pack was investigated and the impact of these events on the total deposition load was quantified. This quantitative assessment provides fundamental knowledge on further investigations and impact related studies tackling the above mentioned fields of e.g. nutrient input and microbiological studies regarding the bacterial community.

Literature

Aherne, J., Farrell, E.P., 2002. Deposition of sulphur, nitrogen and acidity in precipitation over Ireland: chemistry, spatial distribution and long-term trends. Atmospheric Environment 36, 1379–1389. https://doi.org/10.1016/S1352-2310(01)00507-6

Avila, A., 1996. Time trends in the precipitation chemistry at a mountain site in Northeastern Spain for the period 1983–1994. Atmospheric Environment 30, 1363–1373. https://doi.org/10.1016/1352-2310(95)00472-6

Avila, A., Alarcón, M., Queralt, I., 1998. The chemical composition of dust transported in red rains-its contribution to the biogeochemicl cycle of a holm oak forest in Catalonia (Spain). Atmospheric Environment 32, 179–191. https://doi.org/10.1016/S1352-2310(97)00286-0

Barkan, J., Alpert, P., 2010. Synoptic analysis of a rare event of Saharan dust reaching the Arctic region. Weather 65, 208–211. https://doi.org/10.1002/wea.503

Cehak, K., Chalupa, K., 1985. Observations of various chemical contaminants of the precipitation at a BAPMoN station in the Eastern Pre-Alpine Region. Archives for meteorology, geophysics, and bioclimatology Series B, 307–322.

Chuvochina, M.S., Marie, D., Chevaillier, S., Petit, J.-R., Normand, P., Alekhina, I.A., Bulat, S.A., 2011. Community Variability of Bacteria in Alpine Snow (Mont Blanc) Containing Saharan Dust Deposition and Their Snow Colonisation Potential. Microbes and Environments 26, 237–247. https://doi.org/10.1264/jsme2.ME11116

De Angelis, M., Gaudichet, A., 1991. Saharan dust deposition over Mont Blanc (French Alps) during the last 30 years. Tellus B 43, 61–75.

Egger, W., 2019. Luftgüte in Tirol - Jahresbericht 2018.

Escudero, M., 2005. Wet and dry African dust episodes over eastern Spain. Journal of Geophysical Research 110. https://doi.org/10.1029/2004JD004731

Field, J.P., Belnap, J., Breshears, D.D., Neff, J.C., Okin, G.S., Whicker, J.J., Painter, T.H., Ravi, S., Reheis, M.C., Reynolds, R.L., 2010. The ecology of dust. Frontiers in Ecology and the Environment 8, 423–430. https://doi.org/10.1890/090050

Firmkranz, J., 2019. Untersuchungen zur Niederschlagschemie in Österreich.

Franzén, L.G., Hjelmroos, M., Kållberg, P., Rapp, A., Mattsson, J.O., Brorström-Lundén, E., 1995. The Saharan dust episode of south and central Europe, and northern Scandinavia, March 1991. Weather 50, 313–318. https://doi.org/10.1002/j.1477-8696.1995.tb06139.x

Gabbi, J., Huss, M., Bauder, A., Cao, F., Schwikowski, M., 2015. The impact of Saharan dust and black carbon on albedo and long-term mass balance of an Alpine glacier. The Cryosphere 9, 1385–1400. https://doi.org/10.5194/tc-9-1385-2015

Greilinger, M., Schöner, W., Winiwarter, W., Kasper-Giebl, A., 2016. Temporal changes of inorganic ion deposition in the seasonal snow cover for the Austrian Alps (1983–2014). Atmospheric Environment 132, 141–152. https://doi.org/10.1016/j.atmosenv.2016.02.040

Huang, Y., Wang, Y., Zhang, L., 2008. Long-term trend of chemical composition of wet atmospheric precipitation during 1986–2006 at Shenzhen City, China. Atmospheric Environment 42, 3740–3750. https://doi.org/10.1016/j.atmosenv.2007.12.063

Kutuzov, S., Shahgedanova, M., Mikhalenko, V., Ginot, P., Lavrentiev, I., Kemp, S., 2013. High-resolution provenance of desert dust deposited on Mt. Elbrus, Caucasus in 2009&ndash;2012 using snow pit and firn core records. The Cryosphere 7, 1481–1498. https://doi.org/10.5194/tc-7-1481-2013

Lehmann, C.M.B., Bowersox, V.C., Larson, R.S., Larson, S.M., 2007. Monitoring Long-term Trends in Sulfate and Ammonium in US Precipitation: Results from the National Atmospheric Deposition Program/National Trends Network. Water Air Soil Pollut: Focus 7, 59–66. https://doi.org/10.1007/s11267-006-9100-z

Maupetit, F., Delmas, R.J., 1994. Snow chemistry of high altitude glaciers in the French Alps. Tellus B: Chemical and Physical Meteorology 46, 304–324. https://doi.org/10.3402/tellusb.v46i4.15806

Okuda, T., Iwase, T., Ueda, H., Suda, Y., Tanaka, S., Dokiya, Y., Fushimi, K., Hosoe, M., 2005. Long-term trend of chemical constituents in precipitation in Tokyo metropolitan area,

Japan, from 1990 to 2002. Science of The Total Environment 339, 127–141. https://doi.org/10.1016/j.scitotenv.2004.07.024

Peter, H., Hörtnagl, P., Reche, I., Sommaruga, R., 2014. Bacterial diversity and composition during rain events with and without Saharan dust influence reaching a high mountain lake in the Alps: Bacteria in rainfall with and without Saharan dust influence. Environmental Microbiology Reports 6, 618–624. https://doi.org/10.1111/1758-2229.12175

Pongratz, T., 2018. Luftreinhaltung in der Steiermark - Jahresbericht 2017. Bericht Nr. Lu-07-2018.

Psenner, R., 1999. Living in a dusty world: airborne dust as a key factor for alpine lakes. Water, Air, & Soil Pollution 112, 217–227.

Puxbaum, H., Simeonov, V., Kalina, M., Tsakovski, S., Löffler, H., Heimburger, G., Biebl, P., Weber, A., Damm, A., 2002. Long-term assessment of the wet precipitation chemistry in Austria (1984–1999). Chemosphere 48, 733–747. https://doi.org/10.1016/S0045-6535(02)00125-X

Rizzolo, J.A., Barbosa, C.G.G., Borillo, G.C., Godoi, A.F.L., Souza, R.A.F., Andreoli, R.V., Manzi, A.O., Sá, M.O., Alves, E.G., Pöhlker, C., Angelis, I.H., Ditas, F., Saturno, J., Moran-Zuloaga, D., Rizzo, L.V., Rosário, N.E., Pauliquevis, T., Santos, R.M.N., Yamamoto, C.I., Andreae, M.O., Artaxo, P., Taylor, P.E., Godoi, R.H.M., 2017. Soluble iron nutrients in Saharan dust over the central Amazon rainforest. Atmospheric Chemistry and Physics 17, 2673–2687. https://doi.org/10.5194/acp-17-2673-2017

Rodhe, H., Granat, L., 1984. An evaluation of sulfate in European precipitation 1955–1982. Atmospheric Environment 18, 2627–2639.

Rogora, M., Mosello, R., Arisci, S., Brizzio, M.C., Barbieri, A., Balestrini, R., Waldner, P., Schmitt, M., Stähli, M., Thimonier, A., Kalina, M., Puxbaum, H., Nickus, U., Ulrich, E., Probst, A., 2006. An Overview of Atmospheric Deposition Chemistry over the Alps: Present Status and Long-term Trends. Hydrobiologia 562, 17–40. https://doi.org/10.1007/s10750-005-1803-z

Rogora, M., Mosello, R., Marchetto, A., 2004. Long-term trends in the chemistry of atmospheric deposition in Northwestern Italy: the role of increasing Saharan dust deposition. Tellus B: Chemical and Physical Meteorology 56, 426–434. https://doi.org/10.3402/tellusb.v56i5.16456

Schreiner, E., 2017. Analyse der Messungen zur Nassen Deposition seit 1983.

Schulz, M., Prospero, J.M., Baker, A.R., Dentener, F., Ickes, L., Liss, P.S., Mahowald, N.M., Nickovic, S., García-Pando, C.P., Rodríguez, S., Sarin, M., Tegen, I., Duce, R.A., 2012. Atmospheric Transport and Deposition of Mineral Dust to the Ocean: Implications for Research Needs. Environmental Science & Technology 46, 10390–10404. https://doi.org/10.1021/es300073u

Schwikowski, M., Döscher, A., Gäggeler, H.W., Schotterer, U., 1999. Anthropogenic versus natural sources of atmospheric sulphate from an Alpine ice core. Tellus B: Chemical and Physical Meteorology 51, 938–951. https://doi.org/10.3402/tellusb.v51i5.16506

Simeonov, V., Puxbaum, H., Tsakovski, S., Sarbu, C., Kalina, M., 1999. Classification and receptor modeling of wet precipitation data from central Austria (1984-1993) 16.

Swap, R., Garstang, M., Greco, S., Talbot, R., Kållberg, P., 1992. Saharan dust in the Amazon Basin. Tellus B 44, 133–149. https://doi.org/10.1034/j.1600-0889.1992.t01-1-00005.x

Tsakovski, S., Puxbaum, H., Simeonov, V., Kalina, M., Löffler, H., Heimburger, G., Biebl, P., Weber, A., Damm, A., 2000. Trend, seasonal and multivariate modelling study of wet precipitation data from the Austrian Monitoring Network (1990–1997). J. Environ. Monitor. 2, 424–431. https://doi.org/10.1039/b004170j

Vet, R., Artz, R.S., Carou, S., Shaw, M., Ro, C.-U., Aas, W., Baker, A., Bowersox, V.C., Dentener, F., Galy-Lacaux, C., Hou, A., Pienaar, J.J., Gillett, R., Forti, M.C., Gromov, S., Hara, H., Khodzher, T., Mahowald, N.M., Nickovic, S., Rao, P.S.P., Reid, N.W., 2014. A global assessment of precipitation chemistry and deposition of sulfur, nitrogen, sea salt, base cations, organic acids, acidity and pH, and phosphorus. Atmospheric Environment 93, 3–100. https://doi.org/10.1016/j.atmosenv.2013.10.060

Weil, T., De Filippo, C., Albanese, D., Donati, C., Pindo, M., Pavarini, L., Carotenuto, F., Pasqui, M., Poto, L., Gabrieli, J., Barbante, C., Sattler, B., Cavalieri, D., Miglietta, F., 2017. Legal

immigrants: invasion of alien microbial communities during winter occurring desert dust storms. Microbiome 5. https://doi.org/10.1186/s40168-017-0249-7

Article (peer-reviewed)

This chapter corresponds to the following peer-reviewed publication in its original form:

Greilinger, M., Baumann-Stanzer, K., Skomorowski, P., Schauer, G., Schöner, W., & Kasper-Giebl, A. (2018). Contribution of Saharan dust to ion deposition loads of high alpine snow packs in Austria (1987-2017). Frontiers in Earth Science, 6, 126. doi: 10.3389/feart.2018.00126

The study was conceived in the terms of scientific collaborations with the first author being main responsible for the content and realization of the work. The detailed author contributions can be found in the respective section in the article.

Contribution of Saharan Dust to Ion Deposition Loads of High Alpine Snow Packs in Austria (1987–2017)

Marion Greilinger[1,2]*, Gerhard Schauer[3], Kathrin Baumann-Stanzer[3,4], Paul Skomorowski[3,4], Wolfgang Schöner[5] and Anne Kasper-Giebl[2]

[1] Climate Monitoring and Cryosphere, Central Institution for Meteorology and Geodynamics, Vienna, Austria, [2] Environmental and Process Analytics, Institute of Chemical Technologies and Analytics, Vienna University of Technology, Vienna, Austria, [3] Sonnblick Observatory, Central Institution for Meteorology and Geodynamics, Salzburg, Austria, [4] Environmental Meteorology, Central Institution for Meteorology and Geodynamics, Vienna, Austria, [5] Institute of Geography and Regional Research, University of Graz, Graz, Austria

We investigate the influence of Saharan dust on the chemical composition and deposition loads of a 31-year long snow chemistry data set (1987–2017) of high alpine snow packs situated close to the Sonnblick Observatory, a global GAW (Global Atmospheric Watch) station, in the National Park Hohe Tauern in the Austrian Alps. Based on the snow pack of the winter accumulation period 2015/2016, when two Saharan dust events were visible by a reddish color of the snow, we define a pH > 5.6 together with a Ca^{2+} concentration > 10 µeq/l as thresholds to identify Saharan dust affected snow layers. This criterion is checked with an intercomparison with trajectories and on-line aerosol data determined at the Sonnblick Observatory. This check was extended to the accumulation periods 2014/2015 and 2016/2017 before the whole time series is investigated regarding the contribution of Saharan dust to ion deposition loads. Especially Mg^{2+}, Ca^{2+}, and H^+ depositions are strongly affected by Saharan dust input causing, as average values across the 30 years period, increased Mg^{2+} (25%) and Ca^{2+} (35%) contributions of affected snow layers, while the contribution to the snow water equivalent was only 11%. For H^+ Saharan dust affected snow layers show a much lower contribution (2%) while the contribution of other ions is well comparable to the deposition amount expected according to the snow water equivalent of affected snow layers. The pH range of Saharan dust affected snow layers covers 5.58–7.17, while the median value of all samples is 5.40. The long term trends of ion deposition are not affected by the deposition of Saharan dust.

Keywords: mineral dust, Saharan dust, snow chemistry, high alpine snow pack, deposition loads

INTRODUCTION

Deserts serve as a major source for aerosols in the atmosphere with mineral dust as a main contributor to primary aerosol mass. Especially the Sahara, the largest desert in the world, contributes roughly half of the primarily emitted aerosol mass found in the atmosphere and is thus the world's largest source for Aeolian soil dust (Prospero, 1996; Goudie and Middleton, 2001 and references therein). Once in the atmosphere, desert dust can be transported over thousands of kilometers via synoptic wind patterns to regions far beyond (e.g., Prospero, 1996; Moulin et al., 1997). Online aerosol measurements conducted since 2013 at Austria's high alpine Sonnblick

25

Observatory, listed as a global station within the Global Atmospheric Watch Program of the World Meteorological Organization, suggest up to 30 days per year with the influence of mineral dust. Due to the predominant contribution of dust origination from the Sahara the term Saharan dust will be used within this paper. Transported dust can be removed from the atmosphere through wet and dry deposition processes.

If dust is deposited on mountain snow packs it causes several direct and indirect effects. Firstly, Saharan dust deposited onto snow surfaces decreases the albedo due to a darkening of the surface and consequently higher absorption of solar radiation, leading to an earlier removal of the snow cover or increased glacier melt-off (Goudie and Middleton, 2001; Field et al., 2010). This triggering of faster and earlier melt-off due to the dust deposition can potentially result in a lower total and less late-season water supply (Field et al., 2010) due to melt-off already during the season. This is especially important in areas where water supply is scarce. A more recent study of Gabbi et al. (2015) investigated the long-term effect of snow impurities, mainly Saharan dust and Black Carbon, on albedo and glacier mass balance and found that their presence lowered the albedo by 0.04–0.06, thereby increasing melt by 15–19% and reducing the mean annual mass balance.

Secondly, dust plays an important role in the control of global and regional biogeochemical cycles. These effects have been studied mostly in seawater or the Amazonas basin. For seawater especially P and Fe are supposed to be the main actors to estimate the contribution of atmospheric inputs stimulating the productivity of oceanic plankton, thus accelerating CO_2 uptake and stimulating N_2-fixation (Gruber and Sarmiento, 1997; Field et al., 2010; Schulz et al., 2012). For the Amazonas basin, Swap et al. (1992) and Rizzolo et al. (2017) showed that especially Fe^{3+}, Na^+, Ca^{2+}, K^+, and Mg^{2+} are the main constituents introduced via Saharan dust, acting as fertilizer or micronutrients essential for plant growth by offsetting the losses of nutrients due to leaching or weathering of the soil. Many other studies propose the significant influence of Saharan dust on microbiology, nutrient supply, acid neutralization and geochemistry in Europe as well. Avila et al. (1998) for example found that red rains, indicating Saharan dust influence, are important for biogeochemical consequences of a Holm oak forest in Catalonia, Spain, due to addition of nutrient elements such as K^+, Ca^{2+}, and Mg^{2+} and input adding to the neutralizing capacity of the soils in the catchment. The effect of Saharan dust on high alpine snow biogeochemistry is still poorly investigated although many studies propose that the ionic composition and deposition load of snow is of high biogeochemical interest because snow serves as interface where the water and nutrient cycle interact (De Angelis and Gaudichet, 1991; Kuhn, 2001). Marchetto et al. (1995) just showed that for alpine lakes in areas of low weathering rocks, such as silicate rocks also present at the site investigated in this study, lake chemistry, including acidity and alkalinity, is mainly determined by atmospheric deposition. Additionally it is well known that Saharan dust alters the chemical composition and neutralizing capacity of precipitation and, if deposited, also of snow packs and thus influences surface water chemistry (De Angelis and Gaudichet, 1991; Rogora et al., 2004).

If the chemical composition of high alpine snow packs is investigated the main ions analyzed generally are Cl^-, SO_4^{2-}, NO_3^-, NH_4^+, Na^+, K^+, Mg^{2+}, Ca^{2+} as well as the pH and conductivity. Their origin can be assigned to different sources like anthropogenic sources, sea salt or mineral dust (Maupetit and Delmas, 1994). Greilinger et al. (2016) who analyzed the long-term series of snow chemistry data used in this study found three different clusters of ions representing different types of origin. Thereby one cluster representing mineral dust sources was found, positively correlated with Ca^{2+} and Mg^{2+} together with a negative correlation for H^+, representing the alkaline characteristics of mineral dust. Findings are comparable to results from Maupetit and Delmas (1994). It can be proposed that increased Ca^{2+} and Mg^{2+} concentrations change the chemical characteristics of the samples, especially the pH value.

Thirdly, Aeolian dust and as such also Saharan dust, is used by microorganisms to disperse and colonize new habitats. It is assumed, that microorganisms that are able to survive in the harsh conditions of the Sahara and the atmosphere during transport may also be able to colonize other sites with comparably challenging conditions such as the high Alps (Chuvochina et al., 2011) or the Himalaya (Zhang et al., 2008). It has been shown in a recent study of Weil et al. (2017) that those microbial dust passengers introduced to high alpine snow packs via Saharan dust can favor a rapid microbial contamination of sensitive habitats after snowmelt.

Due to the described effects of Saharan dust on mountain snow packs, the main purpose of this paper is to investigate the intensity and frequency of Saharan dust deposited in high alpine snow packs via a retrospective evaluation of a unique high alpine snow chemistry data set of 31 years (1987–2017) and to quantify the impact of these events on the deposition load.

According to Psenner (1999), who investigated the relevance of airborne dust like Saharan dust for the ecology of alpine lakes, an interdisciplinary research is necessary to elucidate the impact of dust on ecological issues. An estimation of the contribution of Saharan dust to the chemical variability of the ecosystems is not easy due to lack of quantitative studies in remote areas but cannot be neglected when dealing with acidification and recovery processes. Thus, our study provides relevant input for further investigations and conclusions, and indicates that the stochastic occurrence of Saharan dust deposition is on the long run a constant factor influencing the terrestrial and aquatic ecosystem of the Alpine region.

MEASUREMENTS AND METHODS

The study area, sampling, and measurement techniques as well as data quality issues are thoroughly described in Greilinger et al. (2016) and are only summarized shortly in this section.

Study Area

Snow profiles were sampled at the Goldbergkees (GOK), a remote glacier field, part of the Goldberggruppe at an elevation of more than 3,000 m.a.s.l. (**Figure 1**) close to the Sonnblick Observatory, listed as a global station within the Global

26

FIGURE 1 | Location of the Goldberggruppe in Austria, the sampling site Goldbergkees (GOK) on a glacier field in the Eastern Alps and of the mountain summit Hoher Sonnblick where the meteorological observatory is situated.
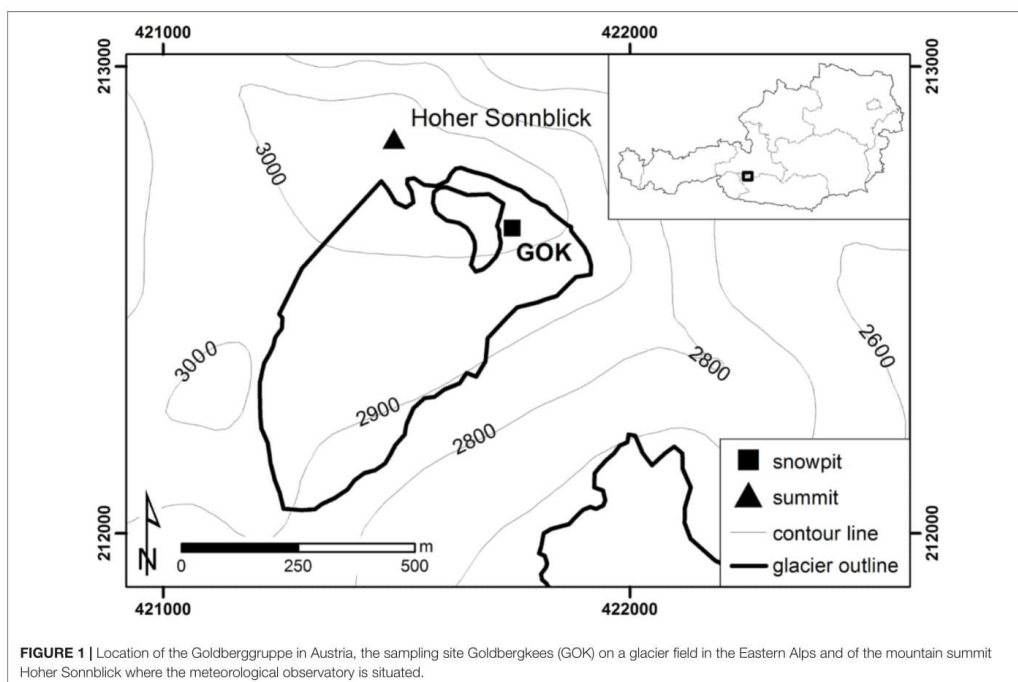
Atmospheric Watch Program of the World Meteorological Organization. The site is not exposed to any local anthropogenic influence.

Snow Sampling and Chemical Analysis

Snow samples representing the whole winter accumulation period are taken annually in a vertical resolution of 10 cm increments just prior to the start of significant snowmelt (usually at the end of April or the beginning of May). Just in 1997 the size of the increments was 40 cm. Note that the respective increments could either represent a portion of a single precipitation event or include mixed information of several events, depending on precipitation amount and settling of the snow cover. After digging a snow pit until the horizon when winter accumulation had started snow samples were taken with a stainless steel cylinder and stored in polyethylene bags. To avoid contamination of the samples gloves and a mask were used during sampling. Samples were taken to the lab frozen and were analyzed immediately after thawing. Analytical protocols changed slightly during the period of observation, but quality assurance was maintained by regular participation in the laboratory intercomparison of the World Data Center for Precipitation Chemistry (Global Atmosphere Watch). Conductivity and pH were determined electrochemically using a conductivity cell and a glass electrode, respectively. Anion (chloride, nitrate and sulfate) and monovalent cation (sodium,

potassium, ammonium) concentrations were determined by suppressed ion chromatography. Bivalent cation (calcium, magnesium) concentrations were determined by atomic absorption spectroscopy until 1993, and only later by ion chromatography. Limits of detections (LODs) changed slightly during the years but were in the range of 0.01 and 0.015 mg/L for all ions and years, aside from sulfate and the time period until 1993, when a LOD of 0.029 mg/L was obtained. More details are given in Winiwarter et al. (1998) and Greilinger et al. (2016) including data quality control, outlier discussion and general presentation of the data.

Trajectory Analysis

In meteorology trajectories are defined as the paths of infinitesimally small particles of air. Such an air parcel, 'marked' at a certain point in space at a given time, can be traced forward or backward in time along its trajectory. In this study, air mass trajectories are calculated using the Flextra model (Stohl et al., 2001) based on meteorological data provided by ECMWF (European Centre for Medium Range Weather Forecast) with a horizontal resolution of 0.2°. The trajectories are starting from Sonnblick Observatory eight times per day (00UTC, 03UTC, 06UTC, 09UTC, 12UTC, 15UTC, 18UTC, and 21UTC) and trace the path of the air parcel backward in time for the previous 96 h, giving an indication where the major part of the air mass came from.

27

Aerosol Measurements

Aerosol sampling is performed via a heated (+20°C) whole air inlet designed according to GAW guidelines, with an upper size cut of 20 μm at a wind speed of 20 m/s. Details about the setup are given in Schauer et al. (2016). Episodes with a dominant influence of dust are continuously identified via the optical properties of the aerosol and the corresponding calculation of the wavelength dependence of the Single Scattering Albedo (SSA) according to Coen et al. (2003). Therefore a three-wavelength polar Nephelometer (Aurora 4000, Ecotech) was used for the determination of the light scattering coefficients at 450, 525, and 635 nm. Absorption coefficients were determined with an Aethalometer (AE33, Magee Scientific) at seven wavelengths, i.e., 370, 470, 525, 590, 660, 880, and 940 nm. A detailed description of the respective calculations can be found in Schauer et al. (2016). Based on this identification and on particulate matter (PM) concentrations a "dust index" is calculated on a routine base. A positive DI is reported when an influence of dust is identified for at least eight half hourly means during the day with a PM concentration above 5 μg/m^3. Mass concentrations of particulate matter are determined via a combination of nephelometry and β-attenuation (Sharp 5030, Thermo Scientific).

RESULTS

Several studies (e.g., Maupetit and Delmas, 1994; Greilinger et al., 2016) investigated the qualitative source assignments of high alpine snow packs using principal component analysis (PCA) and identified a factor related to Ca^{2+}, Mg^{2+} and the pH, being indicative for a marked contribution of Saharan dust. However, to get quantitative information on the contribution of Saharan dust to the respective ion composition or annual deposition loads the investigation of single snow layers is essential.

Identification of Saharan Dust Affected Snow in the Snowpack of the Winter Accumulation Period 2015/2016
Chemistry of the Snow Pack GOK2016

In the snowpack representing the winter accumulation period from September 2015 to April 2016 (=GOK2016), reddish colored snow layers where observed during sampling in about 120–160 cm depth (compare picture of the snow pack in **Figure 2**). Still, this depth has to be regarded as an approximate value and can be inaccurate by about 10–15 cm. This is because sampling is performed in an up to 2 m wide snow pit and the actual sampling of the 10 cm increments might be 0.5–1 m off the position where the depth, the snow morphology and also the color were determined. This "red snow," along the lines of "red rain" as used by Avila et al. (1998), is interpreted as an indicator of long-range transport of mineral dust, most likely originating from the Sahara. Although the color can vary from yellowish to brownish and up to now reddish, we stick to the term "red snow" throughout the paper.

To identify potential Saharan dust affected snow by chemical analysis, we build on a 2-step approach based on

Rogora et al. (2004). They investigated a 15- to 20-year long time series of rain water chemistry data of Northwest Italy and grouped rain events in acid and alkaline events with a pH of 5.6 as the threshold, representing the pH of pure water equilibrated with atmospheric CO_2. Although a pH of 5.6 still represents acid conditions, the samples denoted as "alkaline" feature comparable high pH. Within this work we will use the same notation as Rogora et al. (2004) and denote "alkaline increments" to 10 cm sample increments featuring pH > 5.6. After the identification of the alkaline events, Rogora et al. (2004) characterized Saharan dust episodes, as a subgroup of the alkaline events, via a high Ca^{2+} and alkalinity content, but no strict values are given for this classification.

Using the pH > 5.6 threshold we identified five alkaline increments of 10 cm (**Table 1**). This is one more (350–360 cm) than visually identified as "red snow." These alkaline increments can be further distinguished via their chemical composition. Either an elevated Ca^{2+} concentration often accompanied by increased concentration of the other ions, representing a Saharan dust influence, or an increased NH_4^+ concentration most likely associated to anthropogenic sources in agriculture (Greilinger et al., 2016) was noted. Both, Ca^{2+} and NH_4^+ act as important neutralizing agents for the anions SO_4^{2-} and NO_3^- (Das et al., 2005). The chemical composition of all 10 cm increments is given in **Table 1** and **Figure 2** (right).

Ca^{2+} and Mg^{2+} concentrations of the increments 130–140 cm, 140–150 cm, and 350–360 cm were all above the 87th percentile. The 160–170 cm increment showed elevated concentrations as well, but concentrations of NH_4^+ and NO_3^- were much more pronounced than Ca^{2+} and are the highest observed for the whole snow pack. The pH was actually just slightly above the threshold of 5.6. The 150–160 cm increment showed markedly elevated concentrations of NH_4^+, NO_3^- and SO_4^{2-}, and just slightly elevated Ca^{2+} concentrations. Based on these results we can separate the alkaline increments in one fraction dominated by increased Ca^{2+} concentrations (increments from 130 to 140 cm, 140 to 150 cm, and 350 to 360 cm) and one fraction dominated by increased NH_4^+ concentrations (150–160 cm). As the 160–170 cm increment is featuring both characteristics highest concentrations for NH_4^+ and NO_3^-, but also elevated concentrations of Ca^{2+}, it cannot be clearly assigned to one of the two categories.

Taking 10 μeq/l as threshold (higher than the 85th percentile, close to the arithmetic mean of 8.9 μeq/l and below the concentrations of the six samples showing the upper and detached range of the frequency distribution) four 10 cm increments (130–140 cm, 140–150 cm, 160–170 cm, and 350–360 cm) can be classified as affected by Saharan dust in the 2015/2016 snow pack. This fits nicely to the classification of the alkaline increments given above as it does not include the one from 150 to 160 cm, dominated by increased NH_4^+ concentration. Furthermore the increment at the bottom of the snow pack (350–360 cm) is identified, although it was not visible as 'red snow.' For completeness we want to point out that two increments show Ca^{2+} concentrations higher than 10 μeq/l but a pH less than 5.6. Thus the combination of the pH criterion and the Ca^{2+} threshold is mandatory.

TABLE 1 | Ion concentrations, pH, conductivity, and ion sum of every single 10 cm increments of the snow pack from the accumulation period September 2015 to April 2016.
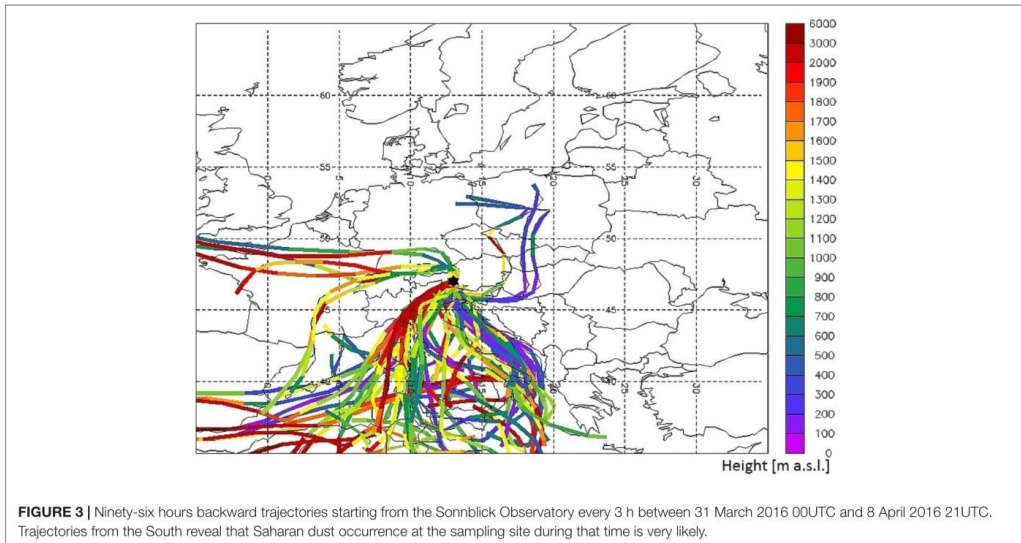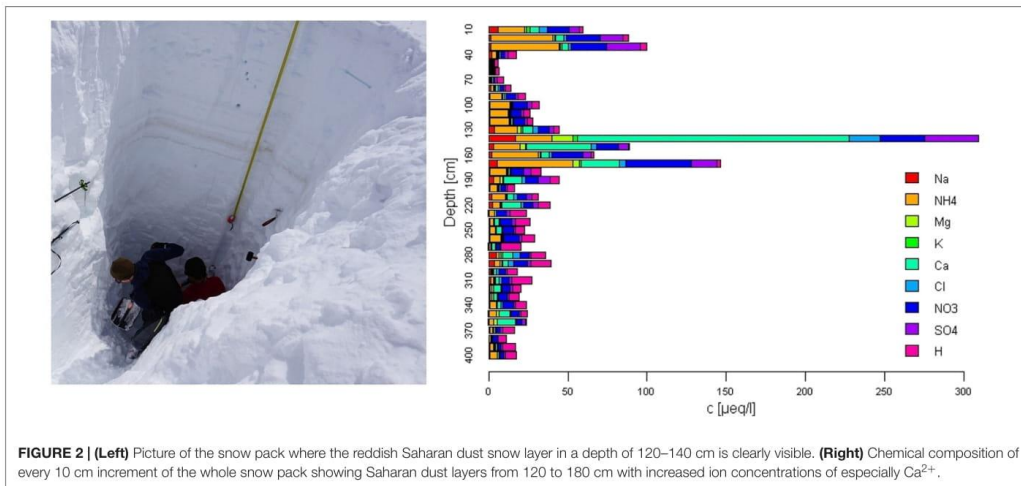
Snow depth (cm)	Ion concentration (μeq/l)									Σ ions (μeq/l)	pH	Conductivity (μS/cm)
	Na^+	NH_4^+	K^+	Mg^{2+}	Ca^{2+}	Cl^-	NO_3^-	SO_4^{2-}	H^+			
0–10	5.96	16.38	2.25	1.46	5.63	5.20	14.09	6.02	2.67	59.66	5.39	9.19
10–20	1.43	39.19	0.72	0.81	5.20	1.53	21.44	14.24	3.77	88.33	5.24	13.36
20–30	1.28	42.99	0.87	0.74	4.21	1.70	22.49	21.31	4.32	99.91	5.17	17.63
30–40	1.56	3.29	0.59	0.16	0.64	1.46	2.00	2.74	5.08	17.52	5.10	4.02
40–50	0.62	0.83	0.22	0.05	0.27	0.45	0.28	0.74	2.43	5.89	5.21	1.91
50–60	0.63	0.76	0.22	0.10	0.53	0.57	0.69	0.68	2.43	6.61	5.21	2.23
60–70	0.85	0.38	0.31	0.07	0.38	1.01	0.63	1.35	4.16	9.14	5.18	1.94
70–80	0.99	1.99	0.34	0.62	1.98	1.01	2.26	1.51	3.23	13.93	5.29	2.13
80–90	0.88	7.39	0.21	0.40	0.73	1.15	5.86	2.08	4.68	23.38	5.24	3.36
90–100	0.50	12.89	0.15	0.27	0.73	0.60	9.07	2.95	4.79	31.95	5.23	4.56
100–110	0.58	11.55	0.22	0.26	0.55	0.95	6.09	1.75	4.03	25.98	5.29	3.66
110–120	0.41	12.60	0.34	0.65	1.26	0.44	7.02	1.82	2.92	27.46	5.43	3.55
120–130	3.54	14.53	1.24	2.21	6.29	3.56	6.47	2.87	3.69	44.40	5.43	4.91
130–140	**16.89**	**22.94**	**2.92**	**13.40**	**171.51**	**19.64**	**28.23**	**33.70**	**0.07**	**309.30**	**7.17**	**28.80**
140–150	**2.77**	**17.11**	**0.56**	**3.44**	**40.87**	**3.32**	**14.01**	**6.43**	**0.32**	**88.83**	**6.49**	**8.38**
150–160	**1.82**	**29.59**	**0.38**	**1.15**	**5.17**	**1.91**	**19.40**	**5.00**	**1.86**	**66.28**	**5.73**	**6.27**
160–170	**5.20**	**47.98**	**1.10**	**3.90**	**24.42**	**3.72**	**41.33**	**16.67**	**2.05**	**146.37**	**5.74**	**13.02**
170–180	0.74	10.50	0.37	0.28	1.35	0.89	8.09	4.09	6.34	32.65	5.25	3.07
180–190	2.83	4.25	0.77	1.43	11.72	2.30	8.06	7.40	5.44	44.20	5.33	3.87
190–200	0.66	4.96	0.08	0.29	0.52	0.92	3.28	0.60	4.96	16.27	5.37	1.04
200–210	2.06	8.16	0.47	0.97	4.18	1.88	5.91	3.27	4.28	31.18	5.40	2.64
210–220	2.29	4.71	0.38	0.97	11.75	2.03	5.81	3.00	7.61	38.55	5.15	3.84
220–230	0.36	2.92	0.18	0.14	0.96	0.27	5.95	2.27	10.92	23.97	5.04	3.80
230–240	0.47	2.46	0.18	0.49	2.93	0.61	7.53	2.05	9.30	26.02	5.11	3.31
240–250	0.37	3.75	0.16	0.44	3.17	1.03	6.57	1.21	6.05	22.75	5.25	2.31
250–260	0.37	7.21	0.22	0.12	1.02	0.49	9.64	1.75	7.79	28.61	5.14	3.70
260–270	0.32	1.08	0.08	0.30	2.38	0.45	2.77	0.46	12.20	20.04	5.00	3.73
270–280	4.41	1.89	1.34	1.31	6.15	4.61	5.57	1.42	8.84	35.54	5.14	3.64
280–290	3.42	3.41	0.67	1.29	3.53	3.55	8.27	2.51	12.81	39.46	5.01	5.10
290–300	1.03	1.16	0.37	0.32	1.96	1.81	3.66	1.17	6.72	18.20	5.29	1.45
300–310	1.12	1.73	0.42	0.56	2.51	1.73	4.71	1.70	12.69	27.17	5.03	3.74
310–320	0.65	1.36	0.24	0.67	4.41	0.96	4.78	1.76	5.41	20.24	5.40	1.32
320–330	0.49	1.59	0.07	0.67	2.45	0.63	5.79	1.04	6.45	19.18	5.20	2.45
330–340	0.80	3.74	0.16	0.59	2.30	0.98	7.01	1.41	6.45	23.44	5.20	2.70
340–350	0.30	4.47	0.08	1.52	7.20	0.42	5.06	1.25	4.19	24.49	5.44	1.28
350–360	**0.35**	**2.75**	**0.08**	**1.90**	**11.57**	**0.49**	**3.89**	**2.09**	**0.70**	**23.82**	**6.22**	**1.12**
360–370	0.51	2.08	0.19	0.12	1.07	0.73	2.39	1.41	7.97	16.47	5.13	2.37
370–380	0.28	1.01	0.07	0.12	0.48	0.33	3.38	0.20	5.39	11.26	5.30	0.99
380–390	0.46	2.98	0.34	0.32	0.92	0.70	1.92	1.17	8.08	16.89	5.21	1.71
390–400	0.46	4.65	0.09	0.15	0.79	0.67	2.35	1.12	7.21	17.49	5.26	1.55
Min	0.28	0.38	0.07	0.05	0.27	0.27	0.28	0.20	0.07	5.89	5.00	0.99
1st quantile	0.47	1.97	0.18	0.27	0.89	0.61	3.36	1.24	3.58	18.03	5.17	2.08
2nd quantile	0.77	4.00	0.33	0.58	2.42	1.00	5.89	1.79	5.02	25.24	5.25	3.46
Mean	1.77	9.13	0.49	1.12	8.89	1.92	8.09	5.51	5.36	41.07	5.36	4.74
3rd quantile	1.88	11.81	0.57	1.19	5.31	1.89	8.14	3.07	7.31	38.78	5.39	4.16
Max	16.89	47.98	2.29	13.40	171.51	19.64	41.33	33.70	12.81	309.30	7.17	28.80

Bold values represent the alkaline increments using a pH > 5.6 for identification.

Comparison With Backward Trajectories and Aerosol Measurements

Based on the recording of precipitation events and snow height measurements the increments affected by Saharan dust can roughly be assigned to respective time periods. To confirm the influence of Saharan dust during these time periods backward trajectories and on-line aerosol measurements are used.

29

FIGURE 2 | (Left) Picture of the snow pack where the reddish Saharan dust snow layer in a depth of 120–140 cm is clearly visible. **(Right)** Chemical composition of every 10 cm increment of the whole snow pack showing Saharan dust layers from 120 to 180 cm with increased ion concentrations of especially Ca^{2+}.

FIGURE 3 | Ninety-six hours backward trajectories starting from the Sonnblick Observatory every 3 h between 31 March 2016 00UTC and 8 April 2016 21UTC. Trajectories from the South reveal that Saharan dust occurrence at the sampling site during that time is very likely.

The 10 cm increments from 130 to 150 cm and 160 to 170 cm represent precipitation events occurring in spring and can be assigned to a strong Saharan dust event in April, which is documented by backward trajectories for the period from 31 March 2016 00UTC until 8 April 2016 21UTC given in **Figure 3**. The frame of the image includes only the coastal area of Egypt and Tunisia and not the Sahara as such because the high resolution meteorological data of the ECMWF (horizontal resolution of 0.2°) is not available further south. Backward trajectories running southward out of the frame and descending from high altitudes are highly likely to come from the Sahara. On-line aerosol measurements at Sonnblick Observatory indicate that this event can be separated in two episodes. The first episode lasts from 31 March until 3 April 2016 and the second one, which was three times stronger regarding the mass concentration of particulate matter starting at 4 April 2016. Due to wind drift accumulation and precipitation, causing a slight increase in snow height in-between the episodes (measured by an automatic ultrasonic sensor next to the sampling site and shown in **Supplementary Figure 1**) it is plausible that they are separated in the snow

30

TABLE 2 | Years and depth where visible red snow was recorded in handwritten protocols and photographs during sampling and associated snow sample increments featuring a pH > 5.6 and a Ca^{2+} concentration of >10 µeq/l.

	Year	Depth recorded in protocols (cm)	Depth of snow sample increments (cm)	Ca^{2+} > 10 µeq/l
1	1987	80–84	75–85	+
2	1987	130	115–125	+
3	1987	370	365–375	+
4	1991	106–109	100–110	+
5	1992		210–220	+
6	1993	Snow surface	−	
7	1994	27–32	20–30 and 30–40	+
8	1995	290–292	280–290	+
9	1995	351–351.5*	−	−
10	1996	9–10	10–20	+
11	1996	130–140	130–140	+
12	1996	220–230	210–220	+
13	1997	368–370**	−	−
14	1997	377–381**	−	−
15	1997	520–527	500–540	+
16	2000	234–240	230–240	+
17	2003	240–241	240–250	+
18	2007	200	210–220	+
19	2012	150	150–160	+
20	2014	95–100	90–100	+
21	2014	184–189	180–190	+
22	2016	120–130	130–140	+
23	2016	130–140	140–150	+

*Indicates that there is a note in the metadata that Saharan dust was not continuously present. **Indicates that in 1997 the height of the sampling increments was 40 cm, leading to a loss of information due to dilution. The pH of these layers was 5.48, hence they slightly missed the pH-criterion.*

cover by one 10 cm increment. The 350–360 cm increment, showing an increased pH and a slight increase in the ion sum and Ca^{2+} concentration, represent snow samples from autumn (November and possibly also December 2015), which were concentrated in this depth due to an almost stable snow cover height during this time. Backward trajectories as well as on-line aerosol measurements indicate an influence of Saharan dust, though much lower than in spring 2016, during several days in November and December 2015 (**Supplementary Figures 2–4**) and thus justify the chemical identification of this increment.

Concluding, reasonable agreement of the identification of Saharan dust episodes between backward trajectories, aerosol measurements and the snow pack was obtained. This allows to extend the presented approach to the entire data set to retrospectively identify Saharan dust affected samples of snow packs back until 1987.

Retrospective Identification of Saharan Dust Layers

For 12 years (1987, 1991–1997, 2000, 2003, 2014, and 2016) hand written records reveal the presence of visible red snow in the respective snow pack. Besides, photographs of the snow packs are available since 2004, except for 2015. They show red snow for the years 2007, 2012, 2014, and 2016. Thus in total 23 layers within 14 years feature visually present red snow (listed in **Table 2**). Their position within the snow pack is reported in

the column named "depth recorded in protocols." The respective depth of affected increments identified via the pH and Ca^{2+} criterion is also reported in **Table 2** in the column "depth of snow sample increments." Thereby it is important to mention that the recorded snow depth need not correspond exactly to the sample increments of the same layer due to variations in the snow pit as described earlier. Additionally it is possible, that the Saharan dust layer (SDL) is split into two 10 cm sample increments or that it is much thinner than the sample increment, both leads to a dilution of the concentration in the affected layer.

Table 2 shows that 19 out of the 23 layers with red dust identified by visual inspection are identified using the pH > 5.6 and Ca^{2+} > 10 µeq/l thresholds. Reasons for this mismatch can be easily given. In 1995 it was recorded that the colored layer was not continuously present across the width of the snow pit. Hence it is not contradicting that Ca^{2+} concentrations were not markedly elevated. In 1997 sample increments were 40 cm instead of 10 cm, leading to a dilution and thus to a poorer sensitivity of the analytical approach. The respective increment showed a pH value of 5.48 which is only slightly lower than the used threshold of 5.6. In 1993 Saharan dust was visible on the snow surface but the respective increment only matched the Ca^{2+} criterion but, with a pH of 4.78, not the pH criterion. Maybe other influences on the surface (e.g., snow surface–air interactions) do play a role for the pH. Excluding those layers from the evaluation all recorded red dust layers could be verified by the chemical analysis.

The total data set covers 28 years of snow pack data (1987–2017, except 1988, 1989, and 1990 due to missing values for bivalent cations) and comprises 1,163 chemically analyzed 10 cm increments. Increments which were identified to feature Saharan dust input are here named as "SDLs," although they do not necessarily represent different stratigraphic layers or single events. Based on the chemical information we find 394 alkaline layers (equal to 34% of the whole data set) using the pH criterion only. For comparison, the mean pH of all samples is 5.44 with 75th percentile and 90th percentile values of 5.70 and 6.15, respectively. Including the Ca^{2+} criterion this number of layers decreases to 104 (equal to 9% of the whole data set or 26% of the alkaline layers) with pH values ranging from 5.58 to 7.17. As it was the case for the GOK2016 snow pack there are more sample increments chemically identified as SDLs than samples showing a visible appearance of red snow. More precisely we find five times more based on chemistry compared to the visual identification.

Some validation can be given for the accumulation periods 2014/2015 and 2016/2017, as back trajectories and on-line aerosol data are available for these years as well. In both years, no red snow was visible, but in case of the 2016/2017 period (GOK2017) one SDL was chemically identified in the lower part of the snow pack. Backward trajectories indicate the influence of Saharan dust in October 2016 and also two much weaker episodes in spring 2017 (compare **Supplementary Figures 5** and **6**). Complementary on-line aerosol measurements yielded a positive dust index during the respective time periods. Thus the SDL identified in the bottom part of the snow pack much likely represents the event in October 2016. The spring events in February and March 2017 are, using the present methods, not identified in the snow pack. Still sample increments which can be assigned to the relevant time period meet the pH criterion and show a Ca^{2+} concentration of 9.72 μeq/l, i.e., only slightly below the threshold of 10 μeq/l. Within the snow pack of the 2014/2015 accumulation period (GOK2015) no SDLs were chemically identified. Again backward trajectories and on-line aerosol data shows some influence during early winter at the end of November and beginning of December 2014 (**Supplementary Figure 7**), which is not reflected in the lowest part of the snow pack. This seems surprising, but snow height measurements revealed the absence of wet deposition during these events. During spring time the situation was similar to the conditions described for the GOK2017 and the GOK2016 snow pack. A Saharan dust influence occurred in March 2015 (backward trajectories given in **Supplementary Figure 8**) and the respective sample increments again meet the pH criterion, but were slightly below the 10 μeq/l Ca^{2+} threshold (Ca^{2+} concentration of 9.48 μeq/l). This intercomparison suggests that it is most likely that no overestimation of SDLs occurs when the criteria defined within this paper are used. Weak events might even be missed. Furthermore the influence of Saharan dust, and not just a general influence of mineral dust, is likely for all identified events.

In literature markedly higher Ca^{2+} values can be found to identify Saharan dust affected samples. Maupetit and Delmas (1994) report a value of 23.8 μeq/l for alkaline snow samples collected in the French Alps. A Ca^{2+} threshold of 20 μeq/l was also used by Schwikowski et al. (1999) to classify ice

TABLE 3 | Overview and seasonality of the number of Saharan dust layers (SDLs) using different Ca^{2+} thresholds of 28 years of snow pack data (1987–2017, missing data in 1988, 1989, and 1990).

	Ca^{2+} > 10 μeq/l	Ca^{2+} > 20 μeq/l
Total years investigated	28	28
Total amount of analyzed increments	1,163	1,163
Total amount of alkaline layers (pH > 5.6)	394	394
Years with minimum one SDL	26	16
Years without SDLs	2	12
Years with more than one SDL	19	8
SDLs via pH > 5.5 and Ca^{2+} threshold	104	45
SDLs in fall (September to November)	32	17
SDLs in winter (December to February)	48	19
SDLs in spring (March to April)	24	9

core data from an Alpine ice core (Colle Gnifetti). Of course these concentrations are strongly driven by the respective accumulation rates and thus can vary from site to site. Still we want to elucidate how sensitive the classification is to respective thresholds. If we would use a threshold of 20 μeq/l, the recovery in the chemical analysis of the visually identified reddish SDLs would decrease. Consequently the number of identified SDLs of the whole data set including all increments (not only the visually noticeable ones) decreases as shown in **Table 3**. Despite this decreasing trend the snow pack still experiences an impact of Saharan dust during more than half of the years when the 20 μeq/l criterion is used. Regarding only years with more than one identified layer (reflecting a repeated or longer lasting Saharan dust influence) more than two-thirds of the years are affected when the 10 μeq/l Ca^{2+} threshold is used. This number decreases to about one-third for the higher threshold. Obviously the level of the threshold influences the number of detected SDLs as well as years affected, but, as will be shown later, the respective deposition loads are affected much less.

If the snowpack is subdivided into the different seasons of fall (September to November), winter (December to February) and spring (March and April) according to Greilinger et al. (2016), it seems as if the most Saharan dust events occur during winter (**Table 3**). This result seems surprising, since a clear fall and spring maximum can be found for Saharan dust in the atmosphere (Coen et al., 2003). Possible explanations are that potential events occurring in September might have been melted away or that they occurred without snowfall, remained airborne and were thus not deposited in or on the snow pack. Besides, during September rain is still very likely at the sampling site which might wash away already deposited Saharan dust on the snow or glacier surface or enables a deposition with rain due to rain water run-off. Events occurring in May, still accounting to the spring maximum given in Coen et al. (2003), were not captured in the snow pack analysis due to sampling end of April, latest beginning of May. Also the snow water equivalent is on average much higher for the winter period (mean over the period 1987–2017 of 663 mm) compared to fall or spring (mean over the period 1987–2017 of 491 mm and 447 mm, respectively). Thus, a Saharan dust deposition during snowfall is more likely

TABLE 4 | Mean relative ion composition of the mean overall annual depositions (MOAD) including all layers, as well as for SDLs and non-SDLs separately using the 10 µeq/l Ca^{2+} threshold.

	Cl^-	NO_3^-	SO_4^{2-}	Na^+	NH_4^+	K^+	Mg^{2+}	Ca^{2+}	H^+
All	8.5%	18.1%	13.9%	9.6%	16.5%	2.6%	2.7%	15.6%	12.9%
SDLs	7.2%	13.3%	11.0%	7.6%	12.7%	2.4%	4.1%	39.6%	2.1%
Non-SDLs	9.1%	18.7%	14.3%	10.3%	16.5%	2.8%	1.9%	11.9%	14.4%

TABLE 5 | Mean overall annual depositions (MOAD) in meq/m² and snow water equivalent (SWE) in mm of all years (1987–2017) and all layers, SDLs and non-SDLs as well as the absolute and relative contribution of the respective ions.

		MOAD (meq/m²)	SWE (mm)	Cl^-	NO_3^-	SO_4^{2-}	Na^+	NH_4^+	K^+	Mg^{2+}	Ca^{2+}	H^+
Ca > 10 µeq/l	All	70.2	1579	6.0	12.7	9.8	6.7	11.6	1.8	1.6	10.9	9.0
	SDLs	10.0	172	0.7	1.3	1.1	0.8	1.3	0.2	0.4	3.9	0.2
		(14%)	(11%)	(11%)	(10%)	(11%)	(11%)	(12%)	(11%)	(25%)	(35%)	(2%)
	Non-SDLs	60.5	1420	5.5	11.3	8.6	6.2	10.0	1.7	1.2	7.2	8.7
		(86%)	(89%)	(89%)	(90%)	(89%)	(89%)	(88%)	(89%)	(75%)	(65%)	(98%)
Ca > 20 µeq/l	SDLs	8.7	125	0.5	1.0	0.9	0.5	0.9	0.1	0.3	4.4	0.1
		(11%)	(8%)	(7%)	(7%)	(8%)	(7%)	(8%)	(5%)	(16%)	(32%)	(1%)
	Non-SDLs	70.9	1508	6.3	13.0	10.9	6.8	11.0	1.8	1.6	9.3	10.3
		(89%)	(92%)	(93%)	(93%)	(92%)	(93%)	(92%)	(95%)	(84%)	(68%)	(99%)

in winter than in fall or spring. The increased number of SDLs in winter is also biased by single years (e.g., 1996 and 2014) where a huge number of layers were identified, all occurring in the winter period.

Influence of Saharan Dust Layers on the Relative Ion Composition

The mean relative ion composition was calculated for all layers together as well as for SDLs and non-SDLs separately. Results are presented in **Table 4**. Note that non-SDLs account for 89% of the snow water equivalent (**Table 5**) and hence also for the majority of the analyzed snow layers and the water deposited.

The relative ion composition of non-SDLs is almost identic to the ion composition if all layers are considered. The ratio between the relative contributions of most of the single ions within non-SDLs to those of the entire snow pack is slightly above 1 aside from Mg^{2+} and Ca^{2+} showing ratios of 0.7 and 0.8, respectively.

For SDLs, the relative ion composition is different to the ion composition of the entire snow pack. Mg^{2+} is slightly increased with a ratio between the relative contributions of SDLs to those of all layers of 1.4, whereas Ca^{2+} is much more increased with a ratio of 2.5. H^+ is markedly lower in SDLs with a ratio of only 0.1 between the relative contributions of non-SDLs to those of all layers. Contributions of all other ions are slightly decreased in SDLs, compared to the contributions if all layers are considered, with ratios between 0.7 and 0.9.
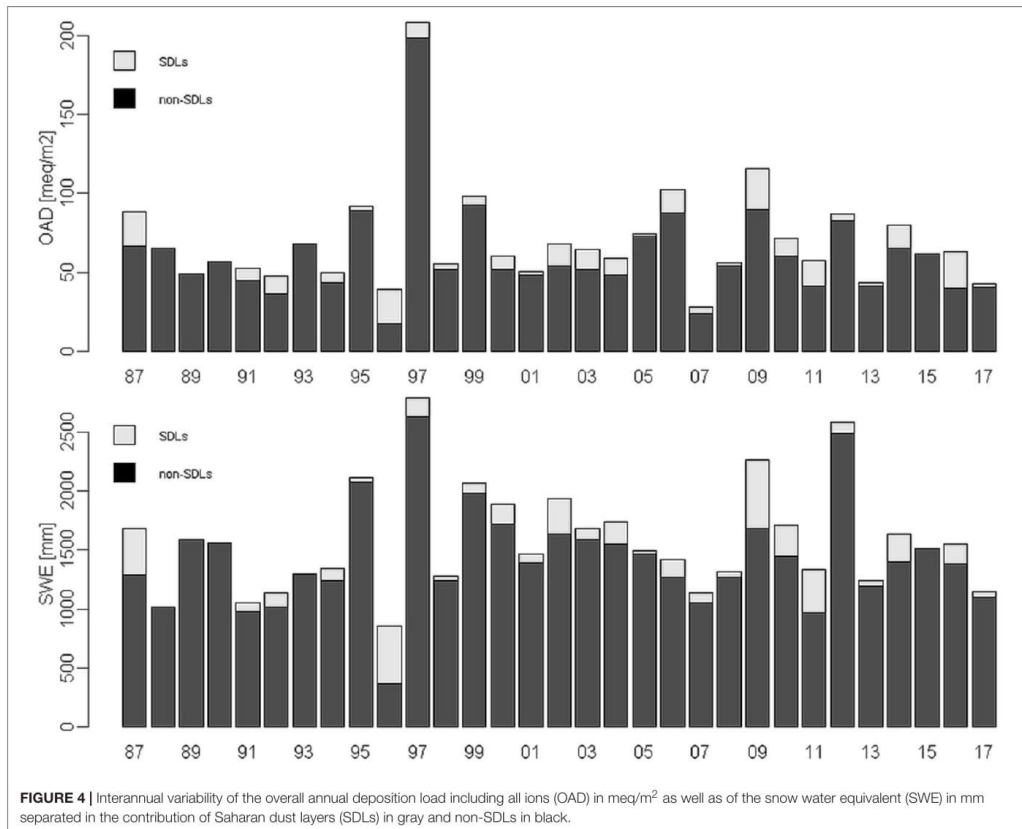
Influence of Saharan Dust Layers on Mean Annual Ion Deposition Loads

Table 5 lists the mean overall annual deposition (MOAD, sum of all ions analyzed) as well as the mean annual deposition loads of the respective ions and the snow water equivalent of the complete data set (1987–2017), calculated via averaging the respective annual values. The same was performed for the contribution of the SDLs and the non-SDLs, calculated as sum over all SDL or non-SDL layers of the respective years and averaging these annual values. In addition to the absolute values the relative contributions of SDLs and non-SDLs to the overall "MOAD," to the snow water equivalent and to the deposition loads of the single ions are listed as percentage values given in parenthesis. Note that the sums of SDL and non-SDL deposition loads need not match the overall annual loads. This is due to the fact that years without any SDL were not considered when splitting annual averages into SDL and non-SDL contributions. This approach was taken to base the averages of SDL and non-SDL contributions on the same data set, i.e., the same years. This accounts for the year to year variability, which has to be expected and which is discussed later.

For most of the single ions the contribution of SDLs and non-SDLs to the mean annual deposition load is similar to the respective contribution of the snow water equivalent, ranging between 10–12% and 88–90%, respectively. This indicates, that the concentrations of these ions is almost similar between SDLs and non-SDLs. Only Mg^{2+} and Ca^{2+} show much higher contributions of SDLs (25% and 35%, respectively), whereas H^+ shows a much lower contribution of only 2% compared to the snow water equivalent.

Interestingly, the contributions of the deposition loads of single ions but also of MOAD to the entire data set do not vary a lot when the Ca^{2+} threshold is increased from 10 to 20 µeq/l (**Table 5**). At first this seems surprising as the number of identified increments did go down by a factor of three when the threshold was increased. Still the deposition load is very much driven by the maximum concentrations which usually largely exceed 20 µeq/l. Thus annual deposition loads are not very much affected by the different thresholds.

FIGURE 4 | Interannual variability of the overall annual deposition load including all ions (OAD) in meq/m^2 as well as of the snow water equivalent (SWE) in mm separated in the contribution of Saharan dust layers (SDLs) in gray and non-SDLs in black.
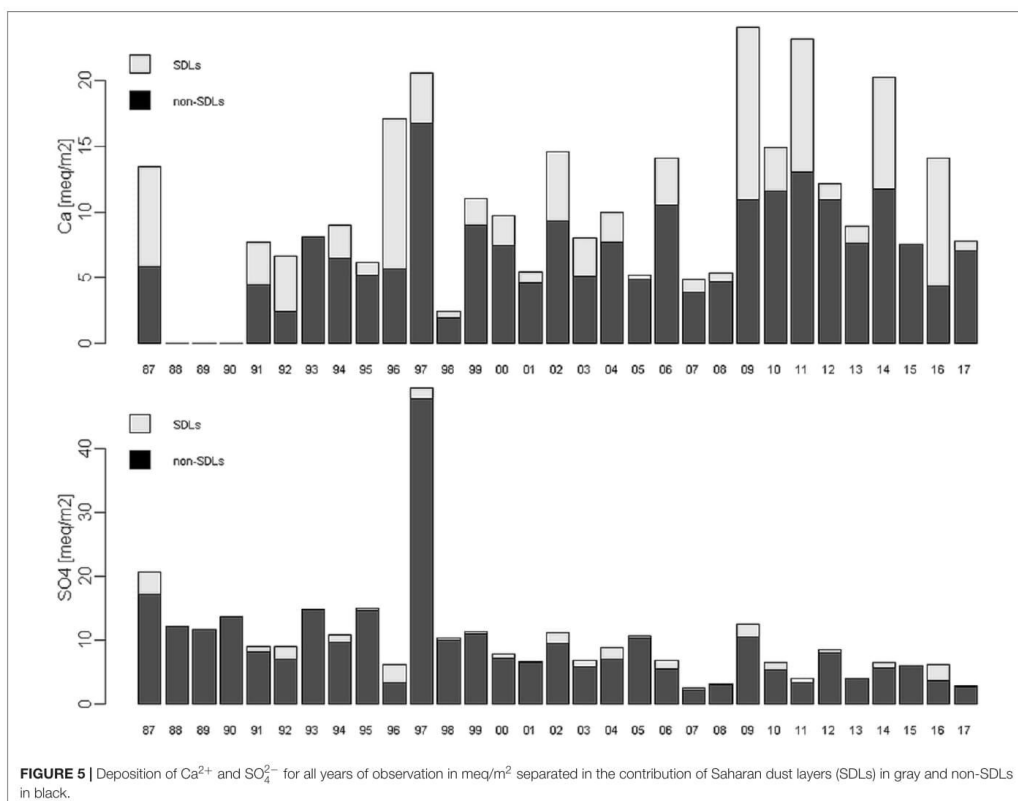
Interannual Variabilities of the Influence of Saharan Dust Layers on Ion Deposition

The interannual variability of the overall annual deposition load including all ions (OAD) as well as of the snow water equivalent is displayed in **Figure 4**.

The interannual variability of the OAD results for 9 of the 26 years with SD influence in a 13–19% contribution of SDLs whereas 2 years (1996 and 2016) show much higher contribution up to 55% and 36%, respectively (compare **Figure 4**). Likewise, also the annual depositions of the single ions show a high interannual variability with different trends. A detailed investigation of these annual trends, not quantifying the influence of deposited dust, can be found in Greilinger et al. (2016). Here results are exemplarily shown for Ca^{2+} and SO_4^{2-} in **Figure 5**. SO_4^{2-} depositions show a declining trend caused by decreasing emissions of sulfur dioxide (Greilinger et al., 2016). This trend is not altered if the deposition loads related to the deposition of SD would be deducted. Regarding the

deposition of Ca^{2+} no significant time trend can be observed using the Mann-Kendall Test with a two-sided p-value below 5% for level of significance when the overall depositions are considered (Kendall's tau = 0.246 and 2-sided-p = 0.06). Also the contribution of SDLs to the annual Ca^{2+} deposition does not show any statistical trend (Kendall's tau = −0.119 and 2-sided-p = 0.38).

A boxplot shown in **Figure 6**, displaying the contribution of SDLs to the annual deposition of the single ions, reflects the interannual variability. The first box represents the interannual variability of the contribution of the SDLs to the annual snow water equivalent, showing a less than 10% for most of the years whereas outliers outside the upper whisker in the boxplot show 3 years where contributions were higher (1996, 2009, and 2011). In 1996 it was highest with 53%. Two years (1996 and 2006) were observed where all ions show a more than 25% contribution, for 1996 even more than 45%. For Ca^{2+} and Mg^{2+} more years were found with contributions of SDLs to the annual ion deposition load higher than 25%. For Ca^{2+} 16 years (1987, 1991, 1992,

34

Greilinger et al.

Saharan Dust Deposition in Snow

FIGURE 5 | Deposition of Ca^{2+} and SO_4^{2-} for all years of observation in meq/m^2 separated in the contribution of Saharan dust layers (SDLs) in gray and non-SDLs in black.

1994, 1996, 1998, 2000, 2002, 2003, 2004, 2006, 2007 2009, 2011, 2014, and 2016) where identified and five of these years (1987, 1992, 1996, 2009, and 2016) show contributions of more than 45%, in 1992, 1996, and 2016 even more than 60%. For Mg^{2+} 10 years (1987, 1991, 1996, 2001, 2002, 2003, 2007, 2011, 2014, and 2016) showed contributions above 25%, in 1987 and 2016 even more than 50%. Contributions for H^+ are always very low with maximum values of 5%. Contributions of single years (1996, 2004, 2009, and 2010) marked as outliers in **Figure 6** were higher with contributions of 33%, 18%, 14%, and 8%, respectively.

From these results we find 2 years, 1996 and 2016, which show remarkable high contributions of SDLs to the OAD as well as to the annual ion deposition. For both years red colored snow layers were already visually observed during sampling of the snow pack (**Table 2**) but the contribution of the SDLs to the annual snow water equivalent differ strongly with a contribution of 57% in 1996 but only 11% in 2016. This reveals, that in 1996 the contributions of SDLs to the annual ion deposition is high due to a high number of SDLs (12 layers) whereby the deposition load of these SDLs was not very high (Ca^{2+} concentrations between 15.0 and 42.7 μeq/l). In contrast to this, the high contributions

of SDLs to the annual ion deposition in 2016 is associated to only three SDLs with very high Saharan dust input (Ca^{2+} concentrations of 24.4 μeq/l, 40.9 μeq/l, and 171.5 μeq/l).

The boxplot also underlines the main findings discussed before that the contribution of SDLs to the annual deposition loads is markedly different to the contribution of the snow water equivalent for Mg^{2+}, Ca^{2+}, and H^+ because these ions are most affected by Saharan dust. Regarding Cl^-, Na^+, and K^+, ions which are related to Saharan dust too but most likely have additional sources as well, the distributions are shifted to elevated contributions, but the differences to snow water equivalent are much less pronounced. The smallest influence can be seen for NO_3^-, SO_4^{2-}, and NH_4^+, but still 75th percentiles and whiskers reach up to markedly higher contributions of SDLs than can be expected due to the snow water equivalent of those layers.

DISCUSSION

In the following our results about the contribution of SDLs to the mean annual deposition loads are compared to those

FIGURE 6 | Boxplot of the annual contributions of Saharan dust layers (SDLs) to the snow water equivalent (SWE) and the annual depositions of the single ions. The box represents the 25th and 75th percentile, the bold black line shows the median and whiskers extend to the most extreme data point which is no more than 1.5 times the interquartile range of the box. Dashed lines mark 25% and 45% contributions of SDLs.

of (Avila and Rodà, 1991), analyzing the dissolved nutrient amounts during red rains in Montseny Mountains, Spain from 1983 to 1988. They found that red rains are responsible for 46% Ca^{2+} input, between 20 and 25% for Na^+, K^+, Cl^-, and Mg^{2+} input and between 7 and 16% for SO_4^{2-}, NO_3^-, and NH_4^+ input featuring high interannual variability with coefficients of variations between 26 and 68% for the single ions. Still red rains contribute only 5% of the total annual precipitation for the study period, pointing to a higher relative influence of single events of red rains in Spain than in the present study. Rogora et al. (2004) report results on the impact of Saharan dust deposition on the long-term trends of atmospheric deposition in Italy from 1984 to 2002. They found that contribution of Saharan dust events to the annual precipitation amount was in average 10% whereas the mean contribution of the respective ions during these events where 43% Ca^{2+}, 20–24% of Mg^{2+}, Na^+, and Cl^- and 11–16% of NO_3^-, SO_4^{2-}, NH_4^+, and K^+, what is more similar to our results. Maupetit and Delmas (1994), investigating the snow chemistry of glaciers in the French Alps from 1989 to 1991, found alkaline samples to contribute 19% on average over all years, representing between 22 and 52% of the ionic load, with the highest amount for Ca^{2+}. Values of Maupetit and Delmas (1994) are highest, most likely due to the fact that they did not distinguish between alkaline samples originating from Saharan dust or from increased NH_4^+ concentrations, both acting as buffering agents. If no Ca^{2+} criterion would have been used in the present study the number of affected increments would have been more than threefold.

Regarding the nutrient input via Saharan dust the importance of Ca^{2+}, Mg^{2+}, and K^+ is mentioned in literature (e.g., Avila et al., 1998). Our data set shows that the input of Ca^{2+} and Mg^{2+} definitely is driven by long-range transport of mineral dust, while no marked effect becomes visible for K^+. In this case other sources, e.g., the more regional influence of combustion processes, are more important. The same is the case for Na^+, another ion, whose input could have been driven by mineral dust (e.g., Swap et al., 1992; Rizzolo et al., 2017).

Additionally to the influence of Saharan dust on ion deposition loads we suggest that Saharan dust in snow may

36

Greilinger et al.   Saharan Dust Deposition in Snow

not only directly influence microbiology by acting as fertilizer and additional nutrient input to increase biomass but rather influences the metabolism, respiration, and productivity of microbes (Pulido-Villena et al., 2008; Reche et al., 2009; Schulz et al., 2012). In this respect, the changed acidity could be an important parameter as well. We found the pH to be distinctly different in SDLs compared to unaffected snow layers, providing distinctly different habitat conditions for microorganisms surviving within high alpine snow packs. Also the community diversity in high alpine snow is changed due to Saharan dust input (Zhang et al., 2008; Chuvochina et al., 2011). Due to the fact that Saharan dust introduces a variety of bacteria and microbial species to areas far away from their origin, it can be assumed that, especially in remote alpine snow, the accomplished input of Saharan dust simulate the natural habitat of those microbes so they can survive in very harsh and contrary conditions to their original habitat.

SUMMARY AND CONCLUSION

We investigated the intensity and frequency of Saharan dust deposited in high alpine snow retrospectively for a unique long-term data set of high alpine snow chemistry.

Based on a chemical criterion (pH > 5.6 and Ca^{2+} concentration > 10 µeq/l) we provide a robust method to identify SDLs within high alpine snow. Results for the use of a higher Ca^{2+} threshold (20 µeq/l) show, that it hardly affect the annual deposition loads whereas the number of identified layers goes down.

While contributions of SDLs and unaffected layers (10–12% and 88–89%, respectively) to the deposition load of Cl^-, NO_3^-, SO_4^{2-}, Na^+, NH_4^+, and K^+ is similar to the contribution of the snow water equivalent (11% and 86%, respectively), markedly elevated contributions of SDLs were observed for Mg^{2+} (25%) and Ca^{2+} (35%), while the impact of H^+ becomes negligible (2%). Also the relative ion composition in SDLs underlines the influence on Mg^{2+}, Ca^{2+}, and H^+.

Generally SO_4^{2-} depositions show a declining trend caused by decreasing emissions of sulfur dioxide but this trend is not altered if the deposition loads related to the deposition of Saharan dust would be deducted. Regarding the deposition of Ca^{2+} no significant time trend was observed at all.

Using the suggested Ca^{2+} threshold of 10 µeq/l, only 2 out of 28 investigated years without Saharan dust influence were observed. Two thirds of the affected years showed even more than

one SDL. This is the case, although a 3-year comparison of the identified SDLs using backward trajectories and on-line aerosol measurements showed that we might miss weak events.

An estimation of the contribution of Saharan dust events to the chemical variability of the ecosystems is not easy due to lack of quantitative studies in remote areas but cannot be neglected. Our results provide relevant input not only on ion deposition loads. They can be used for further investigations and conclusions on the influence of Saharan dust on the albedo of snow and glacier surfaces, on the biogeochemistry of high alpine snow as well as on the microbiology of remote areas.

AUTHOR CONTRIBUTIONS

MG and AK-G conceived the study. MG processed the data and wrote the manuscript together with AK-G. GS performed and evaluated the aerosol sampling at the site and calculated the DI. KB-S and PS performed the backward trajectory analysis. WS was part of the team initiating the snow chemistry monitoring and ensuring ongoing sampling for most of the years. All co-authors commented on the results and on the manuscript content.

ACKNOWLEDGMENTS

SUPPLEMENTARY MATERIAL

The Supplementary Material for this article can be found online at: https://www.frontiersin.org/articles/10.3389/feart.2018.00126/full#supplementary-material

REFERENCES

Avila, A., Alarcón, M., and Queralt, I. (1998). The chemical composition of dust transported in red rains-its contribution to the biogeochemicl cycle of a holm oak forest in Catalonia (Spain). *Atmos. Environ.* 32, 179–191. doi: 10.1016/S1352-2310(97)00286-0

Avila, A., and Rodà, F. (1991). Red rains as major contributors of nutrients and alkalinity to terrestrial ecosystems at Montseny (NE Spain). *Orsis* 6, 215–229.

Chuvochina, M. S., Marie, D., Chevaillier, S., Petit, J.-R., Normand, P., Alekhina, I. A., et al. (2011). community variability of bacteria in alpine snow (mont blanc) containing saharan dust deposition and their snow colonisation potential. *Microbes Environ.* 26, 237–247. doi: 10.1264/jsme2.ME11116

Coen, M. C., Weingartner, E., Schaub, D., Hueglin, C., Corrigan, C., Schwikowski, M., et al. (2003). Saharan dust events at the Jungfraujoch: detection by wavelength dependence of the single scattering albedo and analysis of the events during the years 2001 and 2002. *Atmos. Chem. Phys. Discuss.* 3, 5547–5594. doi: 10.5194/acpd-3-5547-2003

Das, R., Das, S. N., and Misra, V. N. (2005). Chemical composition of rainwater and dustfall at Bhubaneswar in the east coast of India. *Atmos. Environ.* 39, 5908–5916. doi: 10.1016/j.atmosenv.2005.06.030

De Angelis, M., and Gaudichet, A. (1991). Saharan dust deposition over mont blanc (French Alps) during the last 30 years. *Tellus B* 43, 61–75. doi: 10.3402/tellusb.v43i1.15246

Field, J. P., Belnap, J., Breshears, D. D., Neff, J. C., Okin, G. S., Whicker, J. J., et al. (2010). The ecology of dust. *Front. Ecol. Environ.* 8, 423–430. doi: 10.1890/090050

Gabbi, J., Huss, M., Bauder, A., Cao, F., and Schwikowski, M. (2015). The impact of Saharan dust and black carbon on albedo and long-term mass balance of an Alpine glacier. *Cryosphere* 9, 1385–1400. doi: 10.5194/tc-9-1385-2015

Goudie, A. S., and Middleton, N. J. (2001). Saharan dust storms: nature and consequences. *Earth Sci. Rev.* 56, 179–204. doi: 10.1016/S0012-8252(01)00067-8

Greilinger, M., Schöner, W., Winiwarter, W., and Kasper-Giebl, A. (2016). Temporal changes of inorganic ion deposition in the seasonal snow cover for the Austrian Alps (1983–2014). *Atmos. Environ.* 132, 141–152. doi: 10.1016/j.atmosenv.2016.02.040

Grell, G. A., Peckham, S. E., Schmitz, R., McKeen, S. A., Frost, G., Skamarock, W. C., et al. (2005). Fully coupled "online" chemistry within the WRF model. *Atmos. Environ.* 39, 6957–6975. doi: 10.1016/j.atmosenv.2005.04.027

Gruber, N., and Sarmiento, J. L. (1997). Global patterns of marine nitrogen fixation and denitrification. *Glob. Biogeochem. Cycles* 11, 235–266. doi: 10.1029/97GB00077

Kuhn, M. (2001). The nutrient cycle through snow and ice, a review. *Aquat. Sci. Res. Boundaries* 63, 150–167. doi: 10.1007/PL00001348

Marchetto, A., Mosello, R., Psenner, R., Bendetta, G., Boggero, A., Tait, T., et al. (1995). Factors affecting water chemistry of alpine lakes. *Aquat. Sci.* 57, 81–89. doi: 10.1007/BF00878028

Maupetit, F., and Delmas, R. J. (1994). Snow chemistry of high altitude glaciers in the French Alps. *Tellus B Chem. Phys. Meteorol.* 46, 304–324. doi: 10.3402/tellusb.v46i4.15806

Moulin, C., Lambert, C. E., Dulac, F., and Dayan, U. (1997). Control of atmospheric export of dust from North Africa by the North Atlantic Oscillation. *Nature* 387, 691–694. doi: 10.1038/42679

Prospero, J. M. (1996). "Saharan dust transport over the North Atlantic Ocean and Mediterranean: an overview," in *Impact Desert Dust Mediterr,* eds S. Guerzoni and R. Chester (Alphen aan den Rijn: Kluwer Academic Publishers), 133–151. doi: 10.1007/978-94-017-3354-0_13

Psenner, R. (1999). Living in a dusty world: airborne dust as a key factor for alpine lakes. *Water Air Soil Pollut.* 112, 217–227. doi: 10.1023/A:1005082832499

Pulido-Villena, E., Wagener, T., and Guieu, C. (2008). Bacterial response to dust pulses in the western Mediterranean: implications for carbon cycling in the oligotrophic ocean: bacterial response to dust pulses. *Glob. Biogeochem. Cycles* 22:GB1020. doi: 10.1029/2007GB003091

Reche, I., Ortega-Retuerta, E., Romera, O., Villena, E. P., Baquero, R. M., and Casamayor, E. O. (2009). Effect of Saharan dust inputs on bacterial activity and community composition in Mediterranean lakes and reservoirs. *Limnol. Oceanogr.* 54, 869–879. doi: 10.4319/lo.2009.54.3.0869

Rizzolo, J. A., Barbosa, C. G. G., Borillo, G. C., Godoi, A. F. L., Souza, R. A. F., Andreoli, R. V., et al. (2017). Soluble iron nutrients in Saharan dust over the central Amazon rainforest. *Atmos. Chem. Phys.* 17, 2673–2687. doi: 10.5194/acp-17-2673-2017

Rogora, M., Mosello, R., and Marchetto, A. (2004). Long-term trends in the chemistry of atmospheric deposition in Northwestern Italy: the role of increasing Saharan dust deposition. *Tellus B Chem. Phys. Meteorol.* 56, 426–434. doi: 10.3402/tellusb.v56i5.16456

Schauer, G., Kasper-Giebl, A., and Močnik, G. (2016). Increased PM concentrations during a combined wildfire and Saharan dust event observed at high-altitude sonnblick observatory, Austria. *Aerosol Air Qual. Res.* 16, 542–554. doi: 10.4209/aaqr.2015.05.0337

Schulz, M., Prospero, J. M., Baker, A. R., Dentener, F., Ickes, L., Liss, P. S., et al. (2012). Atmospheric transport and deposition of mineral dust to the ocean: implications for research needs. *Environ. Sci. Technol.* 46, 10390–10404. doi: 10.1021/es300073u

Schwikowski, M., Döscher, A., Gäggeler, H. W., and Schotterer, U. (1999). Anthropogenic versus natural sources of atmospheric sulphate from an alpine ice core. *Tellus B Chem. Phys. Meteorol.* 51, 938–951. doi: 10.3402/tellusb.v51i5.16506

Stohl, A., Haimberger, L., Scheele, M. P., and Wernli, H. (2001). An intercomparison of results from three trajectory models. *Meteorol. Appl.* 8, 127–135. doi: 10.1017/S1350482701002018

Swap, R., Garstang, M., Greco, S., Talbot, R., and Kållberg, P. (1992). Saharan dust in the Amazon Basin. *Tellus B* 44, 133–149. doi: 10.1034/j.1600-0889.1992.t01-1-00005.x

Weil, T., De Filippo, C., Albanese, D., Donati, C., Pindo, M., Pavarini, L., et al. (2017). Legal immigrants: invasion of alien microbial communities during winter occurring desert dust storms. *Microbiome* 5:32. doi: 10.1186/s40168-017-0249-7

Winiwarter, W., Puxbaum, H., Schöner, W., Böhm, R., Werner, R., Vitovec, W., et al. (1998). Concentration of ionic compounds in the wintertime deposition: results and trends from the Austrian Alps over 11 years (1983–1993). *Atmos. Environ.* 32, 4031–4040. doi: 10.1016/S1352-2310(97)00252-5

Zhang, S., Hou, S., Wu, Y., and Qin, D. (2008). Bacteria in Himalayan glacial ice and its relationship to dust. *Biogeosci.* 5, 1741–1750. doi: 10.5194/bg-5-1741-2008

38

Supplementary material

This chapter corresponds to the supplementary material of the peer-reviewed publication

Greilinger, M., Baumann-Stanzer, K., Skomorowski, P., Schauer, G., Schöner, W., & Kasper-Giebl, A. (2018). Contribution of Saharan dust to ion deposition loads of high alpine snow packs in Austria (1987-2017). Frontiers in Earth Science, 6, 126. doi: 10.3389/feart.2018.00126
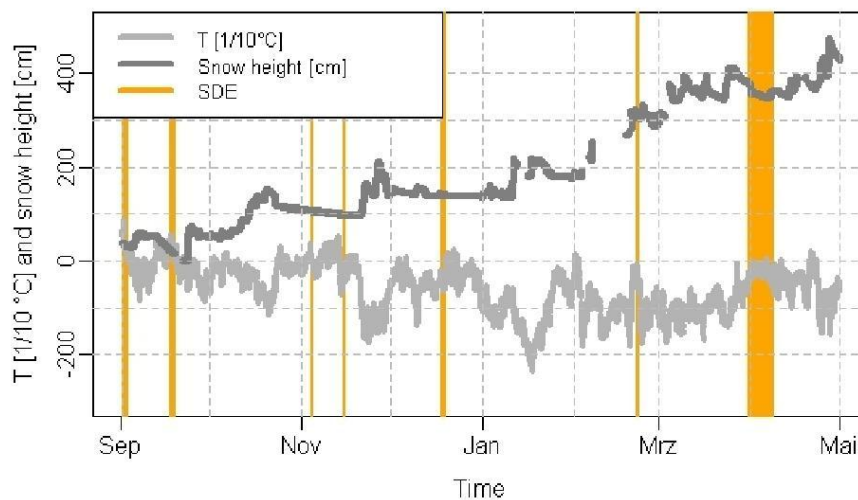
Supplementary Material

Contribution of Saharan dust to ion deposition loads of high alpine snow packs in Austria (1987-2017)

Marion Greilinger[1,2,*], Gerhard Schauer[1], Kathrin Baumann-Stanzer[1], Paul Skomorovski[1], Wolfgang Schöner[3], Anne Kasper-Giebl[2]

* Correspondence:
Marion Greilinger
Marion.greilinger@zamg.ac.at

Supplementary Figure 1: Time series of T in [1/10°C] (lightgrey) and snow height in [cm] (darkgrey). SD episodes are marked in orange.
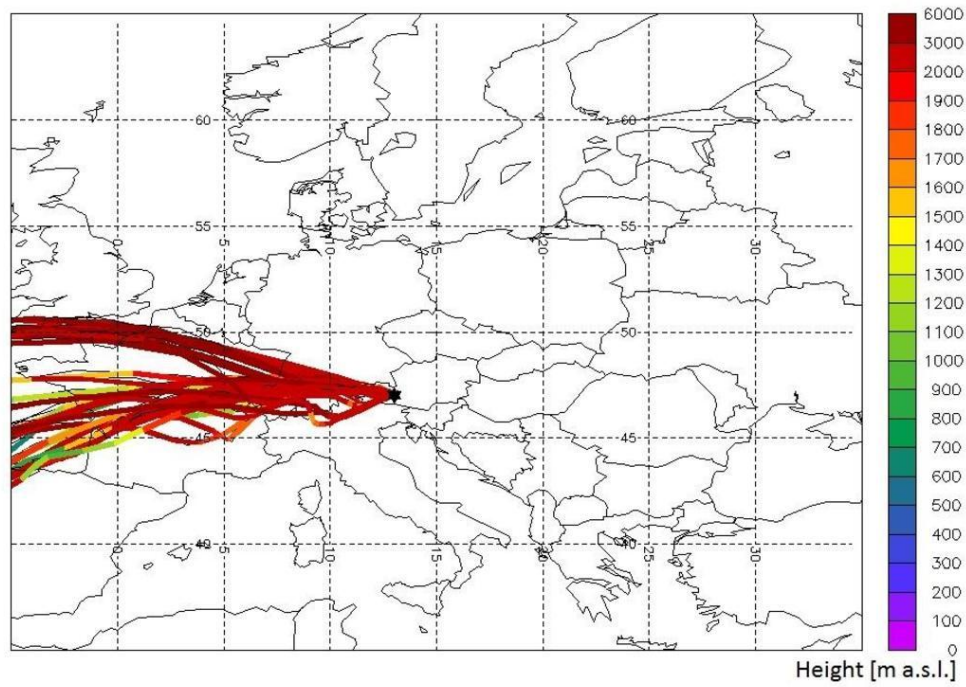
Supplementary Material

Evaluation of backward trajectories and aerosol measurements for the accumulation period 2015/2016

Backward trajectories indicate an influence of SD from 04.11.2015 until 07.11.2015. On-line aerosol measurements yield a positive DI on 04.11.2015 only, as particulate matter concentration on the following days were too low to allow reliable calculations. Thus trajectories were plotted for the whole time period between 04.11. and 07.11.2015. A number of trajectories originate from the Southwest and reveal that SD occurrence at the sampling site during part of this time period is very likely.
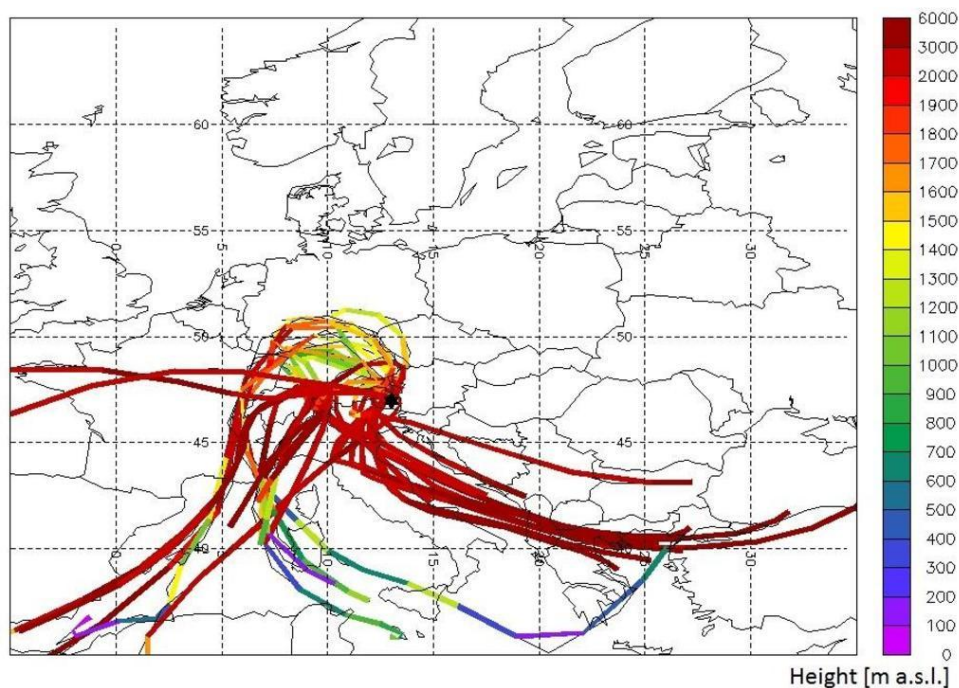
Supplementary Figure 2: 96 hours backward trajectories starting from the Sonnblick Observatory every three hours between 04.11.2015 00UTC and 07.11.2015 21UTC.

Furthermore aerosol measurements give a positive DI for 18.12.2015 and 19.12.2015. During these days backward trajectories show an influence of air masses from the west (Supplementary Figure 3), which seems surprising at a first glance. Comparing these results with the calculations of WRFChem model forecast calculations for these days according to Grell et al. (2005) the transport of SD from the West as shown also by the backward trajectories to western and even northern parts of Europe becomes visible (Supplementary Figure 4). Thus an influence of SD is also likely for the December period.

2

Supplementary Figure 3: 96 hours backward trajectories starting from the Sonnblick Observatory every three hours between 17.12.2015 00UTC and 20.12.2015 21UTC.

3

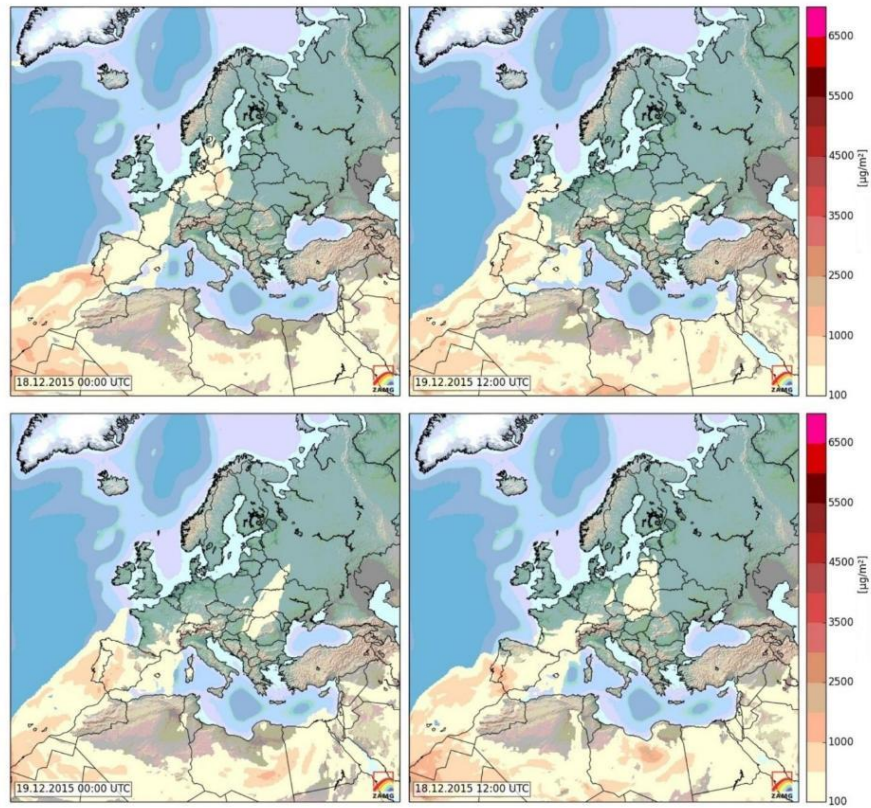**Evaluation of backward trajectories and aerosol measurements for the accumulation period 2016/2017**

Backward trajectories as well as aerosol measurements indicate an influence of SD during two time periods in October 2016. Based on aerosol measurements an influence of SD is given on 15.10.2016 and later again on 24.10. and 25.10.2016, while backward trajectories point to slightly longer periods (15.10. - 19.10. 2016 as well as 23.10. - 25.10.2016). Note that the DI determined via aerosol measurements is just reported for mass concentrations above 5 µg/m³. Supplementary Figure 5 summarizes backward trajectories determined for the whole time period of 15.10. until 25.10.2016. Trajectories from the South reveal that SD occurrence at the sampling site during that time is very likely. In between (20.10. – 22.10.2016) trajectories originating from the West are recorded.
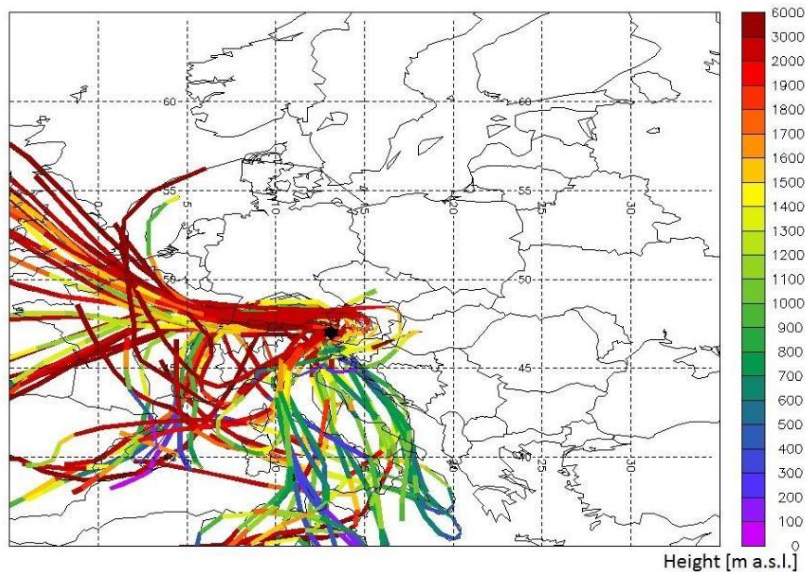
Supplementary Figure 5: 96 hours backward trajectories starting from the Sonnblick Observatory every three hours between 15.10.2016 00UTC and 25.10.2016 21UTC.

During spring 2017 trajectory analyses reveal an influence of air masses originating from the South or Soutwest for a time period in February 2017 and March 2017 (Supplementary Figure 6).Thus the occurrence of SD at the sampling site again is very likely and is confirmed by on-line aerosol measurements (SDI indicating SD during 12.2.-14.2.2017, as well as on 23.3. and 24.3.2017).

5

Supplementary Material

Supplementary Figure 4: Dust concentration over Europe (mg/m^2) in the whole air column up to 50 hPa simulated with WRFChem for 18.12.2015 00UTC and 12UTC as well as for 19.12.2015 00UTC and 12 UTC showing a SD influence over Austria or at least over Western Europe.

4

Supplementary Material

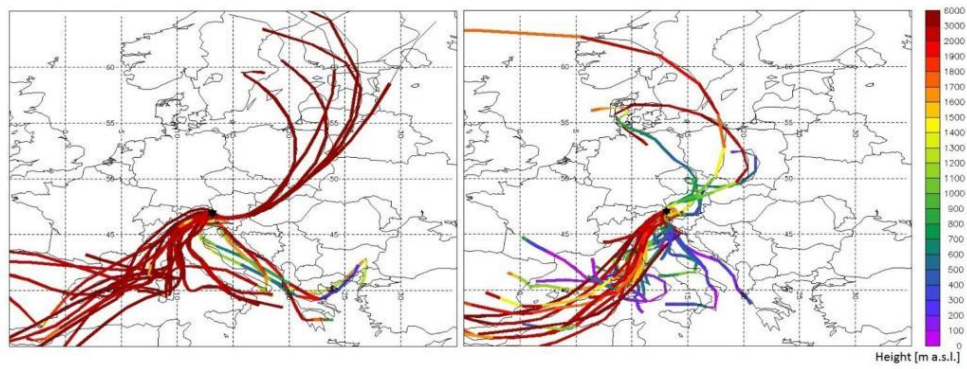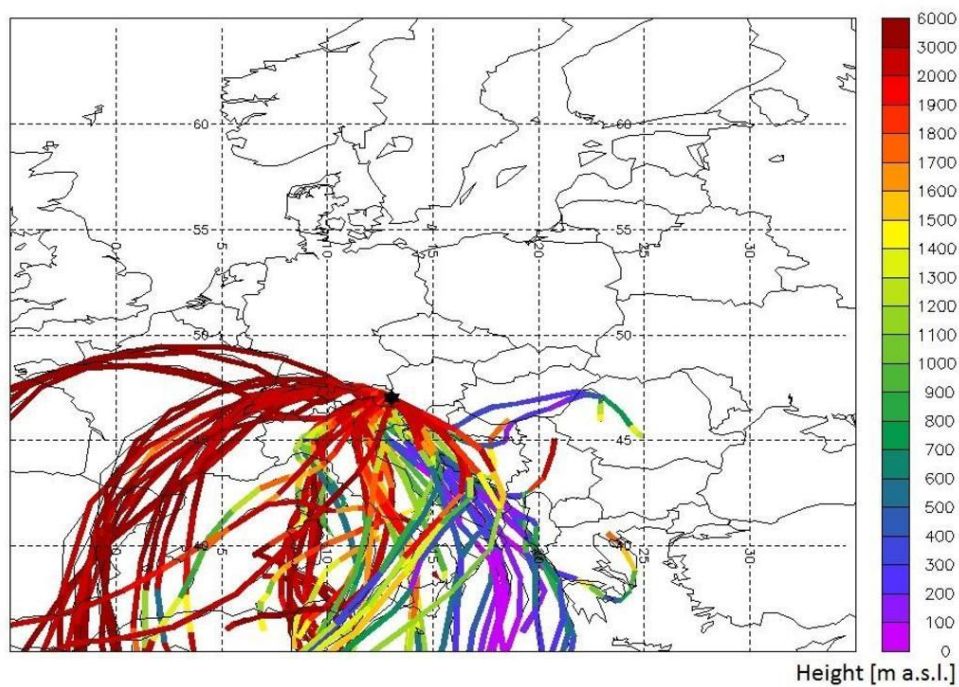**Supplementary Figure 6:** 96 hours backward trajectories starting from the Sonnblick Observatory every three hours between 12.02.2017 00UTC - 15.02.2017 21UTC (left) and 23.03.2017 00UTC - 26.03.2017 21UTC (right).

6

Evaluation of backward trajectories and aerosol measurements for the accumulation period 2014/2015

Backward trajectories as well as aerosol measurements indicate an influence of SD during late November and early December 2014. Supplementary Figure 7 summarizes backward trajectories determined for the time period of 24.11. until 03.12.2014. Most of the trajectories originate from the South revealing that SD occurrence at the sampling site during that time is very likely. The SDI determined by aerosol measurements pointed to SD for most of the days (24.11., 25.11., 26.11., 01.12., 3.12.2014). was

Another time period with backward trajectories originating from the South was observed during March 2015. However, the situation during the respective time period (17.3. – 26.03.2015) was less pronounced. Aerosol measurements point to an influence of SD during 18.3., 21.3., 23.3, 24.3. and 25.3.2015.

Supplementary Figure 7. 96 hours backward trajectories starting from the Sonnblick Observatory every three hours between 24.11.2014 00UTC and 03.12.2014 21UTC.

7

Supplementary Material
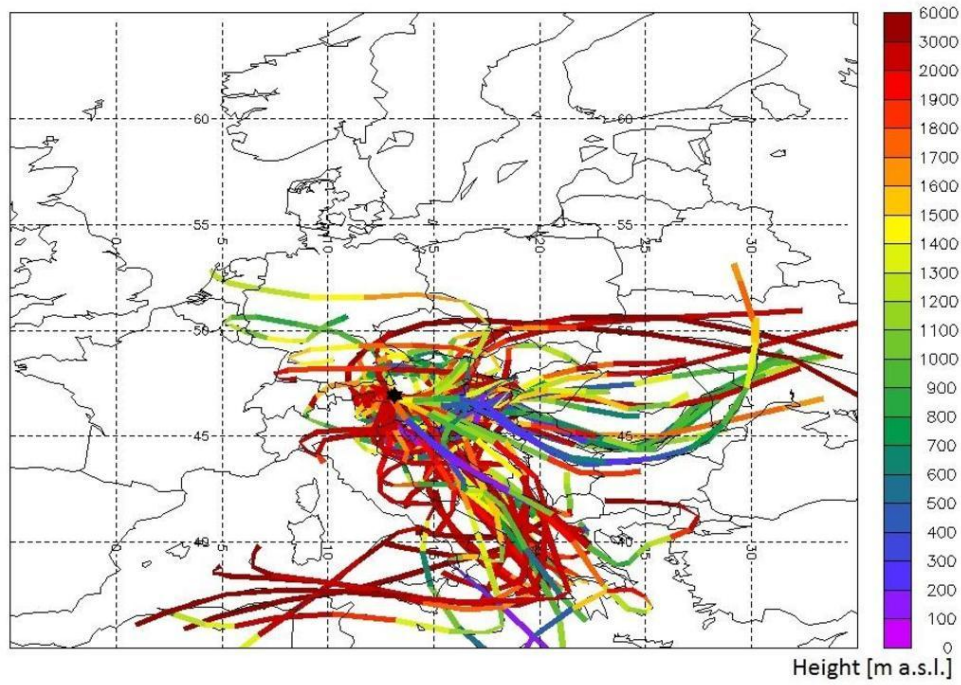
Supplementary Figure 8. 96 hours backward trajectories starting from the Sonnblick Observatory every three hours between 17.03.2015 00UTC and 26.03.2015 21UTC.

8

Chapter 3
Influence of mineral dust on PM_{10} concentrations

Background and aim

Due to the impact of PM on human health, causing serious cardiovascular diseases and increased mortality (e.g. Pope, 2000), the European Commission has established limit values for PM concentration within the air quality directive 2008/50/EC. Limit values for various PM parameters, such as PM_{10} and $PM_{2.5}$ are given therein which may be exceeded only on a limited amount of days per year. The limit value for PM_{10} is set to 50µg/m³ which may be exceeded on only 35 days per year. A more comprehensive description of limit values was already given earlier, in Table 4. The main goal of the regulation is to avoid, prevent and reduce harmful effects of ambient air pollution on human health and the environment as a whole. To achieve this, the EU member states have to assess their ambient air quality and apply counter measures if the amount of days with concentrations above the limit values is exceeded on a regular basis.

As described in the directive 2008/50/EC, concentrations of regulated pollutants, in particular in the case of PM and SO_2, may exceed the set limit values due to the contribution from natural sources such as desert dust or volcanoes. The directive offers the possibility to provide evidence that the exceedance is due, in part or as a whole, to natural sources which can be assessed but not controlled. If the contribution of a natural source can be quantified its contribution may thus be subtracted from the daily mass concentration, which might affect the compliance with air quality limit values.

The natural contributions of desert dust assessed in the directive can vary significantly depending on the place where they are measured and are especially relevant in Southern and South-eastern Europe due to their vicinity to the dry regions in Africa, mainly the Saharan desert, and the Arabian Peninsula, e.g. the Negev desert (Pey et al., 2013). Many studies investigated the contribution of desert dust on the daily PM_{10} load for several years (compare Table 5), highlighting the significant input especially for the Mediterranean region.

The methodology provided by the directive 2008/50/EC for the subtraction of desert dust contribution from the daily PM_{10} load is based on a method developed in Spain and Portugal for the application in both countries (Escudero et al., 2007). The method allows a quantification of the desert dust contribution on a daily basis which can be used for a subtraction from the daily PM_{10} load. The procedure can be described by two steps. Firstly, dates affected by desert dust transport have to be identified and secondly the net dust load (NDL) on the daily PM_{10} record has to be quantified. The identification of desert dust events can be based on different supporting information like trajectory analysis, model forecasts and/or satellite data, which have to be screened and interpreted. The second step, the quantification phase, requires a continuous PM_{10} monitoring at a single selected and representative regional background site providing the reference or background load (BGL). Thereby the BGL represents the moving 40th percentile of the measured PM_{10} 15 days before and 15 days after the investigated day, where days influenced by desert dust are excluded. The 40th percentile was selected from validation studies from the Iberian Peninsula (Pey, 2007). The NDL at the regional background site, representing the contribution of desert dust to PM_{10}, is then estimated as difference between the measured daily PM_{10} load and the calculated BGL. In the directive it is clearly stated that the use of this statistical measure has not been validated for other countries. It might be preferable to use the average or the median of the PM_{10} concentrations measured 15 days before and 15 days after the investigated day, excluding desert dust affected days, to determine the BGL. Member states applying this method should provide an evidence that reliable estimations of the BGL and subsequently on the NDL can be achieved to avoid an underestimation of the NDL and an overestimation of the desert dust

contribution. Thus, the choice of a representative background station and the definition of its spatial representativeness plays an important role. A validation of the NDL is recommended in the directive via measurement campaigns and the determination of a 'crustal load'. According to the directive the measurements of the elements calcium, aluminium, iron, magnesium and potassium is used to subsequently quantify the crustal load. Therefore, the stoichiometric mass of $CaCO_3$, $MgCO_3$, Al_2O_3 and Fe_2O_3 is calculated, while K is included as the element and SiO_2 is indirectly quantified via $3*Al_2O_3=SiO_2$.

Table 5: Contribution of desert dust on the daily PM10 load as provided in the respective studies.

Study	Observation
Rodríguez et al. (2001) PM_{10}, TSP, 24h Iberian Peninsula Spain (1996-1999)	• 23-55% of the daily exceedances of the EU limit value during Saharan dust episodes • 63% of the Saharan dust intrusion from May to September • Peak PM_{10} levels during Saharan dust episodes >150μg/m³
Viana et al. (2002) PM_{10}, 24h Canary Islands Spain (1998-2000)	• 25% of the days affected by desert dust • Winter 600-700 μg/m³ • Summer <75 μg/m³ • Fall 400-500 μg/m³
Achilleos et al. (2014) PM_{10}, 24h Nicosia Cyprus (1993-2008)	up to 470 μg/m³ due to desert dust
Pey et al. (2013) PM_{10}, 24h Mediterranean Basin (2001-2011)	• 30-37% of the days affected by desert dust at Southern sites • <20% of the days affected by desert dust at Northern sites • 35-43% desert dust contribution on the daily PM_{10} in SE Spain, Crete and Cyprus • 19-25% DD of daily PM_{10} in SW and central Spain, Sardinia, South Greece • 6-10% DD of daily PM_{10} in populated areas • 35-50% of PM_{10} from DD (peak 80%) • 2-5% extreme DD days (>100μg/m³) • 5-25% moderate DD days (30-99μg/m³) • 50-70% low DD days (1-10μg/m³)

Querol et al. (2009) applied this method to the whole Mediterranean basin with participants from Greece, Cyprus, Spain, Italy and France, aiming to quantify the African dust contribution to mean PM_{10} levels recorded. A common methodology has been applied to 21 stations, of which some only cover a few years within the time frame ranging from 1996 to 2007 and some covering that whole timespan. To identify days influenced by African dust outbreaks NCEP meteorological maps, HYSPLIT4 back trajectories, aerosol maps from NRL (Naval Research Laboratory, USA) and SKIRON, BSC-DREAM dust maps and satellite images from the NASA SeaWIFS project were used. The daily BGL was obtained by computing the monthly moving 30th percentile (as suggested by Escudero et al., 2007) at the respective regional background stations after a prior exclusion of desert dust affected days.

Pey et al. (2013) performed the same analysis as Querol et al. (2009) extending the time series from 2007 to 2011 and exchanging some of the stations but still investigating 19 stations in total. The methodology used for the identification of African dust outbreaks is the same as in the previous study of Querol et al. (2009) but for the computation of the BGL the monthly moving 40th percentile was used, excluding the days impacted by African dust. They propose that they use the 40th percentile instead of the 30th percentile initially published by Escudero et al. (2007) for conservative reasons because the 40th percentile is the official method as given in the EU directive. This alternate use of the 30th or the 40th percentile of the same regions point out the problems of fixing defined thresholds for the evaluation process.

Cuspilici et al. (2017) studies the Saharan dust influence on PM_{10} in Sicily from 2013 to 2015. They used HYSPLIT back trajectories, the BSC-DREAM model and the NAAPS (Navy Aerosol Analysis and Prediction System for estimating the concentration of mineral aerosol as a function of the aerosol optical thickness) for the identification of Saharan dust affected days. Only days exceeding the daily limit value of 50μg/m³, as set by the European Commission, were subjected to this procedure. For the quantification of the Saharan dust contribution to the PM_{10} loads, the regional BGL was computed by the monthly moving 50th percentile. It is not clearly stated if Saharan dust affected days were excluded for this computation or not. They chose the 50th percentile to follow the recommendation of the directive that when the 40th percentile cannot be validated with chemical measurements the more conservative 50th percentile should be used.

Barnaba et al. (2017) investigated the applicability of the directive for Italy from 2012 to 2014. They proposed an adapted methodology where they used each site as a reference for its own background load and used the 50th moving percentile from a +/- 3 day time-window instead of the monthly moving percentile.

The studies listed above reveal the importance of validation studies of the application and suitability of the methodology given in the directive as well as the necessity to adopt the procedure for single regions or sites. Until now evaluation studies of the applicability of the directive always focus on the Mediterranean region because the impact of Saharan dust or mineral dust from the Arabian Peninsula is known to be very high. Still significant impact was observed also in the Alpine region e.g. in Austria (Baumann-Stanzer et al., 2018; Schauer et al., 2016), even in the Arctic (Barkan and Alpert, 2010; Franzén et al., 1995). Inventories from the Austrian environmental agency (e.g. Spangl and Nagl, 2019) reveal a regular impact of desert dust leading to exceedance of PM_{10} short-term limit values loads, highlighting the importance of a detailed investigation of the applicability of the air quality directive for Austria.

For evaluation studies the choice of a representative background station and the choice of the statistical parameters used for the computation of the BGL as well as the identification of desert dust affected days are the most important steps. Especially the identification is very crucial because it is a very subjective and hence user-dependent process. Some effort has been made by Barnaba et al. (2017) to introduce an automatic, model-based method to identify desert dust affected days. Also the DIAPASON-Project (Desert dust Impact on Air quality through model Predictions and Advances Sensors ObservatioNs) has implemented a semi-automated system to collect, organize and store the information necessary to identify desert dust advections and to evaluate their contribution to the observed PM_{10} levels. For regions further afar from the source regions the desert dust impact can be overlaid by the local impact which is mostly the case during weak desert dust events. Thus not only the identification of desert dust affected days, but also the selection of a representative background station together with a representative computation of the BGL is very important.

To evaluate the applicability of the air quality directive for Austria a six-year time series from 2013 to 2018 of PM_{10} measurements was investigated for the region of Graz, Styria. The evaluation is focused on days with PM_{10} concentrations exceeding the daily limit value of 50μg/m³ as set by the European Commission. It provides a discussion on the selection of a suitable regional background station as well as a discussion on the statistical approach used for the computation of the BGL. Results reveal an adapted approach of the methodology described in the directive, using the monthly mean average of the PM_{10} concentration at the regional background station, together with threshold criteria to identify only desert dust affected days, skipping the subjective and user-dependent process of identifying desert dust events from satellite, back trajectories or model evaluations. The study highlights that desert dust can be responsible for a limit value exceedance, but in the investigated region the anthropogenic sources are mainly responsible for that. Additionally, the manuscript discusses a number of effects a different interpretation of the guideline might have, e.g. the use of different statistical parameters or the exclusion of Saharan dust affected days for the computation of the BGL. In general the impact of desert dust to a daily PM_{10} limit value exceedance in Austria can be expected to be rather small considering the legal maximum

amount of days exceeding the daily PM_{10} limit value as given in the EU directive but still the scales might be tipped in favour of a transgression of that very maximum where one single day can be crucial (Pongratz, 2018). The presented study reveals the necessity of further evaluation studies regarding the determination of the boundary layer height to better validate the representativeness of the background station together with filter based measurements for a corresponding determination of the crustal load.

Literature

Achilleos, S., Evans, J.S., Yiallouros, P.K., Kleanthous, S., Schwartz, J., Koutrakis, P., 2014. PM10 concentration levels at an urban and background site in Cyprus: The impact of urban sources and dust storms. Journal of the Air & Waste Management Association 64, 1352–1360. https://doi.org/10.1080/10962247.2014.923061

Barkan, J., Alpert, P., 2010. Synoptic analysis of a rare event of Saharan dust reaching the Arctic region. Weather 65, 208–211. https://doi.org/10.1002/wea.503

Barnaba, F., Bolignano, A., Di Liberto, L., Morelli, M., Lucarelli, F., Nava, S., Perrino, C., Canepari, S., Basart, S., Costabile, F., Dionisi, D., Ciampichetti, S., Sozzi, R., Gobbi, G.P., 2017. Desert dust contribution to PM10 loads in Italy: Methods and recommendations addressing the relevant European Commission Guidelines in support to the Air Quality Directive 2008/50. Atmospheric Environment 161, 288–305. https://doi.org/10.1016/j.atmosenv.2017.04.038

Baumann-Stanzer, K., Greilinger, M., Kasper-Giebl, A., Flandorfer, C., Hieden, A., Lotteraner, C., Ortner, M., Vergeiner, J., Schauer, G., Piringer, M., 2018. Evaluation of WRF-Chem Model Forecasts of a Prolonged Sahara Dust Episode over the Eastern Alps. Aerosol and Air Quality Research. https://doi.org/10.4209/aaqr.2018.03.0116

Cuspilici, A., Monforte, P., Ragusa, M.A., 2017. Study of Saharan dust influence on PM 10 measures in Sicily from 2013 to 2015. Ecological Indicators 76, 297–303. https://doi.org/10.1016/j.ecolind.2017.01.016

Escudero, M., Querol, X., Pey, J., Alastuey, A., Pérez, N., Ferreira, F., Alonso, S., Rodríguez, S., Cuevas, E., 2007. A methodology for the quantification of the net African dust load in air quality monitoring networks. Atmospheric Environment 41, 5516–5524. https://doi.org/10.1016/j.atmosenv.2007.04.047

Franzén, L.G., Hjelmroos, M., Kållberg, P., Rapp, A., Mattsson, J.O., Brorström-Lundén, E., 1995. The Saharan dust episode of south and central Europe, and northern Scandinavia, March 1991. Weather 50, 313–318. https://doi.org/10.1002/j.1477-8696.1995.tb06139.x

Pey, J., 2007. Caracterización fisico-química de los aerosoles atmos´fericos en el mediterráneo occidental. Universitat Politècnica de Catalunya, Barcelona.

Pey, J., Querol, X., Alastuey, A., Forastiere, F., Stafoggia, M., 2013. African dust outbreaks over the Mediterranean Basin during 2001-2011: PM10 concentrations, phenomenology and trends, and its relation with synoptic and mesoscale meteorology. Atmos. Chem. Phys. 13, 1395–1410. https://doi.org/10.5194/acp-13-1395-2013

Pongratz, T., 2018. Luftreinhaltung in der Steiermark - Jahresbericht 2017. Bericht Nr. Lu-07-2018.

Pope, C.A., 2000. What Do Epidemiologic Findings Tell Us about Health Effects of Environmental Aerosols? Journal of Aerosol Medicine 13, 335–354. https://doi.org/10.1089/jam.2000.13.335

Querol, X., Pey, J., Pandolfi, M., Alastuey, A., Cusack, M., Pérez, N., Moreno, T., Viana, M., Mihalopoulos, N., Kallos, G., Kleanthous, S., 2009. African dust contributions to mean ambient PM10 mass-levels across the Mediterranean Basin. Atmospheric Environment 43, 4266–4277. https://doi.org/10.1016/j.atmosenv.2009.06.013

Rodrı´guez, S., Querol, X., Alastuey, A., Kallos, G., Kakaliagou, O., 2001. Saharan dust contributions to PM10 and TSP levels in Southern and Eastern Spain. Atmospheric Environment 35, 2433–2447. https://doi.org/10.1016/S1352-2310(00)00496-9

Schauer, G., Kasper-Giebl, A., Močnik, G., 2016. Increased PM Concentrations during a Combined Wildfire and Saharan Dust Event Observed at High-Altitude Sonnblick Observatory, Austria. Aerosol and Air Quality Research 16, 542–554. https://doi.org/10.4209/aaqr.2015.05.0337

Spangl, W., Nagl, C., 2019. Jahresbericht der Luftgütemessung in Österreich 2018. REP-0675.

Viana, M., Querol, X., Alastuey, A., Cuevas, E., Rodrı´guez, S., 2002. Influence of African dust on the levels of atmospheric particulates in the Canary Islands air quality network. Atmospheric Environment 36, 5861–5875. https://doi.org/10.1016/S1352-2310(02)00463-

Article (peer-reviewed)

This chapter corresponds to the following peer-reviewed publication in its original form:

Greilinger, M., Zbiral, J., Kasper-Giebl, A. (2019) Desert dust contribution to PM10 loads in Styria (Southern Austria) and impact on exceedance of limit values from 2013-2018. Applied Sciences, 9, 2265, doi: 10.3390/app9112265

The study was conceived in the terms of scientific collaborations with the first author being main responsible for the content and realization of the work. The detailed author contributions can be found in the respective section in the article.

applied
sciences

MDPI

Desert Dust Contribution to PM$_{10}$ Loads in Styria (Southern Austria) and Impact on Exceedance of Limit Values from 2013–2018

Marion Greilinger [1,2,*], Johannes Zbiral [2] and Anne Kasper-Giebl [2]

[1] Department of Climate Research, Zentralanstalt für Meteorologie und Geodynamik (ZAMG), 1190 Vienna, Austria

[2] Institute for Chemical Technologies and Analytics, Vienna University of Technology, 1060 Vienna, Austria; johannes.zbiral@tuwien.ac.at (J.Z.); anneliese.kasper-giebl@tuwien.ac.at (A.K.-G.)

[*] Correspondence: marion.greilinger@zamg.ac.at; Tel.: +43-1-36026-2232

check for
updates

Abstract: From a legislators point of view, the contribution of natural sources to PM$_{10}$ loads is relevant since their impact can be subtracted from the daily limit value of PM$_{10}$ as regulated in a working staff paper by the European Commission (EC), supporting the European Air Quality Directive (2008/50/EC). This work investigates its applicability for two stations in Austria over a time period of six years (2013 to 2018), as the occurrence of long-range transport of desert dust is observed on a regular base. Different stations and different statistical parameters were evaluated to determine the regional background load and subsequently the net dust load (NDL). Results reveal an adapted approach of the methodology described by the EC, using the +/− 15-day mean average of the PM$_{10}$ at the regional background station, together with threshold criteria to identify only desert dust affected days. The results of calculated NDLs were in good agreement with crustal loads determined on filter samples during two desert dust events in 2016. Thus, the application of the EC method for a region in Central Europe, which experiences a regular but less pronounced impact of desert dust than stations in the Mediterranean, is discussed.

Keywords: air quality; desert dust; mineral dust; PM exceedance; net dust load; background load; particulate matter

1. Introduction

Particulate matter (PM) concentrations are known to have severe impact not only on global climate and atmospheric chemistry ([1] and references therein) but also on human health [2,3]. Regarding the findings from these studies, the European Commission (EC) has established limit values for PM in the air quality directive 2008/50/EC. Therein, a daily limit for PM$_{10}$ of 50 μg/m^3 is stated, which may be exceeded on 35 days per year. Also for other PM fractions such as PM$_{2.5}$ limit values are given by the EC; however, within this study, only PM$_{10}$ is investigated.

Close to populated areas, exceedance of the limit values of PM$_{10}$ are caused mainly by anthropogenic sources such as energy production, traffic and industry, although natural sources can contribute as well [4]. The relative importance of the different sources depends strongly on regional and temporal scales, often the urban impact adds to a marked initial pollution load [5,6]. Especially in the Mediterranean region natural mineral dust sources are known as important contributors to PM$_{10}$ exceedance [7–9]. If exceedance of limit values can be attributed to a natural phenomenon such as particle intrusion from arid regions (e.g., the Sahara, or the Arabian or Lybian deserts), they can be discounted. The EC provides a commission working staff paper [10] describing this procedure

for Spain. In the underlying study of Escudero et al. [11] a methodology for quantifying the daily African PM_{10} load during dust outbreaks for Southern Europe is proposed, using Spain as study area. They determined the regional background load via applying a monthly moving 30th percentile to the PM_{10} load at a regional background site, excluding the days affected by African dust transport and validated the methodology via crustal loads determined by chemical speciation of PM_{10} filters. Within the working staff paper of the EC it is clearly stated that the use of this approach has not been validated for other countries and that no certainty exists on its accuracy for application. A recent study of Barnaba et al. [7] investigates the applicability of the EC methodology for Italy, describing limitations and drawbacks in the identification of desert dust days as well as in the quantification of the regional background load. Specific solutions for Italy are proposed and introduced. In their adapted methodology, they use each site as reference for its own background load, reduced the time window over which the background load is determined and introduced an automatic, model-based method to identify desert dust affected days.

It is well known that desert dust outbreaks regularly occur in Austria [12–14], although their impact is less pronounced than in the Mediterranean region. Their influence on air quality has not been investigated so far and a discussion of the EC methodology for the subtraction of desert dust contributions is completely missing.

This study presents the first validity check of the applicability of the EC methodology for Austria. This is of high relevance as both facts, exceedances of short-term limit values of PM_{10} and the influence of desert dust occur in Austria. The critical application of a methodology developed for the Mediterranean region to a country within Central Europe is of special interest for continuative use. We evaluate whether long-range transport of desert dust can be quantified via the EC methodology and whether the respective subtractions would influence the exceedance of the short-term limit value for PM_{10}, taking the urban-traffic sampling site Graz Don Bosco as main example. We compared three different stations for their suitability to be regarded as the regional background station, required for applying the EC methodology. Furthermore, different statistical parameters for the computation of the net dust load that can then be discounted from the exceeding daily PM_{10} load of the respective station were tested, as suggested by the EC. The calculated amounts of the net dust loads of two desert dust events in 2016 were compared with measured mineral dust loads based on chemical analyses of the respective filters to verify the results.

The evaluation comprises a six-year data basis from January 2013 to December 2018 and is focused on days with PM_{10} concentrations > 50 μg/m^3, exceeding the daily limit value. The possible impact of desert dust to the overall load of PM_{10} would be interesting, but goes beyond the scope of this study.

2. Materials and Methods

2.1. Study Area

Overall PM_{10} concentrations in Austria show a declining trend [15]. Nevertheless PM_{10} concentrations in Styria, especially at sites within its capital city Graz, regularly exceed the short-term limit value [16]. Therefore, the region around Graz was selected as study area. Graz is located in Styria, in the southern part of Austria, southeast of the main ridge of the Alps (Figure 1) and is the second largest city in Austria, with about 300.000 inhabitants. Exceedances of PM_{10} short-term limit values are mainly due to the specific orographic situation and the combination of local pollution sources, the regional transport of particulate matter and the possible input of long-range transport.

The climate of Graz can be classified as continental but its orography plays a key role in the atmospheric dynamics, and hence, in the air quality of the city. The location in a valley basin facilitates a shielding effect of the Alps, and therefore, a lack of wind especially during winter, preventing vertical mixing. This makes the occurrence of inversions and fog more likely [17].'Due to the increased occurrence of inversion conditions, PM concentrations are supposed to be increased regularly leading to an exceedance of limit values. To highlight the importance of emission reduction measures the

applicability and impact of the EC methodology for an urban-traffic station Graz Don Bosco (DB) and an urban-background station Graz Süd (GS) was investigated on a six-year data basis from January 2013 to December 2018. Three stations (Masenberg, MB; Bockberg, BB; Lustbühel, LB) were taken into account as potential regional background station for the calculation of the net dust load following the EC methodology. Filter samples of a rural (Gratwein, GW) and a suburban site (Graz Ost GO), sampled during two desert dust episodes in February and April 2016, together with filters of DB for the event in February only, were used to validate the calculated net dust loads.
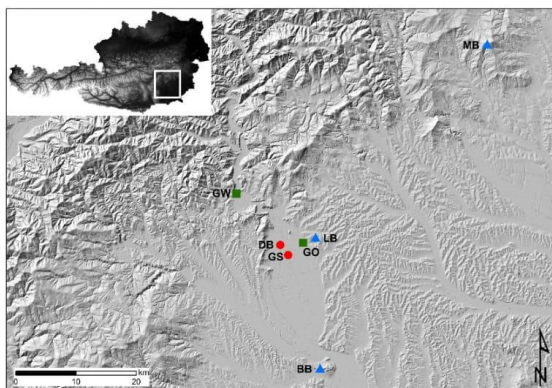

Figure 1. Location of the air quality monitoring stations selected for this study as listed in Table 1. Stations of investigation (Graz Don Bosco, DB, and Graz Süd, GS) are marked by red dots. Potential background stations, mandatory for the determination of the net dust load as proposed by the European Commission, are marked with blue triangles. Stations were filter samples for validation purposes were taken are marked via green squares.

2.2. PM_{10} Measurements and Sampling

PM_{10} concentrations at DB as well as at GS were gravimetrically measured according to the European standard reference method EN12341:2014 using a Digitel high volume sampler DHA80. PM_{10} measurements at MB, BB and LB were derived using a beta attenuation mass monitor MetOne BAM 1020 (EN 16450:2017) The equivalence of this method to the reference method has to be proven and is shown in the annual reports of the environmental agency [18] and the provincial government of Styria [19].

At the stations GO and GW PM_{10} samples of the two mineral dust episodes in February and April 2016 were collected on quartz fiber filters (Pallflex Tissuquartz) using a Digitel high volume sampler DHA80. Again, sampling was carried out according to EN12341:2014. The same filter material was used in DB to investigate the event in February. Sample changes, maintenance of the stations and gravimetric analysis were performed by the specialist department of the provincial government of Styria within the framework of the ambient air quality monitoring. Table 1 summarizes the location, measured parameters as well as the measurement and sampling devices.

Table 1. Monitoring stations used in the present study. See locations in Figure 1.

Station	LON [°]	LAT [°]	Elevation [m a.s.l.]	Device
Graz Don Bosco (DB)	15.41643	47.05702	358	Digitel HVS DHA80
Graz Süd (GS)	15.43306	47.04167	345	Digitel HVS DHA80
Graz Lustbühel (LB)	15.49369	47.06700	473	MetOne BAM 1020
Bockberg (BB)	15.49583	46.87139	449	MetOne BAM 1020
Masenberg (MB)	15.88222	47.34806	1180	MetOne BAM 1020
Graz Ost (GO)	15.46638	47.05944	366	Digitel HVS DHA80
Gratwein (GW)	15.32361	47.13555	382	Digitel HVS DHA80

2.3. Chemical Filter Analysis

XRF analysis was used to determine the crustal load (CL) on the PM_{10} quartz fiber filters sampled during the two dust events in February and April 2016. Measurements were performed using a Panalytical Axios Advanced wavelength dispersive X-ray fluorescence spectrometer with a Rhodium target X-ray tube. The tube was set at 50 kV with a current of 50 mA and a 20 mm aperture for exposure and an exposure time of 20 seconds per channel was used. Filter samples were put into a holder with a central opening of 27 mm in diameter. A set of eight filter holders with one filter blank and seven samples were put into the instrument and were automatically transferred to the analytical chamber one by one. Following the procedure described by Peng et al [20] a certified standard soil (San Joaquin soil from National Institutes of Standards, USA, NIST SRM 2709) was used for calibration. Concentrations of Mg, Ca, Fe and Al were determined and the respective crustal components such as SiO_2, Al_2O_3, Fe_2O_3, $CaCO_3$ and $MgCO_3$ were stoichiometrically calculated. The content of SiO_2 was indirectly determined from the content of Al using the relation $SiO_2 = 2*Al_2O_3$ [21]. Potassium was not included in the calculation of the CL, as it is well known that wood combustion used for residential heating is a dominant contributor to particulate matter concentrations within the region [22,23]. The CL was then computed by adding the concentrations of the major crustal components (SiO_2, Al_2O_3, Fe_2O_3, $CaCO_3$ and $MgCO_3$) similar to the approach of Escudero et al. [11] proposed in the EC guideline.

3. Results and Discussion

3.1. PM_{10} Levels at the Stations Graz Don Bosco (DB) and Graz Süd (GS)

Daily PM_{10} levels recorded at the stations DB (urban-traffic) and GS (urban-background) exceed the 50 μg/m^3 on 242 and 196 days, respectively, within the six-year period from January 2013 to December 2018, thereby exceeding the 35 day/year limit in six years and one year, respectively. The time series are plotted in Figure 2 showing that maximum PM_{10} values, and hence, exceedance of limit values mostly occur during wintertime. This pattern of the seasonal variation is observed at both stations and is characteristic for stations in this region. The increase of PM concentrations during winter can on one hand be attributed to an enhanced influence of inorganic secondary aerosols due to lower air temperature and increased humidity and also to a stronger influence of wood combustion used for residential heating, as well as regional transport of PM [22,24]. Furthermore, meteorological conditions with wintertime inversions favor an enrichment of PM concentrations in the boundary layer. During wintertime inversion conditions are very likely in the area of Graz due to the orographic situation of the region, allowing air pollutants to concentrate over several days until the inversion is cleared out and concentrations drop [17].

On top of these seasonal variations the influence of long-range transported desert dust may occur. As an example, an intensive desert dust episode in April 2016 is marked by a red star in Figure 2. The identification, intensity and duration of this event, covering large parts of Austria, was already thoroughly described by Baumann-Stanzer et al. [12]. Still a number of less pronounced events took place. Such events, identified via the use of WRF-Chem model forecasts [12], FLEXTRA

back-trajectories [25] as well as the dust ensemble forecasts and forecast comparisons provided by the WMO sand and dust storm warning advisory and assessment system (https://sds-was.aemet.es/forecast-products/dust-forecasts), are marked in orange in Figure 2. Additionally optical aerosol properties measured at the high mountain global GAW station Hoher Sonnblick in the Austrian Alps are used for the identification of desert dust (DD) occurrence [14]. The aim of this study was the quantification of DD contributions for days with PM_{10} exceedances only. An additional influence of desert dust might have occurred during periods of lower PM_{10} concentrations as well.
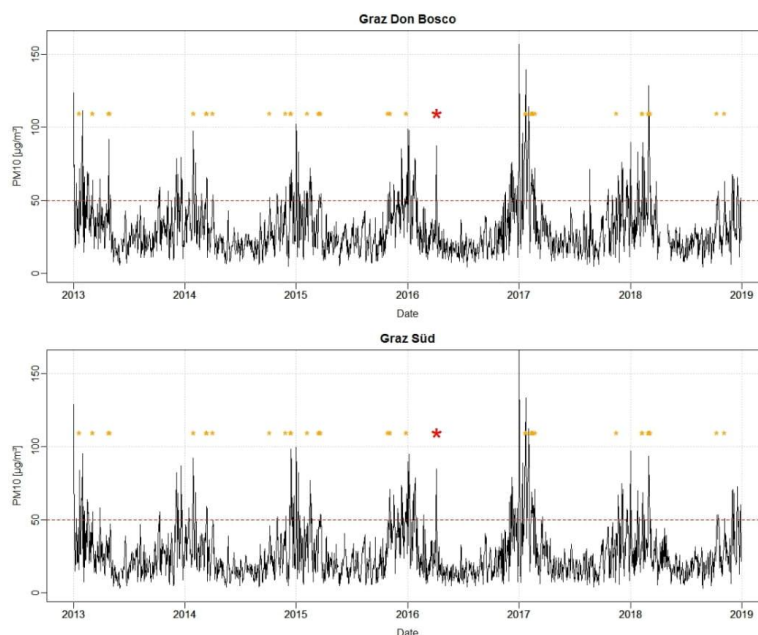

Figure 2. Particulate matter (PM_{10}) time series of the two stations under investigation. The red line marks the 50 $\mu g/m^3$ limit value set by the European Commission. Orange stars mark desert dust events on days where the PM_{10} concentration was > 50 $\mu g/m^3$. The red star marks an intense Saharan dust event in April 2016.

3.2. Determination of Background Loads According to the EC Methodology

The EC methodology [10] for the evaluation of desert dust (DD) contributions is based on two steps. Firstly, dates affected by DD transport have to be identified and secondly, the net dust load (NDL) on the daily PM_{10} record has to be quantified. The identification of DD events is based on several supporting information like trajectory analysis, model forecasts and/or satellite data, which have to be screened and interpreted. A number of models, back-trajectory calculations or data bases for satellite data are suggested by the EC methodology, but later evaluations included other sources as well [7,11] showing the technical and organizational change in that field. In case the various information portals give diverse results for the identification of a DD event further evaluations and comparisons are needed. The second step, the quantification phase, requires a continuous PM_{10} monitoring at a single selected regional background site representative for the region under investigation, providing the reference or background load (BGL). The BGL represent a moving 30-day average value (mean, median or 40th percentile as suggested by the EC) of the 15 days before and 15 days after the investigated day, where days influenced by DD are excluded. The NDL at the regional background site, representing the

contribution of DD to PM_{10}, is then estimated as difference between the measured daily PM_{10} load and the calculated BGL:

$$NDL_{RB} = PM10_{RB} - BGL_{RB} \qquad (1)$$

Within a first approach to estimate the influence of DD for Austria we do not exclude days with DD influence for calculating the NDL. This is a difference to the EC methodology and can be regarded as a more conservative approach. Doing so, we want to consider two main facts. Even if DD is a driver for BGLs at the respective sites and respective days in Austria, other sources might contribute markedly as well and an exclusion of days with influence of DD would eliminate these effects as well. Secondly, modeling tools used for the characterization of DD reveal some uncertainty, which influences the determination of days which could be rejected. This uncertainty might be more pronounced for Austria than for regions closer to the source. The uncertainty is supposed to increase with longer transport time because atmospheric dispersion of air pollutants is a very complex process with very high uncertainties in chemical transport models. Thus, we did not put this elimination step to the beginning of our evaluation procedure. As a matter of fact we will get a potential overestimation of the BGL at the regional background station and hence an underestimation of the according NDL for the respective day. Thus, a potentially lower value of a DD contribution is subtracted compared to reality. Some discussion of the systematical error introduced by this approach will be given later.

Regarding the quantification phase, we compared the 30-day mean, median and 40th percentile for the computation of the BGL at three potential regional background stations (compare Figure 3). The calculated BGL based on the mean is generally higher than the BGL based on the median or the 40th percentile, regarding all three stations. As may be expected from Equation (1), the estimated NDL decreases as the percentile for the computation of the BGL increases. Again, we decided to stick to a more conservative approach and use the 30-day mean for further computation of the BGL. Using the median or the 40th percentile would reduce the average BGL by 4–11% and 13–21%, respectively, depending on the station used (MB, BB or LB). The BGL calculated based on the 30-day mean varies between 10–50 $\mu g/m^3$ for BB and LB and between 4–21 $\mu g/m^3$ for MB and is reduced to 5–45$\mu g/m^3$ (BB and LB) and 3–19 $\mu g/m^3$ (MB) when the 40th percentile criterion is applied.
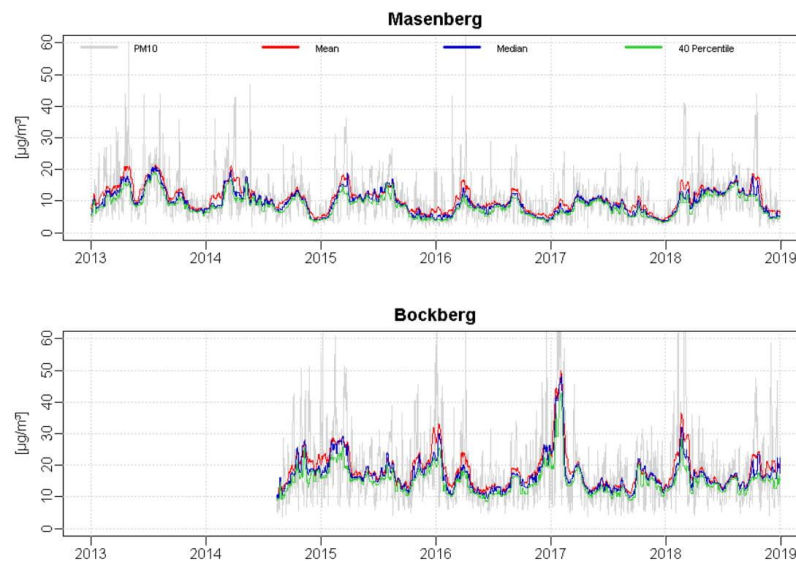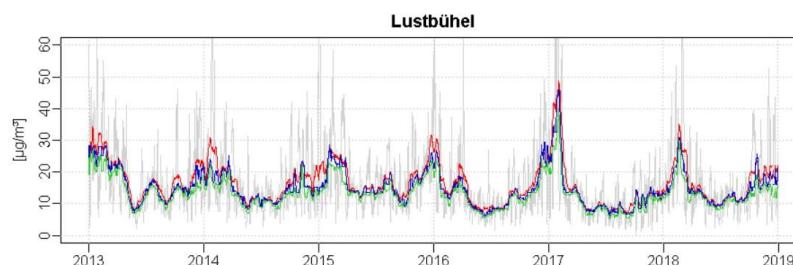

Figure 3. *Cont.*

Figure 3. Background load (BGL) of three potential background stations using either the mean (red), the median (blue) or the 40th percentile (green) of the 30-day period for calculation.

3.3. Selection of a Suitable Regional Background Station

According to Equation (1) the NDLs of the respective days, calculated as the difference between PM_{10} and BGL, will vary around zero. Negative values represent days where the BGL is larger than the central PM_{10} value and vice versa.

In Figures 3 and 4 it can be seen that the time series of MB feature different characteristics than the one of BB and LB. PM_{10} values of BB and LB tend to cover a wider range compared to MB and show a seasonality similar to DB and GS with increased values especially during winter. Correspondingly, BGLs of BB and LB (Figure 3) show this seasonality as well and NDLs (Figure 4) yield a much larger scatter during the wintertime, than during summer. Negative NDL outliers at BB and LB were found to occur mostly during winter and could be traced back to days at the end of an inversion weather situation where the PM_{10} concentration suddenly drops due to an air mass exchange. Days with inversion weather conditions, meaning an inversed vertical temperature profile with lower values at lower altitudes compared to higher ones, were identified using the daily mean temperature at the TAWES stations at the airport of Graz (337 m a.s.l.) and on top of Schöckel (1445 m a.s.l.). If the daily mean temperature at the airport of Graz was lower than the one at Schöckel the day was classified as inversion day. Inversion days occur all years whereas their number varies from year to year. Thus, for single years and during short time measurement campaigns BB and LB might serve as suitable background stations for Graz, but not over a longer period of several years. Positive NDL outliers at BB and LB are of course identical with PM_{10} outliers and occur mostly during winter, again reflecting the inversion weather situation where PM_{10} concentrations are enhanced. Due to this seasonal dependence, BB and LB are ineligible as regional background stations to compute the NDL. The calculated NDL at these stations cannot be interpreted as such due to the substantial influence of inversion weather conditions. It rather reflects a "pollution load" pointing to a variety of influencing factors from anthropogenic and natural sources.

NDLs of MB are similar between winter and summer and, as a matter of fact, for the whole data set. Negative NDL outliers were found to be associated to days with precipitation rather than inversion weather situations shortly before or after. During precipitation the PM_{10} concentration suddenly drops and becomes lower than during the previous and subsequent days representing the BGL. Positive outliers of the NDL are again identical with outliers of PM_{10}, but were quite equally distributed between the different seasons. The single outlier for the BGL was observed on July 25, 2013 related to a Saharan dust episode a few days later. Due to averaging over 30 days, also other days are influenced by this Saharan dust episode. Their BGL values were found to be only slightly smaller than the upper whisker and are therefore not highlighted.
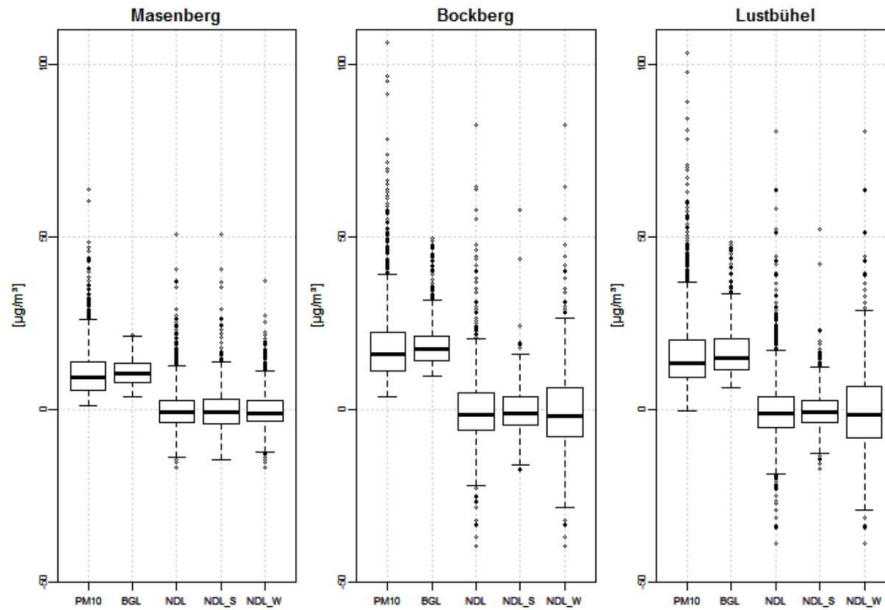
Figure 4. Boxplot of the daily mean PM_{10}, the background loads (BGL) calculated based on the mean as well as the net dust loads (NDL) for the whole years as well as for the summer (NDL_S) and winter period (NDL_W) of the three potential background stations.

Results show that MB represents a suitable background station because it is largely independent of inversion weather situations and hence seasonality. Based on an urban climate analysis study of Graz [17] it can be assumed that the representativeness of the background condition observed on MB is applicable for the stations in Graz. Thus, we investigate the contribution of desert dust on PM_{10} measurements using MB to compute the BGL based on the mean of a 30-day period without extracting desert dust affected periods. This approach represents a modified methodology compared to the one proposed by the EC (40th percentile, exclusion of DD days) which was established for Spain, but the demand for its validation for other countries is clearly highlighted.

Due to its definition (see Equation (1)) the NDL is computed via a subtraction of the BGL from the daily PM_{10} value and is likely to vary around zero. BGL values (representing a 30-day average PM_{10} load) might be higher than the PM_{10} load of a single day due to precipitation or increased vertical mixing after a period of stable atmospheric conditions on that special day, leading to negative NDL values. These negative values are just a consequence of the day to day variability and are, therefore, set to zero for further evaluation. Hence, the NDL of MB can be interpreted as a reduction potential in $\mu g/m^3$ due to the influence of desert dust lowering PM_{10} levels observed at other stations in the investigated region. Table 2 gives an overview of the main statistical parameters describing the NDL before and after negative values were set to zero.

Table 2. NDL in $\mu g/m^3$ of the Masenberg station, most suitable to act as regional background station, before and after negative values were set to zero.

	Before Setting Negative NDLs to Zero	After Setting Negative NDLs to Zero
Minimum	−16.82	0
25th percentile	−3.79	0
Median	−0.91	0
75th percentile	2.79	2.79
Maximum	50.60	50.60

3.4. Application of the Modified Methodology

Table 3 shows the number of days exceeding the 50 $\mu g/m^3$ daily PM_{10} limit at the two investigated stations DB and GS as well as the number of days exceeding this limit after the subtraction of the NDL_{MB}. Throughout the six-year period 242 days exceed the daily limit value at the urban-traffic station DB, which comes up to five out of six years exceeding the 35 day/year limit. At the urban-background station GS 196 days exceed the daily limit value, whereas only in 2017 the 35 day/year limit was exceeded due to a longer lasting pollution episode in January and February.

Subtracting the NDL_{MB} without any further evaluation of the presence of DD, 40 days of the 242 days at DB fall below the 50 $\mu g/m^3$ limit, reducing the years which exceed the 35 day/year limit to three years (2013, 2017 and 2018) in contrast to the five years given before. For GS 35 days of 196 days fall below the 50 $\mu g/m^3$ limit, not influencing the exceedance of the 35 day/year limit. After an identification of DD days based on model result, back trajectories and optical aerosol measurements as described earlier, results reveal that of the 40 and 35 days at DB and GS, only 20 (DB) and 15 (GS) days show an influence of DD (compare Table 3, columns DD days). Obviously only for those days a subtraction of the NDL_{MB} is allowed and the solely determination of NDL_{MB} is not sufficient.

The selection of DD days could be included before subtracting the NDL_{MB}, corresponding to the EC methodology. This would identify 51 out of 242 days at DB and 37 out of the 196 days at GS with a possible influence of DD. Subtractions of NDL_{MB} for these special days would again give the number of reductions listed in Table 3 (5th column for DB and 9th column for GS).

As already discussed, the identification of DD days using models together with back trajectories is a very subjective process. Barnaba et al [7] developed an automated and user-independent process for the identification of DD days, still using model calculations. As such, a user-independent process was not yet established for Austria. Therefore, we evaluate a method for the identification of DD days based on the time series of the PM_{10} measurements at the background site only.

Table 3. Number of days with daily $PM_{10} > 50$ $\mu g/m^3$ at the urban-traffic station Graz Don Bosco (DB) and the urban-background station Graz Süd (GS), number of days which are exceeding or falling below the 50 $\mu g/m^3$ limit value after the subtraction of the NDL of the regional background station MB (NDL_{MB}) without any further evaluation as well as with the identification of desert dust (DD) days via model calculations. Amount of days exceeding the limit of 35 days/year with PM_{10} concentrations > 50 $\mu g/m^3$ are marked in bold.

Year	PM_{10} DB > 50 $\mu g/m^3$	$PM_{10 DB}$-NDL_{MB} > 50 $\mu g/m^3$	PM_{10} DB-NDL_{MB} ≤ 50 $\mu g/m^3$	DD Days DB	PM_{10} GS > 50 $\mu g/m^3$	$PM_{10 GS}$-NDL_{MB} > 50 $\mu g/m^3$	$PM_{10 GS}$-NDL_{MB} ≤ 50 $\mu g/m$	DD Days GS
2013	**44**	**36**	8	4	31	25	6	1
2014	27	16	11	7	23	18	5	3
2015	**39**	30	9	5	35	29	6	3
2016	**39**	35	4	2	34	29	5	3
2017	**54**	**49**	5	1	**43**	**37**	6	1
2018	**39**	**36**	3	1	30	23	7	4
Sum	242	202	40	20	196	161	35	15

Considering only days with a possible contribution of DD similar features of NDL_{MB} and BGL_{MB} become visible, which define additional criteria to avoid undue reductions even when only NDL_{MB}

values are considered. The resulting thresholds (BGL_{MB}: 12 µg/m^3 and NDL_{MB}: 10 µg/m^3) are based on a descriptive approach, but give a better understanding of the several factors influencing NDL_{MB}.

BGL_{MB} concentrations, determined as a 30-day average, should not fall below 12 µg/m^3, a value close to the annual average concentration of PM_{10} determined at Masenberg. We want to point out that monthly averaged PM_{10} values of the whole period of 6 years vary between 6–8 µg/m^3 for November, December and January and between 10–14 µg/m^3 for all other months. Setting a threshold for BGL_{MB} at 12 µg/m^3 will preclude the determination of a DD event valid for reduction, during the winter month and also during most of the year 2017. Still a lower threshold value would lead to the identification of events not associated with the influence of DD, but by other sources or general differences between the background site at 1180 m asl and the urban sites in Graz. Furthermore, the calculated NDL_{MB} should be at least 10 µg/m^3 and thus account for a substantial part of the PM_{10} concentration, at least at the background site. This can be regarded as a precondition as the method should identify DD events which influence the air quality in Austria markedly. Ohterwise, low concentration values more affected by random variations could account for undue reductions of PM_{10} levels. This is especially important during days when daily limit values at polluted sites are exceeded only slightly. The identified NDL_{MB} threshold is close to the 95th percentile of 10.9 µg/m^3.

These thresholds were applied to the 242 days exceeding the 50 µg/m^3 daily PM_{10} limit within the six-year period at DB only, since this is the more critical station regarding the 35 day/year limit. Now the amount of days still exceeding the limit value is very well comparable as if DD days were identified using model and trajectory analysis. An influence on the exceedance of the 35 day/year limit remains scarce (compare column 3 and 5 in Table 4) and occurs only in one year (2015) when the adapted methodology using the thresholds led to no reduction below the 35 day/year limit, whereas it would fall below if the identified DD days were used.

The general agreement and disagreement with the evaluation of identified DD days is given as contingency table (see columns 6 to 10 in Table 4), while evaluations of the single days are given in the supplement (Table S1).

Table 4. Column 1: Amount of days of PM_{10} exceedance at DB, Column 2: Identified desert dust days (iDD), amount of DD days leading to a reduction below 50 µg/m^3 shown in brackets, Column 3: Remaining days exceeding the daily limit after deduction of the NDL_{MB} on identified DD days, Column 4: Estimated desert dust days (eDD) due to the threshold criteria, amount of estimated DD days leading to a reduction below 50 µg/m^3 shown in brackets. Column 5: Remaining days exceeding the daily limit after deduction of the NDL_{MB} on estimated DD days Column 6–10: Contingency table (TP = true positives, TN = true negatives, FP = false positives, FN = false negatives, NAs = no PM_{10} data from Masenberg available).

	1	2	3	4	5	6	7	8	9	10
Year	$PM_{10\,DB}$ > 50µg/m^3	Identified DD Days (iDD)	$PM_{10\,DB}$ > 50µg/m^3 iDD Days	Estimated DD Days (eDD)	$PM_{10\,DB}$ > 50µg/m^3 eDD Days	TP	TN	FP	FN	NAs
2013	44	8 (4)	40	6 (5)	39	3	32	3	4	2
2014	27	10 (7)	20	4 (4)	23	4	17	0	6	0
2015	39	10 (5)	34	3 (3)	36	3	28	0	7	1
2016	39	2 (2)	37	2 (2)	37	2	37	0	0	0
2017	54	11 (1)	53	0 (0)	54	0	43	0	10	1
2018	39	10 (1)	38	6 (1)	38	4	27	2	6	0
Sum	242	51 (20)	222	21 (15)	227	16 (6.6%)	184 (76.0%)	5 (2.1%)	33 (13.6%)	4 (1.7%)

In total 16 days (6.6%) were identified as true positive (TP) DD days, whereas 184 days (76.0%) were identified as true negatives (TN). This means, that 82% of the days exceeding the daily limit were correctly classified in DD and non-DD days using the thresholds. Regarding the remaining days, five days (2%) were identified as false positive (FP) DD days, while 34 days (13.6%) were found to be false negatives. For 20 of these days some uncertainty of the classification of DD days based on model and

trajectory analysis remains, i.e., the visualizations showed slightly different results or the influence can be expected to be very small. The other 14 days show a clear influence of DD. Still all 34 days need further investigations, as this classification as false negatives could easily be an effect of the systematic error introduced by our calculation of the BGL. Adjusting the calculation procedure for every DD event could overcome this limitation, but this adjustment could also make the identification of DD days slightly more subjective.

For 15 out of these 34 days the NDL_{MB} was below 2 $\mu g/m^3$ while PM_{10} concentrations at DB ranged from 51 to 139 $\mu g/m^3$ with a mean value of 64 $\mu g/m^3$, indicating on one hand that DD is not the main influence on PM_{10} concentrations at this site, on the other hand that an increase of NDL_{MB} via a reduction of the BGL would allow to reach a reduction below the daily limit value in single cases. A repeated evaluation of the model and trajectory results revealed that for these 15 days the DD identification could easily be biased by subjectivity since results from the models and trajectories do not show a clear picture. An additional four days show an NDL_{MB} below 4 $\mu g/m^3$ while PM_{10} concentrations at DB range from 56 to 92 $\mu g/m^3$—again pointing to both statements. These days could be clearly identified as DD days and thus point to a limitation of the threshold method. Thus, the evaluation of single events remains of great importance, but should be supported by a chemical analysis of the crustal loads as given below exemplarily for two cases.

3.5. Validation of the NDL_{MB} Based on Two Case Studies in 2016

In order to validate the NDL_{MB} chemical analyses of filter samples collected at three sites (Graz Don Bosco, DB; Graz Ost, GO; Gratwein, GW; compare Figure 1) were used to determine the crustal loads. This analysis was performed for three days (23.02.2016, 05.04.2016 and 06.04.2016) featuring desert dust intrusion in was thoroughly described earlier.

For the strong transport event of desert dust in April, measured CLs match the calculated NDL_{MB} very well, indicating that the NDL_{MB} is mainly composed of mineral matter. CLs were found to account for more than 70% of the NDL_{MB} with values ranging from 41.2 $\mu g/m^3$ at GO to 39.0 $\mu g/m^3$ at GW for the 5th of April 2016, compared to the NDL_{MB} of 50.6 $\mu g/m^3$ and from 31.5 $\mu g/m^3$ at GO to 25.3 $\mu g/m^3$ at GW for the 06th of April 2016, compared to the NDL_{MB} of 35.3 $\mu g/m^3$.

For the dust event in February, measured CLs are more than 50% lower (17.7 $\mu g/m^3$ at DB, 16.5 $\mu g/m^3$ at GO and 10.9 $\mu g/m^3$ at GW) than the calculated NDL_{MB} (37.1 $\mu g/m^3$) pointing to additional contributions of other particulate matter sources. This result underlines the need of the threshold criteria. Using those the NDL_{MB} is not allowed to be considered for a reduction, because the BGL is too low. Based on WRF-Chem model forecasts is can also be expected that the SD intrusion during this event was rather weak and other, maybe anthropogenic sources, dominate the NDL.

4. Summary and Conclusions

The study investigates the applicability of the methodology suggested by the European Commission (EC) to assess the contribution of desert dust (DD), to PM_{10} loads in the region of Graz in Southern Austria over a time period of six years from January 2013 to December 2018.

The station Masenberg (MB) could be identified as a suitable regional background station and the BGL_{MB} was calculated without an exclusion of DD affected days. Furthermore thresholds for the calculated BGL_{MB} and the NDL_{MB} of 12 $\mu g/m^3$ and 10 $\mu g/m^3$ were used to identify whether the NDL_{MB} is really defined by DD and may be subtracted. We want to point out that this procedure is a more conservative approach than given in the EC guideline, representing the highest computable BGL, and thus the lowest NDL.

A detailed investigation of all days exceeding the daily limit PM_{10} concentration showed that the risk of undue reductions is rather small. Within 16% of days which were not correctly classified, concentrations were not reduced for 33 days (false negatives), while an undue reduction happened only during five days (false positives). The evaluation of these false negative days reveals the limitations of

the method. Both calculation of NDLs and their restriction via thresholds and interpretation of models and trajectories might be biased.

It is obvious that using the proposed approach the BGL_{MB} will be overestimated as soon as the DD influence holds longer than one day, leading to a corresponding underestimation of the NDL_{MB}. Still, the calculated NDL_{MB} is higher than the crustal loads chemically measured on quartz fiber filters sampled during two DD events in 2016.

Overall the influence of the subtraction of natural sources (i.e., desert dust) from PM_{10} concentrations at two sites in Graz yielded a number of reductions; however, on an annual basis, changes of the amount of days exceeding the daily limit were found to be rather small.

Within this study, we investigated stations in the region of Graz, representing a hot spot regarding PM_{10} concentrations in Austria. Due to the limitation to days exceeding the daily limit, the impact on mean annual concentrations of the proposed approach was not assessed. Additionally, the applicability of the proposed approach to other stations needs further investigation and remains of great importance, but should be supported by a chemical analysis of the crustal loads.

References

1. Pachauri, R.K.; Mayer, L. *Intergovernmental Panel on Climate Change*; Climate change 2014: Synthesis report; Intergovernmental Panel on Climate Change: Geneva, Switzerland, 2015; ISBN 978-92-9169-143-2.

2. Dockery, D.; Pope, A. *Epidemiology of Acute Health Effects: Summary of Time-Series Studies*; Particles in our air: Concentrations and health effects; Wilson, R., Spengler, J.D., Eds.; Harvard University Press: Cambridge, MA, USA, 1997; ISBN 0-674-24077-4.

3. Schwartz, J.; Dockery, D.W.; Neas, L.M. Is Daily Mortality Associated Specifically with Fine Particles? *J. Air Waste Manag. Assoc.* **1996**, *46*, 927–939. [CrossRef] [PubMed]

4. Karagulian, F.; Belis, C.A.; Dora, C.F.C.; Prüss-Ustün, A.M.; Bonjour, S.; Adair-Rohani, H.; Amann, M. Contributions to cities' ambient particulate matter (PM): A systematic review of local source contributions at global level. *Atmos. Environ.* **2015**, *120*, 475–483. [CrossRef]

5. Lenschow, P. Some ideas about the sources of PM10. *Atmos. Environ.* **2001**, *35*, 23–33. [CrossRef]

6. Puxbaum, H.; Gomiscek, B.; Kalina, M.; Bauer, H.; Salam, A.; Stopper, S.; Preining, O.; Hauck, H. A dual site study of PM2.5 and PM10 aerosol chemistry in the larger region of Vienna, Austria. *Atmos. Environ.* **2004**, *38*, 3949–3958. [CrossRef]

7. Barnaba, F.; Bolignano, A.; Di Liberto, L.; Morelli, M.; Lucarelli, F.; Nava, S.; Perrino, C.; Canepari, S.; Basart, S.; Costabile, F.; et al. Desert dust contribution to PM10 loads in Italy: Methods and recommendations addressing the relevant European Commission Guidelines in support to the Air Quality Directive 2008/50. *Atmos. Environ.* **2017**, *161*, 288–305. [CrossRef]

8. Rodríguez, S.; Querol, X.; Alastuey, A.; Kallos, G.; Kakaliagou, O. Saharan dust contributions to PM10 and TSP levels in Southern and Eastern Spain. *Atmos. Environ.* **2001**, *35*, 2433–2447. [CrossRef]

9. Viana, M.; Querol, X.; Alastuey, A.; Cuevas, E.; Rodríguez, S. Influence of African dust on the levels of atmospheric particulates in the Canary Islands air quality network. *Atmos. Environ.* **2002**, *36*, 5861–5875. [CrossRef]

10. European Union. *Establishing Guidelines for Demonstration and Substraction of Exceedances Attributable to Natural Sources Under the Directive 2008/50/EC on Ambient Air Quality and Cleaner Air for Europe*; European Comission Comission Staff Working Paper; SEC(2011) 208 final; European Union: Brussels, Belgium, 2011.

11. Escudero, M.; Querol, X.; Pey, J.; Alastuey, A.; Pérez, N.; Ferreira, F.; Alonso, S.; Rodríguez, S.; Cuevas, E. A methodology for the quantification of the net African dust load in air quality monitoring networks. *Atmos. Environ.* **2007**, *41*, 5516–5524. [CrossRef]

12. Baumann-Stanzer, K.; Greilinger, M.; Kasper-Giebl, A.; Flandorfer, C.; Hieden, A.; Lotteraner, C.; Ortner, M.; Vergeiner, J.; Schauer, G.; Piringer, M. Evaluation of WRF-Chem Model Forecasts of a Prolonged Sahara Dust Episode over the Eastern Alps. *Aerosol Air Qual. Res.* **2018**. [CrossRef]

13. Greilinger, M.; Schauer, G.; Baumann-Stanzer, K.; Skomorowski, P.; Schöner, W.; Kasper-Giebl, A. Contribution of Saharan Dust to Ion Deposition Loads of High Alpine Snow Packs in Austria (1987–2017). *Front. Earth Sci.* **2018**, *6*, 126. [CrossRef]

14. Schauer, G.; Kasper-Giebl, A.; Močnik, G. Increased PM Concentrations during a Combined Wildfire and Saharan Dust Event Observed at High-Altitude Sonnblick Observatory, Austria. *Aerosol Air Qual. Res.* **2016**, *16*, 542–554. [CrossRef]

15. Spangl, W.; Nagl, C. Jahresbericht der Luftgütemessung in Österreich 2017. *REP-0643* **2018**.

16. Pongratz, T. Luftreinhaltung in der Steiermark—Jahresbericht 2017. *Bericht Nr. Lu-07-2018* **2018**.

17. Lazar, R.; Podesser, A. An urban climate analysis of Graz and its significance for urban planning in the tributary valleys east of Graz (Austria). *Atmos. Environ.* **1999**, *33*, 4195–4209. [CrossRef]

18. Spangl, W.; Nagl, C. Jahresbericht der Luftgütemessung in Österreich 2008. *REP-0231* **2009**.

19. Pongratz, T. Luftreinhaltung in der Steiermark—Jahresbericht 2008. *Bericht Nr. Lu-05-09* **2009**.

20. Peng, G.; Puxbaum, H.; Bauer, H.; Jankowski, N.; Shi, Y. Improved source assessment of Si, Al and related mineral components to PM10 based on a daily sampling procedure. *J. Environ. Sci.* **2010**, *22*, 582–588. [CrossRef]

21. Querol, X. PM10 and PM2.5 source apportionment in the Barcelona Metropolitan area, Catalonia, Spain. *Atmos. Environ.* **2001**, *35*, 6407–6419. [CrossRef]

22. Caseiro, A.; Bauer, H.; Schmidl, C.; Pio, C.A.; Puxbaum, H. Wood burning impact on PM10 in three Austrian regions. *Atmos. Environ.* **2009**, *43*, 2186–2195. [CrossRef]

23. Greilinger, M.; Schöner, W.; Winiwarter, W.; Kasper-Giebl, A. Temporal changes of inorganic ion deposition in the seasonal snow cover for the Austrian Alps (1983–2014). *Atmos. Environ.* **2016**, *132*, 141–152. [CrossRef]

24. Kistler, M.; Kasper-Giebl, A.; Cetintas, E.C.; Ramirez-Santa Cruz, C.; Schreiner, E.; Sampaio-Cordeiro-Wagner, L.; Szidat, S.; Zhang, Y. PMinter Project—Analysis of Particulate Matter in Leibnitz and Arnfels. *Final Rep. Report Number CTA-EAC-11/13-6* **2013**.

25. Baumann, K.; Stohl, A. Validation of a Long-Range Trajectory Model Using Gas Balloon Tracks from the Gordon Bennett Cup 95. *J. Appl. Meteorol.* **1997**, *36*, 711–720. [CrossRef]

Supplementary material

This chapter corresponds to the supplementary material of the peer-reviewed publication

Greilinger, M., Zbiral, J., Kasper-Giebl, A. (2019) Desert dust contribution to PM10 loads in Styria (Southern Austria) and impact on exceedance of limit values from 2013-2018. Applied Sciences, 9, 2265, doi: 10.3390/app9112265

applied sciences

MDPI

Supplement

Table S1: Detailed investigation of the days where the subtraction of the NDL$_{MB}$ reduced the PM 10 load at the urban-traffic station Don Bosco (DB) below the limit value of 50µg/m³. Light green = true negative (TN), Dark green = true positive (TP), light red = false negative (FN), dark red = false positive (FP), NA = missing values

Date	DB [µg/m³]	MB [µg/m³]	BGL [µg/m³]	NDL [µg/m³]	DB-NDL [µg/m³]	DD J/N	BGL >12µg/m³	NDL >10µg/m³	
01.01.2013	123,1	8,1	7,4	0,7	123,1	N	-	-	TN
02.01.2013	71,2	9,6	7,8	1,8	71,2	N	-	-	TN
03.01.2013	74,2	6,0	8,1	0,0	74,2	N	-	-	TN
09.01.2013	61,8	5,9	10,1	0,0	61,8	N	-	-	TN
10.01.2013	54,9	4,9	10,9	0,0	54,9	N	-	-	TN
20.01.2013	71,8	6,6	9,1	0,0	71,8	Y	-	-	FN
21.01.2013	71,4	8,4	9,1	0,0	71,4	Y	-	-	FN
26.01.2013	62,0	25,3	9,1	16,2	45,8	N	-	+	TN
27.01.2013	69,9	7,0	10,3	0,0	69,9	N	-	-	TN
28.01.2013	81,2	8,5	10,7	0,0	81,2	N	-	-	TN
29.01.2013	76,9	6,3	10,9	0,0	76,9	N	-	-	TN
30.01.2013	111,6	3,9	10,9	0,0	111,6	N	-	-	TN
01.02.2013	73,4	7,7	11,5	0,0	73,4	N	-	-	TN
04.02.2013	58,1	7,9	12,4	0,0	58,1	N	+	-	TN
05.02.2013	65,9	5,2	12,4	0,0	65,9	N	+	-	TN
12.02.2013	52,9	26,8	11,7	15,1	37,8	Y	-	+	FN
15.02.2013	69,6	18,4	12,6	5,8	63,8	N	+	-	TN
16.02.2013	67,1	18,1	12,8	5,3	61,8	N	+	-	TN
17.02.2013	60,3	19,7	13,3	6,4	53,9	N	+	-	TN
18.02.2013	65,3	27,1	13,7	13,4	51,9	N	+	+	FP
19.02.2013	68,8	20,2	14,1	6,1	62,7	N	+	-	TN
28.02.2013	53,1	11,9	13,9	0,0	53,1	N	+	-	TN
04.03.2013	52,0	23,7	12,7	11,0	41,0	Y	+	+	TP
05.03.2013	63,9	27,6	12,3	15,3	48,6	Y	+	+	TP
06.03.2013	53,8	12,8	12,1	0,7	53,1	Y	+	-	FN
28.03.2013	64,9	31,6	14,3	17,3	47,6	N	+	+	FP
29.03.2013	62,7	13,6	14,9	0,0	62,7	N	+	-	TN
26.04.2013	91,9	23,0	20,7	2,4	89,6	Y	+	-	FN
01.05.2013	53,7	60,5	19,8	40,7	13,0	Y	+	+	TP
06.10.2013	53,7	6,8	13,8	0,0	53,7	N	+	-	TN
09.10.2013	55,2	35,6	13,2	22,4	32,8	N	+	+	FP
10.10.2013	59,2	22,0	13,4	8,6	50,6	N	+	-	TN
07.11.2013	56,6	6,8	9,1	0,0	56,6	N	-	-	TN
28.11.2013	51,9	6,4	7,7	0,0	51,9	N	-	-	TN
02.12.2013	54,5	9,9	7,3	2,6	51,9	N	-	-	TN
03.12.2013	57,1	11,0	7,1	3,9	53,2	N	-	-	TN
04.12.2013	77,5	5,9	7,3	0,0	77,5	N	-	-	TN
05.12.2013	78,8	11,4	7,1	4,3	74,5	N	-	-	TN
09.12.2013	67,7	7,5	7,7	0,0	67,7	N	-	-	TN
16.12.2013	51,9	NA	7,6	NA	NA	N	-	NA	-
19.12.2013	56,8	NA	7,5	NA	NA	N	-	NA	-
20.12.2013	79,4	11,8	7,3	4,5	74,9	N	-	-	TN
21.12.2013	51,7	11,9	7,0	4,9	46,8	N	-	-	TN
23.12.2013	63,8	7,1	7,0	0,1	63,7	N	-	-	TN
13.01.2014	50,6	4,8	8,4	0,0	50,6	N	-	-	TN
14.01.2014	55,3	12,0	9,1	2,9	52,4	N	-	-	TN
27.01.2014	84,8	11,2	11,5	0,0	84,8	N	-	-	TN
28.01.2014	97,4	16,0	11,1	4,9	92,5	N	-	-	TN
29.01.2014	60,3	36,0	10,6	25,4	34,9	N	-	+	TN
30.01.2014	84,8	26,8	10,7	16,1	68,7	Y	-	+	FN
31.01.2014	52,9	21,2	10,9	10,3	42,6	Y	-	+	FN
05.02.2014	70,5	7,9	11,4	0,0	70,5	N	-	-	TN
06.02.2014	75,6	6,6	11,7	0,0	75,6	N	-	-	TN
25.02.2014	54,8	19,6	13,7	5,9	48,9	N	+	-	TN
12.03.2014	65,8	21,2	16,4	4,8	61,0	N	+	-	TN
13.03.2014	58,1	30,8	16,0	14,8	43,3	Y	+	+	TP
14.03.2014	64,5	31,4	15,9	15,5	49,0	Y	+	+	TP
02.04.2014	53,9	42,9	16,3	26,6	27,3	Y	+	+	TP
03.04.2014	51,6	30,3	16,6	13,7	37,9	Y	+	+	TP
07.10.2014	52,1	18,1	12,2	5,9	46,2	Y	+	-	FN
30.10.2014	54,5	21,1	11,6	9,5	45,0	N	-	-	TN
31.10.2014	52,3	23,9	11,2	12,7	39,6	N	-	+	TN

Date									
27.11.2014	59,3	15,8	6,8	9,0	50,3	Y	-	-	FN
11.12.2014	66,0	2,5	4,8	0,0	66,0	N	-	-	TN
12.12.2014	56,6	4,3	4,6	0,0	56,6	N	-	-	TN
15.12.2014	66,6	4,3	4,4	0,0	66,6	Y	-	-	FN
16.12.2014	70,9	9,2	4,3	4,9	66,0	Y	-	-	FN
18.12.2014	52,5	4,1	4,4	0,0	52,5	N	-	-	TN
19.12.2014	62,0	3,4	4,6	0,0	62,0	N	-	-	TN
23.12.2014	50,5	3,5	4,9	0,0	50,5	N	-	-	TN
24.12.2014	55,3	2,8	4,9	0,0	55,3	N	-	-	TN
01.01.2015	102,3	3,9	4,8	0,0	102,3	N	-	-	TN
02.01.2015	93,5	3,5	5,1	0,0	93,5	N	-	-	TN
03.01.2015	59,2	8,0	5,0	3,0	56,2	N	-	-	TN
08.01.2015	77,4	4,3	5,6	0,0	77,4	N	-	-	TN
09.01.2015	83,1	3,6	5,6	0,0	83,1	N	-	-	TN
13.01.2015	54,4	2,6	5,6	0,0	54,4	N	-	-	TN
27.01.2015	56,2	NA	6,4	NA	NA	N	-	NA	-
03.02.2015	52,8	7,9	10,2	0,0	52,8	N	-	-	TN
04.02.2015	56,6	9,0	10,4	0,0	56,6	N	-	-	TN
07.02.2015	55,1	11,8	10,9	0,9	54,2	Y	-	-	FN
13.02.2015	55,6	16,3	11,3	5,0	50,6	N	-	-	TN
14.02.2015	62,9	19,3	11,7	7,7	55,3	N	-	-	TN
15.02.2015	57,8	16,9	12,0	4,9	52,9	N	-	-	TN
16.02.2015	72,1	31,0	11,5	19,5	52,6	N	-	+	TN
17.02.2015	61,2	26,8	11,6	15,2	46,0	N	-	+	TN
19.02.2015	58,7	16,9	11,9	5,0	53,7	N	-	-	TN
20.02.2015	62,4	10,9	12,2	0,0	62,4	N	+	-	TN
16.03.2015	53,6	24,3	17,5	6,8	46,8	Y	+	-	FN
17.03.2015	51,5	33,4	16,6	16,8	34,7	Y	+	+	TP
20.03.2015	52,2	30,7	17,0	13,7	38,5	Y	+	+	TP
24.03.2015	54,7	35,8	16,9	18,9	35,8	Y	+	+	TP
28.10.2015	54,4	13,0	6,3	6,7	47,7	N	-	-	TN
29.10.2015	51,0	6,0	6,7	0,0	51,0	Y	-	-	FN
04.11.2015	62,3	10,8	7,3	3,5	58,8	Y	-	-	FN
05.11.2015	55,9	11,1	7,3	3,8	52,1	Y	-	-	FN
17.11.2015	60,6	8,1	5,7	2,4	58,2	N	-	-	TN
18.11.2015	53,9	3,6	6,1	0,0	53,9	N	-	-	TN
30.11.2015	55,0	2,5	5,9	0,0	55,0	N	-	-	TN
01.12.2015	56,3	1,3	5,8	0,0	56,3	N	-	-	TN
03.12.2015	56,0	11,7	5,0	6,7	49,3	N	-	-	TN
12.12.2015	85,1	2,1	5,1	0,0	85,1	N	-	-	TN
13.12.2015	73,1	2,8	5,6	0,0	73,1	N	-	-	TN
15.12.2015	50,8	6,8	6,1	0,7	50,1	N	-	-	TN
16.12.2015	64,9	8,3	6,4	1,9	63,0	N	-	-	TN
22.12.2015	51,0	3,3	7,4	0,0	51,0	N	-	-	TN
23.12.2015	50,8	4,1	7,4	0,0	50,8	N	-	-	TN
26.12.2015	52,4	2,7	7,1	0,0	52,4	N	-	-	TN
28.12.2015	57,5	20,3	6,5	13,8	43,7	Y	-	+	FN
29.12.2015	67,5	18,1	6,5	11,6	55,9	Y	-	+	FN
01.01.2016	98,7	4,1	6,7	0,0	98,7	N	-	-	TN
02.01.2016	59,4	11,3	6,4	4,9	54,5	N	-	-	TN
05.01.2016	77,4	2,6	7,4	0,0	77,4	N	-	-	TN
06.01.2016	98,1	3,0	7,5	0,0	98,1	N	-	-	TN
07.01.2016	74,3	4,0	7,8	0,0	74,3	N	-	-	TN
08.01.2016	67,5	3,4	8,0	0,0	67,5	N	-	-	TN
09.01.2016	67,9	3,8	7,9	0,0	67,9	N	-	-	TN
15.01.2016	53,4	3,8	7,4	0,0	53,4	N	-	-	TN
19.01.2016	59,3	17,8	6,0	11,8	47,5	N	-	+	TN
20.01.2016	67,5	7,9	5,8	2,1	65,4	N	-	-	TN
21.01.2016	55,0	6,0	5,9	0,1	54,9	N	-	-	TN
22.01.2016	51,1	15,5	5,6	9,9	41,2	N	-	-	TN
23.01.2016	63,0	9,4	5,9	3,5	59,5	N	-	-	TN
24.01.2016	65,2	5,8	6,0	0,0	65,2	N	-	-	TN
25.01.2016	78,8	2,1	6,2	0,0	78,8	N	-	-	TN
26.01.2016	76,8	2,5	6,2	0,0	76,8	N	-	-	TN
27.01.2016	76,8	8,7	5,9	2,8	74,0	N	-	-	TN
28.01.2016	66,2	7,4	6,1	1,3	64,9	N	-	-	TN
02.02.2016	51,6	2,9	6,3	0,0	51,6	N	-	-	TN
05.04.2016	87,3	63,6	13,0	50,6	36,7	Y	+	+	TP
06.04.2016	68,1	48,3	13,0	35,3	32,8	Y	+	+	TP
16.11.2016	51,8	2,6	5,5	0,0	51,8	N	-	-	TN
17.11.2016	55,5	2,0	5,5	0,0	55,5	N	-	-	TN
30.11.2016	50,6	4,2	5,8	0,0	50,6	N	-	-	TN
01.12.2016	60,9	4,4	5,7	0,0	60,9	N	-	-	TN
05.12.2016	61,8	13,1	5,9	7,3	54,6	N	-	-	TN
06.12.2016	74,7	4,4	6,2	0,0	74,7	N	-	-	TN

Date									
07.12.2016	61,1	10,2	6,0	4,2	56,9	N	-	-	TN
09.12.2016	75,9	2,8	6,0	0,0	75,9	N	-	-	TN
10.12.2016	65,6	2,9	5,8	0,0	65,6	N	-	-	TN
11.12.2016	56,5	3,5	5,7	0,0	56,5	N	-	-	TN
14.12.2016	66,0	2,2	5,6	0,0	66,0	N	-	-	TN
17.12.2016	52,5	3,1	5,3	0,0	52,5	N	-	-	TN
18.12.2016	57,2	4,2	5,3	0,0	57,2	N	-	-	TN
19.12.2016	58,3	9,6	5,1	4,5	53,8	N	-	-	TN
25.12.2016	60,1	2,5	4,9	0,0	60,1	N	-	-	TN
26.12.2016	53,0	2,7	5,5	0,0	53,0	N	-	-	TN
30.12.2016	55,9	2,2	5,8	0,0	55,9	N	-	-	TN
31.12.2016	83,2	2,7	5,6	0,0	83,2	N	-	-	TN
01.01.2017	157,2	2,0	5,4	0,0	157,2	N	-	-	TN
02.01.2017	89,4	4,1	5,6	0,0	89,4	N	-	-	TN
03.01.2017	71,5	5,3	5,8	0,0	71,5	N	-	-	TN
04.01.2017	60,1	3,3	5,8	0,0	60,1	N	-	-	TN
11.01.2017	81,9	9,3	6,9	2,4	79,5	N	-	-	TN
12.01.2017	96,3	4,4	7,3	0,0	96,3	N	-	-	TN
17.01.2017	52,2	9,9	7,8	2,1	50,1	N	-	-	TN
18.01.2017	77,5	12,1	7,8	4,3	73,2	N	-	-	TN
19.01.2017	78,4	9,5	7,9	1,7	76,8	N	-	-	TN
20.01.2017	85,7	7,9	8,0	0,0	85,7	N	-	-	TN
21.01.2017	94,1	3,3	8,1	0,0	94,1	N	-	-	TN
22.01.2017	105,0	6,2	7,8	0,0	105,0	N	-	-	TN
23.01.2017	139,6	9,4	7,7	1,7	137,9	Y	-	-	FN
24.01.2017	113,3	15,6	7,9	7,7	105,6	Y	-	-	FN
25.01.2017	57,1	13,8	8,5	5,3	51,8	Y	-	-	FN
27.01.2017	67,5	12,9	8,8	4,1	63,4	N	-	-	TN
28.01.2017	70,6	9,1	9,6	0,0	70,6	N	-	-	TN
29.01.2017	86,2	5,4	10,4	0,0	86,2	N	-	-	TN
30.01.2017	81,5	6,0	10,5	0,0	81,5	N	-	-	TN
31.01.2017	100,5	9,3	10,5	0,0	100,5	N	-	-	TN
01.02.2017	114,2	6,1	10,7	0,0	114,2	N	-	-	TN
02.02.2017	95,1	5,3	10,6	0,0	95,1	N	-	-	TN
09.02.2017	62,1	21,9	9,1	12,8	49,3	N	-	+	TN
10.02.2017	58,0	18,1	9,0	9,1	48,9	N	-	-	TN
11.02.2017	60,8	18,7	8,8	9,9	50,9	N	-	-	TN
12.02.2017	71,1	25,7	8,3	17,4	53,7	Y	-	+	FN
13.02.2017	64,7	23,2	8,4	14,8	49,9	Y	-	+	FN
14.02.2017	54,0	7,3	8,9	0,0	54,0	Y	-	-	FN
15.02.2017	57,8	NA	8,7	NA	NA	Y	-	NA	-
16.02.2017	56,9	4,5	8,8	0,0	56,9	Y	-	-	FN
17.02.2017	64,2	7,7	8,8	0,0	64,2	Y	-	-	FN
21.02.2017	72,2	2,7	8,8	0,0	72,2	N	-	-	TN
22.02.2017	50,5	7,3	8,7	0,0	50,5	N	-	-	TN
23.02.2017	51,9	7,0	8,6	0,0	51,9	Y	-	-	FN
22.08.2017	71,1	8,8	9,1	0,0	71,1	N	-	-	TN
20.10.2017	57,6	17,9	7,3	10,6	47,0	N	-	+	TN
02.11.2017	53,4	4,3	7,5	0,0	53,4	N	-	-	TN
15.11.2017	51,8	3,4	6,3	0,0	51,8	N	-	-	TN
17.11.2017	51,1	6,7	6,1	0,6	50,5	Y	-	-	FN
21.11.2017	57,6	3,3	5,7	0,0	57,6	N	-	-	TN
22.11.2017	66,9	6,3	5,4	0,9	66,0	N	-	-	TN
23.11.2017	60,9	4,8	5,0	0,0	60,9	N	-	-	TN
24.11.2017	62,3	9,2	4,9	4,3	58,0	N	-	-	TN
28.11.2017	53,8	3,8	4,9	0,0	53,8	N	-	-	TN
04.12.2017	76,3	4,6	4,6	0,0	76,3	N	-	-	TN
05.12.2017	65,9	4,5	4,6	0,0	65,9	N	-	-	TN
07.12.2017	72,2	2,5	4,7	0,0	72,2	N	-	-	TN
19.12.2017	59,1	5,0	4,0	1,0	58,1	N	-	-	TN
20.12.2017	52,1	5,1	4,0	1,1	51,0	N	-	-	TN
21.12.2017	63,7	3,1	4,1	0,0	63,7	N	-	-	TN
22.12.2017	57,4	2,7	4,0	0,0	57,4	N	-	-	TN
24.12.2017	53,0	3,9	3,8	0,1	52,9	N	-	-	TN
26.12.2017	51,0	3,4	3,5	0,0	51,0	N	-	-	TN
31.12.2017	52,8	4,0	3,8	0,2	52,6	N	-	-	TN
01.01.2018	89,9	2,4	4,7	0,0	89,9	N	-	-	TN
05.01.2018	60,1	2,9	4,7	0,0	60,1	N	-	-	TN
23.01.2018	61,7	3,6	6,6	0,0	61,7	N	-	-	TN
24.01.2018	51,5	6,2	6,6	0,0	51,5	N	-	-	TN
25.01.2018	63,2	6,7	6,8	0,0	63,2	N	-	-	TN
26.01.2018	83,3	6,6	7,3	0,0	83,3	N	-	-	TN
29.01.2018	63,5	3,1	7,5	0,0	63,5	N	-	-	TN
09.02.2018	70,9	16,4	9,2	7,2	63,7	Y	-	-	FN
10.02.2018	89,6	17,7	9,4	8,3	81,3	Y	-	-	FN

11.02.2018	59,2	12,9	9,9	3,0	56,2	N	-	-	TN
15.02.2018	64,8	12,6	13,6	0,0	64,8	N	+	-	TN
16.02.2018	79,1	12,0	14,7	0,0	79,1	N	+	-	TN
17.02.2018	61,3	15,4	15,8	0,0	61,3	N	+	-	TN
21.02.2018	51,7	9,6	16,6	0,0	51,7	N	+	-	TN
28.02.2018	67,4	28,0	14,2	13,8	53,6	N	+	+	FP
01.03.2018	100,6	41,0	13,7	27,3	73,3	N	+	+	FP
02.03.2018	128,8	37,4	13,6	23,8	105,0	Y	+	+	TP
03.03.2018	90,5	40,7	13,5	27,2	63,3	Y	+	+	TP
04.03.2018	87,2	39,9	13,7	26,2	61,0	Y	+	+	TP
05.03.2018	73,2	17,9	14,5	3,4	69,8	Y	+	-	FN
06.03.2018	55,6	12,8	14,9	0,0	55,6	Y	+	-	FN
07.03.2018	55,1	8,1	15,0	0,0	55,1	Y	+	-	FN
09.03.2018	60,1	6,1	15,2	0,0	60,1	N	+	-	TN
26.03.2018	62,8	24,2	9,2	15,0	47,8	N	-	+	TN
27.03.2018	53,7	13,6	9,6	4,0	49,7	N	-	-	TN
12.10.2018	51,2	37,1	17,3	19,8	31,4	Y	+	+	TP
16.10.2018	56,6	22,4	17,0	5,4	51,2	N	+	-	TN
17.10.2018	52,6	17,2	17,4	0,0	52,6	N	+	-	TN
06.11.2018	58,2	6,2	8,1	0,0	58,2	N	-	-	TN
07.11.2018	62,9	6,2	8,0	0,0	62,9	Y	-	-	FN
01.12.2018	61,7	6,9	7,1	0,0	61,7	N	-	-	TN
02.12.2018	67,6	6,2	7,0	0,0	67,6	N	-	-	TN
03.12.2018	65,9	2,9	6,9	0,0	65,9	N	-	-	TN
07.12.2018	64,9	4,5	6,9	0,0	64,9	N	-	-	TN
17.12.2018	64,5	5,2	6,2	0,0	64,5	N	-	-	TN
18.12.2018	65,7	7,0	6,1	0,9	64,8	N	-	-	TN
20.12.2018	59,9	8,2	6,9	1,3	58,6	N	-	-	TN
21.12.2018	55,4	4,8	7,0	0,0	55,4	N	-	-	TN
28.12.2018	51,5	7,2	6,9	0,3	51,2	N	-	-	TN

Chapter 4
Identification of light absorbing PM using filters from air quality monitoring networks

Background and aim

The scientific literature reports carbonaceous light absorbing particles and mineral dust to be the main actors of light absorption in the atmosphere (Bergstrom et al., 2007; Moosmüller et al., 2009). The carbonaceous light absorbing particles can be divided into highly light absorbing carbon particles, termed 'Black Carbon (BC)' or 'Light Absorbing Carbon (LAC)' and weakly absorbing organic carbon particles, termed 'Brown Carbon (BrC)' or loosely "organic carbon" (Bergstrom et al., 2007; Moosmüller et al., 2009).

The optical properties, especially scattering and absorption properties of PM, are widely used to differentiate between the different light absorbing particles. A common approach is the investigation of the wavelength dependence of the absorption and scattering coefficients σ_{abs} and σ_{scat}. Based on their measurements at different wavelengths also the extinction coefficient ($\sigma_{ext} = \sigma_{scat} + \sigma_{abs}$) and the Single Scattering Albedo (SSA) can be computed. Thereby the SSA is defined as:

$$SSA = \frac{\sigma_{scat}}{\sigma_{scat} + \sigma_{abs}} = \frac{\sigma_{scat}}{\sigma_{ext}}$$

Once the respective coefficients are determined at different wavelengths, a power-law fit ($y=b*x^{-\alpha}$) can be applied to obtain the respective exponents (α).

$$\sigma_{abs} = b_{abs} * \lambda^{-\alpha_{abs}}$$

$$\sigma_{scat} = b_{scat} * \lambda^{-\alpha_{scat}}$$

$$\sigma_{ext} = b_{ext} * \lambda^{-\alpha_{ext}}$$

$$SSA = b_{SSA} * \lambda^{-\alpha_{SSA}}$$

These exponents can then be used to distinguish the different light absorbing particles such as desert dust, BC or BrC (e.g. Fialho et al., 2005; Meloni et al., 2006). In case of σ_{ext} the respective exponent α_{ext} is often referred to as Angström exponent å.

Coen et al. (2003) developed a new and very sensitive Saharan dust detection method, using the inversion of the wavelength dependence of the SSA during Saharan dust occurrence as indicator. Based on one-hour time resolved σ_{abs} and σ_{scat} measurements at different wavelengths measured from March 2001 to December 2002 at the high alpine site Jungfraujoch, the wavelength dependence of the SSA was investigated. They found (1) an increase of σ_{scat}, σ_{abs} and consequently σ_{ext}, (2) a wavelength independence of σ_{scat} and σ_{ext} resulting in a vanishing of the respective exponents in the power-law fit, (3) a larger absorption exponent and (4) a negative SSA exponent (α_{SSA}) during the presence of Saharan dust. The resulting negative exponent α_{SSA} is due to the larger size of mineral aerosol, which induced the wavelength independence of σ_{scat} due to the dominance of geometric optics. The larger wavelength dependence of σ_{abs} is linked to the Saharan dust chemical composition (e.g. (Sokolik and Toon, 1999) an thus its colour.

A common on-line filter based instrument for the measurement of the absorption coefficient σ_{abs} at different wavelengths is an aethalometer. Using this instrument for the real-time

measurements of the ATN, air is drawn through a filter and the ATN of the light passing through the sample area is measured to compute σ_{abs} at the different wavelength. Subsequently σ_{abs} is expressed for all wavelengths as the result of an additive contribution. The basic idea behind decoupling σ_{abs} into different source contributions is exemplarily shown by the approach of Fialho et al. (2005) to differentiate between dust (σ_{dust}) and BC particles (σ_{BC}). They used the following approach to decouple the influence of Saharan dust and BC at Pico Mountain in the Azores Island:

$$\sigma_{abs} = \sigma_{BC} + \sigma_{dust}$$

To determine the respective absorption exponents α, the power-law fit as given previously is applied to differentiate the contributions of light absorbing particles.

$$\sigma_{abs} = \sigma_{BC} + \sigma_{dust} = b_{BC} * \lambda^{-\alpha_{BC}} + b_{dust} * \lambda^{-\alpha_{dust}}$$

Depending on the chosen source contributions in various studies, different values for the absorption exponent α_{abs} were achieved which are listed in Table 6.

Table 6: Reported values for the source-attibuted absorption exponent α_{abs} as denoted in the respective studies.

Coen et al. (2003)	Fialho et al. (2005)	Sandradewi et al. (2008)	Schauer et al. (2016)
$\alpha_{SDE} = 1.0$	$\alpha_{BC} = 0.8 +/- 0.1$	$\alpha_{traffic} = 1.1$	$\alpha_{wildfires} = 1.3$
$\alpha_{non-SDE} = 1.5\text{-}1.8$	$\alpha_{dust} = 2.9 +/- 0.2$	$\alpha_{wb} = 1.6\text{-}2.1$	$\alpha_{dust} = 3.0$

Schauer et al. (2016) adopted the approach of Fialho et al. (2005) and Coen et al. (2003) for the high alpine Global Atmospheric Watch (GAW) site Hoher Sonnblick in the Austrian Alps to distinguish between a wildfire and a Saharan dust contribution during a combined event. Both, Saharan dust and Brown Carbon, a common tracer for wood burning aerosol, cause an increased wavelength dependence of the σ_{scat} and σ_{abs}, which has to be regarded in the respective evaluations. The approach of Schauer et al. (2016) was further improved to establish an on-line Saharan dust detection, introducing a so called Saharan Dust Index (SDI) due to on-line measurements of the aerosol optical properties and hence the inversion of the α_{SSA}. Such an identification method is especially useful for investigations regarding the frequency of the occurrence of Saharan dust episodes and interpretations of other aerosol parameters such as particle mass, particle numbers or particle size distributions. The implementation of such an algorithm into the aerosol monitoring program enables the possibility of an internal alert system for the occurrence of mineral dust events.

The increased wavelength dependence of σ_{abs} during the presence of desert dust in the atmosphere opens the possibility to develop a method to identify or even quantify desert dust collected on filters loaded within the air quality monitoring networks. Of course a quantification is possible using a detailed chemical analysis of the respective filters, but thereby the filter material acts as a limiting factor. Besides, this kind of analysis is quite time consuming and cost-intensive. Using a transmissometer (OT-21, Magee Scientific) offers the possibility to apply this approach to attenuation measurements at two different wavelengths (880 nm and 370 nm) of filters sampled within the Austrian air quality monitoring networks of the respective provincial governments. It is well known that the attenuation in the near infrared spectrum is dominated by BC and cross sensitivities to mineral dust or organic carbon compounds (BrC) are lowest whereas they strongly enhance the attenuation in the UV (Petzold et al., 2013; Sandradewi et al., 2008). Thus, online ATN measurements at 880nm e.g. using an aethalometer, are commonly used to determine BC concentrations, more precisely equivalent BC (eBC) according to Petzold et al. (2013), using the relationship:

$$eBC = \frac{1}{\sigma} * \frac{\Delta ATN}{\Delta t} * \frac{A}{Q}$$

Thereby σ is the particle mass attenuation cross section of eBC.

The relationship between ATN and eBC concentration is not linear due to the fact that both scattering and absorbing particles on the filter alter the internal reflection of the filter in a way

that it changes the absorption of the aerosol/filter combination. This non-linearity represents the so called 'filter loading effect'. Due to this, as the filter gets darker, eBC concentrations tend to be underestimated. Additionally, scattering aerosol gets interpreted as eBC as well. Therefore empirical correction functions are needed to take these effects into account. Besides the determination of the 'filter loading effect', it is crucial to determine also MAC, the respective mass absorption cross section of eBC at 880 nm. It is well known that these two parameters depend on the aerosol type and have thus be evaluated separately for different station types or locations. Still, the high correlation between ATN measured at 880nm and EC was already shown by Moosmüller et al. (2009) and Weingartner et al. (2003).

Within the presented article two different approaches based on previous works from Drinovec et al. (2015) and Virkkula et al. (2007) are compared to derive a relationship between the optical ATN measurements and the thermal-optically determined Elemental Carbon (EC) from filters loaded within the Austrian air quality monitoring networks. The 'filter loading effect' represented by the so-called 'filter loading parameter k' and the particle absorption cross section MAC, needed for the determination of BC using the ATN measurements from the OT-21 transmissometer at 880 nm, were computed. MAC is presented as σ based on the relationship MAC=σ/C and C=2.14 according to Weingartner et al. (2003) throughout the article. The computation of both parameters, k and MAC (σ), is a mandatory step to investigate eBC from different station types (urban-traffic, rural-background and remote), based on the ATN measurements only.

The approach based on Virkkula et al. (2007) was already used by Davy et al. (2017) investigating BC concentrations based on reflectance and transmittance measurements of PM_{10} samples of different filter materials for urban stations in London (UK). These investigations represent the first mandatory steps to further investigate the source contributions, as k and MAC (σ) has to be retrieved when ATN measurements are used to determine the respective contributions at different wavelengths.

Further investigations were planned to determine k and MAC (σ) for the UV, using a representative tracer, such as for example the iron concentration for desert dust, analogous to the methodology applied for the determination of BC. Due to the fact that almost all filters sampled at the air quality monitoring stations were overloaded for the measurements in the UV at 370 nm, no ATN in the UV could be measured. Thus, only the ATN measurements of the filters at 880 nm are available and were used for further investigations, serving as a first step towards a refinement of the method for the quantification of mineral dust also.

The presented paper highlights the complexity of optical measurements based on ATN and hence the complexity to quantify mineral dust on filters exposed to ambient air, carrying also other particles besides mineral dust

Literature

Bergstrom, R.W., Pilewskie, P., Russell, P.B., Redemann, J., Bond, T.C., Quinn, P.K., Sierau, B., 2007. Spectral absorption properties of atmospheric aerosols. Atmos. Chem. Phys. 7.

Coen, M.C., Weingartner, E., Schaub, D., Hueglin, C., Corrigan, C., Schwikowski, M., Baltensperger, U., 2003. Saharan dust events at the Jungfraujoch: detection by wavelength dependence of the single scattering albedo and analysis of the events during the years 2001 and 2002. Atmospheric Chemistry and Physics Discussions 3, 5547–5594.

Davy, P.M., Tremper, A.H., Nicolosi, E.M.G., Quincey, P., Fuller, G.W., 2017. Estimating particulate black carbon concentrations using two offline light absorption methods applied to four types of filter media. Atmospheric Environment 152, 24–33. https://doi.org/10.1016/j.atmosenv.2016.12.010

Drinovec, L., Močnik, G., Zotter, P., Prévôt, A.S.H., Ruckstuhl, C., Coz, E., Rupakheti, M., Sciare, J., Müller, T., Wiedensohler, A., Hansen, A.D.A., 2015. The "dual-spot" Aethalometer: an improved measurement of aerosol black carbon with real-time loading compensation. Atmospheric Measurement Techniques 8, 1965–1979. https://doi.org/10.5194/amt-8-1965-2015

Fialho, P., Hansen, A.D.A., Honrath, R.E., 2005. Absorption coefficients by aerosols in remote areas: a new approach to decouple dust and black carbon absorption coefficients using seven-wavelength Aethalometer data. Journal of Aerosol Science 36, 267–282. https://doi.org/10.1016/j.jaerosci.2004.09.004

Meloni, D., di Sarra, A., Pace, G., Monteleone, F., 2006. Aerosol optical properties at Lampedusa (Central Mediterranean). 2. Determination of single scattering albedo at two wavelengths for different aerosol types. Atmos. Chem. Phys. 13.

Moosmüller, H., Chakrabarty, R.K., Arnott, W.P., 2009. Aerosol light absorption and its measurement: A review. Journal of Quantitative Spectroscopy and Radiative Transfer 110, 844–878. https://doi.org/10.1016/j.jqsrt.2009.02.035

Petzold, A., Ogren, J.A., Fiebig, M., Laj, P., Li, S.-M., Baltensperger, U., Holzer-Popp, T., Kinne, S., Pappalardo, G., Sugimoto, N., Wehrli, C., Wiedensohler, A., Zhang, X.-Y., 2013. Recommendations for reporting "black carbon" measurements. Atmospheric Chemistry and Physics 13, 8365–8379. https://doi.org/10.5194/acp-13-8365-2013

Sandradewi, J., Prévôt, A.S.H., Szidat, S., Perron, N., Alfarra, M.R., Lanz, V.A., Weingartner, E., Baltensperger, U., 2008. Using Aerosol Light Absorption Measurements for the Quantitative Determination of Wood Burning and Traffic Emission Contributions to Particulate Matter. Environ. Sci. Technol. 42, 3316–3323. https://doi.org/10.1021/es702253m

Schauer, G., Kasper-Giebl, A., Močnik, G., 2016. Increased PM Concentrations during a Combined Wildfire and Saharan Dust Event Observed at High-Altitude Sonnblick Observatory, Austria. Aerosol and Air Quality Research 16, 542–554. https://doi.org/10.4209/aaqr.2015.05.0337

Sokolik, I.N., Toon, O.B., 1999. Incorporation of mineralogical composition into models of the radiative properties of mineral aerosol from UV to IR wavelengths. J. Geophys. Res. 104, 9423–9444. https://doi.org/10.1029/1998JD200048

Virkkula, A., Mäkelä, T., Hillamo, R., Yli-Tuomi, T., Hirsikko, A., Hämeri, K., Koponen, I.K., 2007. A Simple Procedure for Correcting Loading Effects of Aethalometer Data. Journal of the Air & Waste Management Association 57, 1214–1222. https://doi.org/10.3155/1047-3289.57.10.1214

Weingartner, E., Saathoff, H., Schnaiter, M., Streit, N., Bitnar, B., Baltensperger, U., 2003. Absorption of light by soot particles: determination of the absorption coefficient by means of aethalometers. Journal of Aerosol Science 34, 1445–1463. https://doi.org/10.1016/S0021-8502(03)00359-8

Article (peer-reviewed)

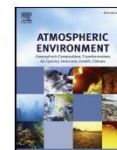This chapter corresponds to the following peer-reviewed publication in its original form:

Greilinger, M., Drinovec, L., Močnik, G., & Kasper-Giebl, A. (2019). Evaluation of measurements of light transmission for the determination of black carbon on filters from different station types. Atmospheric Environment, 198, 1-11, doi: 10.1016/j.atmosenv.2018.10.017

Marion Greilinger conceived the study, designed the figures and wrote the text, . Luka Drinovec and Grisa Močnik helped to set up the models and to interpret the data, Anne Kasper-Giebl contributed to the text, analysis and overall study design.

Evaluation of measurements of light transmission for the determination of black carbon on filters from different station types

Marion Greilinger[a,b,*], Luka Drinovec[c,d], Griša Močnik[c,d], Anne Kasper-Giebl[b]

[a] Zentralanstalt für Meteorologie und Geodynamik (ZAMG),Vienna, 1100, Austria
[b] Technical University of Vienna, Institute for Chemical Technologies and Analytics, Vienna, 1060, Austria
[c] Aerosol d.o.o., Ljubljana, 1000, Slovenia
[d] Jožef Stefan Institute, Ljubljana, 1000, Slovenia

ABSTRACT

We compared two approaches (denoted as Virkkula" and "Drinovec" equations) for the determination of black carbon via attenuation measurements with a transmissometer OT-21 (Magee Scientific) on quartz fiber filters from different station types (urban-traffic, rural-background and remote) within the Austrian air monitoring network. First, we evaluated the entire data set to compare the performance of the models in the determination of the loading parameter k and the mass attenuation cross section σ. Then we investigate k and σ for different station types. The data set comprises 299 filters, all representative for 24 h samples collected with High-Volume-Samplers. Mass concentrations ranged from approximately 5-100 µg m^{-3} and covered all seasons.

Both approaches give statistically indistinguishable results of k with values of $1.00*10^{-3}$ ($\pm 2*10^{-4}$) and $0.97*10^{-3}$ ($\pm 1*10^{-4}$), respectively, if the entire data set is evaluated. The "Drinovec" approach gives slightly lower values for σ than "Virkkula" with values of $32.1 \, m^2 \, g^{-1}$ ($\pm 1.1 \, m^2 \, g^{-1}$) and $35.3 \, m^2 \, g^{-1}$ ($\pm 1.9 \, m^2 \, g^{-1}$). If the data set is restricted to ATN < 300 only, no statistically relevant changes are obtained for k and σ using the "Virkkula" equation. Applying the "Drinovec" equation both parameters, k and σ increase when the data set is restricted.

The investigation of the different station types yields values of k statistically not different from zero, whereas σ values are different for the respective station types. Highest values of $\sigma = 33.7 \, m^2 \, g^{-1}$ ($\pm 1.4 \, m^2 \, g^{-1}$) were observed for the remote, followed by $\sigma = 31.8 \, m^2 \, g^{-1}$ ($\pm 0.5 \, m^2 \, g^{-1}$) for the rural-background station and lowest values of $\sigma = 24.4 \, m^2 \, g^{-1}$ ($\pm 0.5 \, m^2 \, g^{-1}$) for the urban-traffic stations, possibly reflecting the respective aerosol type.

Based on the results for k and σ using either overall values or station type specific values we performed an extensive validation, discussing the application of the transmissometer measurements for a quick, easy and non-destructive quantification of eBC on either fresh sampled or archived filters of different station types. Applying the method for stations not classified as urban, rural or remote a deviation of eBC and EC values up to 23% can be expected. If the station type is known and the respective k and σ values are used this deviation goes down to 10% or lower. This would allow users to obtain long-term time-series going back to times when no on-line instruments were existing, and to obtain these data sets for sites where no on-line instruments are installed even now.

1. Introduction

Carbonaceous particles are one of the main constituents of ambient particulate matter. The carbonaceous fraction can be separated into organic carbon (OC), elemental carbon (EC) and carbonate based on its thermal stability, and is regulated in these terms in the EU Directive 2008/50/EC. The fraction of carbonaceous particles strongly absorbing

visible light is commonly called black carbon (BC) (Bond et al., 2013). While the thermally refractive part of carbonaceous matter (EC) also exhibits strong light absorption, the relationship between BC and EC depends on a number of parameters like particle size, absorption enhancing coatings, interaction with the filters (Moosmüller et al., 2009) and also on the thermal protocol used for analysis.

A variety of methods for the on-line or off-line measurements of EC
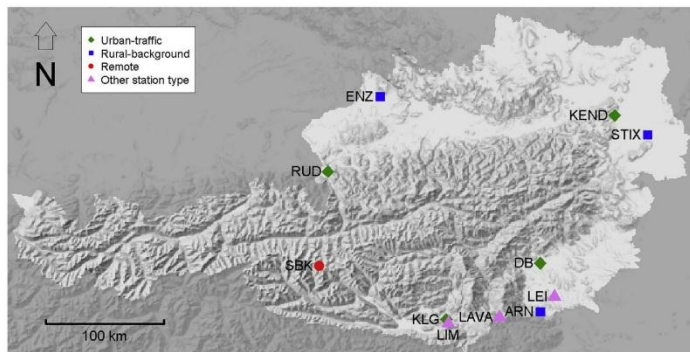

Fig. 1. Location of the sampling sites used in this study. Quartz fiber filters of 4 urban-traffic stations (green diamonds), 4 rural-background stations (blue squares) and one remote station (red dots) were used for the model setup and model testing. Three stations (purple triangles) of different types than the others were used for model testing. (For interpretation of the references to colour in this figure legend, the reader is referred to the Web version of this article.)

or BC exists. A very frequently used on-line instrument is the Aethalometer, determining light absorption by measuring the transmission of light through a continuously darkening filter spot (Drinovec et al., 2015). Common setups for off-line measurements are thermal methods (e.g. Cachier et al., 1991), based on a stepwise combustion procedure or the more advanced thermal-optical methods, considering the evolution of the optical properties of the sample during the stepwise heating process (e.g. Cavalli et al., 2010). For the latter method, several temperature protocols exist, differing in the used temperature set points and residence times at each temperature step. Due to the increasing importance of consistent OC and EC measurements required by the EU Directive 2008/50/EC for the purpose of providing information on the amount and chemical composition of particulate matter, efforts for the harmonization of aerosol measurements, and hence also for EC determinations, were pursued. The thermal-optical measurement with the EUSAAR2 temperature program is the reference method for the determination of EC and OC collected on filters (EN 16909:2017-06, 2017).

Limitations of the above mentioned methods are that the on-line determination demands the operation of specific instruments like an Aethalometer or a continuously operated OC/EC analyzer. The offline thermal-optical method allows a better spatial distribution at low instrument cost, but is quite time consuming with a lot of manual work and filters of materials other than quartz fiber cannot be measured directly. Thus, routine monitoring of EC or BC in existing national ambient air monitoring networks is ambitious. Still it would be of great interest and value because EC or BC, mainly emitted into the atmosphere through incomplete combustion of fossil fuels, represents an important part of particulate matter (PM) in urban areas, being responsible for serious health effects, and its optical properties make it an important component regarding radiative transfer. Depending on the mixing state (externally or internally) BC is able to directly affect the radiation budget due to the strong absorption of solar radiation as well as indirectly by acting as cloud condensation or ice nuclei thereby altering the cloud microphysical properties (Bond et al., 2013; Penner et al., 1998; Zhang and Wang, 2011).

In several air quality networks no routine on-line BC measurements are performed, but routine collection of daily PM10 or PM2.5 filter samples is implemented. These filters could be used for retrospective EC or BC determination using off-line instrumentation. In doing so, a rather cheap and easy method would provide the opportunity to perform comprehensive monitoring and obtain long-term time-series. Also archived filters could be used to extend the time series into the past.

Davy et al. (2017) estimated particulate BC concentrations based on reflectance and transmittance measurements of PM10 samples of different filter materials for urban stations in London (UK). They derived a relationship between the optical measurements and thermal-optically

measured EC. This relationship was used as a model to determine equivalent BC concentrations (eBC) where no EC measurements were available. Referring to (Petzold et al., 2013), the term eBC is used to describe the mass BC concentrations derived from optical methods, such as the transmissometer, and will be used throughout the article.

Within this work quartz fiber filters from selected routine monitoring sites in the Austrian ambient air network, representing different station types (urban-traffic, rural-background and remote), were used to quantify eBC based on transmissometer measurements. It is well known that the overall chemical composition of aerosol samples varies depending on the location of the station and this variation influences the optical properties. Thus, different station types have to be considered to develop a method applicable to the wide range of stations operated within air quality networks.

The performance of two different approaches for the determination of eBC from transmissometer measurements, as well as the observed k, σ and MAC values for the different station types, are compared. We present a comparison of the two different approaches to calculate eBC, as well as an analysis covering station types ranging from urban to background stations. Robust offline measurements of eBC on either fresh or archived filters from different station types and routinely sampled within ambient air monitoring networks would provide a quick, easy and non-destructive method for the monitoring of eBC. This would allow users to obtain long-term time-series going back to times when no on-line instruments were existing, and to obtain these data sets for sites where no on-line instruments are installed even now.

2. Measurements and methods

2.1. Measurement sites and sampling

Daily PM10 quartz fiber filter samples of the previous measurement campaigns, PMinter (Kistler et al., 2013b, 2013a) and AQUELLA (Bauer et al., 2007a, 2007b; Jankowski et al., 2008), collected at 11 official air quality monitoring stations in Austria were used in this study (compare Fig. 1 and Table 1). The stations represent different types (urban-traffic, rural-background, remote and suburban-background) classified according to the IPR (Implementing Provisions on Reporting) Guidance from the European Commission (2013). Two of these stations were mobile stations with no official classification, but they can be regarded as "regional background" and "urban background" stations, respectively. Filters were randomly chosen to represent the different aerosol types of the year (more details listed in Table 1). Mass concentrations (PM10) covered a wide concentration range from below $5\,\mu g\,m^{-3}$ up to $100\,\mu g\,m^{-3}$. Sampling was performed using High-Volume-Samplers (Digitel DA 80) at all stations. The same brand of filters was always used (Pallflex Tissuequartz 2500QAT-UP), but batches were obviously

2

Table 1

Overview of stations used in this study and number of filters for the model development and validation. *denotes that the station classification is not the official classification of the IPR Guidance from the European Commission, but was defined for single measurement campaigns.

ID	Station	Station Type	Number of Filters	Sampling period
DB	Graz Don Bosco	Urban-traffic	23	Jan–Dec 2004 (AQUELLA)
KEND	Wien Kendlerstraße	Urban-traffic	19	Jan–Dec 2004 (AQUELLA)
RUD	Salzburg Rudolfsplatz	Urban-traffic	27	Jan–Dec 2004 (AQUELLA)
KLG	Klagenfurt Völkermarktstraße	Urban-traffic	29	Jan, Feb, Jul 2011 (PMinter)
STIX	Stixneusiedl	Rural-background	30	Jan, Feb 2005 (AQUELLA)
ENZ	Enzenkirchen	Rural-background	30	Apr 2005–Jan 2006 (AQUELLA)
ARN	Arnfels	Rural-background	20	Jan, Feb, Mar 2011 (PMinter)
SBK	Hoher Sonnblick	Remote	46	Nov 2006–Feb 2008
LAVA	Lavamünd	Regional background*	30	Nov 2004–Jul 2005 (AQUELLA)
LEI	Leibnitz	Suburban-background	20	Jan, Feb, Jul 2011 (PMinter)
LIM	Limmersdorf	Urban-background*	25	Jan, Feb, Jul 2011 (PMinter)

different during the course of the years. Filters were archived at $-20\,°C$.

2.2. Transmissometry

A filter punch with 36 mm diameter was used for analysis with an OT-21 transmissometer (Aerosol d.o.o., Magee Scientific Corp.). The OT-21 measures the transmission of light through a particle-loaded filter at 880 nm and 370 nm. The attenuation ($ATN = -100*\ln(I/I_0)$) measured at 880 nm, where I and I_0 are the respective transmission intensities through the loaded and unloaded filter, is assumed to be proportional to the mass of light absorbing material on the filter, that is equivalent BC, eBC. This method is not straightforward, since light transmittance is not reduced only by the light absorbing material on the filter, but also by scattering aerosols as well as by interactions between filter fibers and accumulated aerosol. A more detailed discussion on these artefacts as well as their handling can be found in Coen et al. (2010) and Virkkula et al. (2015).

As we used archived filters, I_0 was not available and we had to assume an average value characteristic for this type of filters. Based on the evaluation of 30 filters originating from three different batches an estimate of the variation of I_0 was obtained. ATN values reported here are calculated with an average value of I_0. Considering the minimum and maximum values obtained for a variation of ATN of $\pm\ 8$ has to be expected. This will become important for low filter loadings only.

Measurements at 370 nm were not evaluated in this study because most of the filters exceed the maximum limit of detection for the measurement of the attenuation at this wavelength (they are "too dark"). Thus, all further measurements refer to an ATN at 880 nm. Gundel et al. (1984) defined a useful range of ATN measurements of 25–300 where saturation effects are rather small. Filters used in this study show maximum values up to ATN = 500, where a filter loading effect expressed by a non-linear dependency between ATN and EC and described by the filter loading parameter k, can be expected (e.g. Drinovec et al., 2015 and references therein).

2.3. Elemental carbon (EC) measurement

A filter punch with 10 mm in diameter was used for analysis with the OC-EC analyzer from Sunset Lab, using the EUSAAR2 reference temperature program as defined in the standard EN16909:2017. The EC content loaded on the filter is given as surface density B in $\mu g\ cm^{-2}$. Limits for the EC concentration using the thermal-optical method as given in the EN16909:2017 range from 0.2 to 38 $\mu g\ cm^{-2}$. Filters used in this study show maximum values of only 26 $\mu g\ cm^{-2}$. The average uncertainty of the EC concentrations can be given as 16%.

2.4. Relationship between attenuation and thermal-optical EC

To determine the EC concentration loaded on a filter based on ATN

measurements only, it is crucial to determine the filter loading parameter k, describing the non-linearity of the relationship, as well as the aerosol specific mass attenuation cross section σ. Two different approaches for the mathematical fit of the calibration curve describing the relationship between measured EC and ATN were investigated.

The first approach follows Davy et al. (2017), who use a quadratic fit to relate $\ln(I_0/I)$ with atmospheric eBC concentrations. Rearranging the quadratic equation (see Eq. (1) and Eq. (2) in Davy et al., 2017) an expression similar to the correction function introduced by Virkkula et al. (2007) for Aethalometer data is obtained. Therefore, the first approach (see Eq. (1)) is denoted "Virkkula equation" throughout the manuscript. The second approach is based on Drinovec et al. (2015), and uses the dual-spot loading effect compensation algorithm used at on-line Aethalometer BC measurements. It is denoted as "Drinovec equation" throughout the manuscript (see Eq. (2)).

Note following differences of our Eq. (1) in respect to the notation given in Davy et al., (2017). In order to be consistent with the "Drinovec" equation we use ATN instead of $\ln I_0/I$, utilizing the relationship $\frac{ATN}{100} = -\ln\left(\frac{I}{I_0}\right)$. Furthermore, we relate ATN to the EC surface density B in $\mu g cm^{-2}$ obtained on the filters, while Davy et al., 2017 use atmospheric eBC concentrations in $\mu g m^{-3}$.

Virkkula equation: $B_{calc} = \frac{1}{\sigma}*ATN*(1 + k*ATN)$ (1)

Drinovec equation: $B_{calc} = -\frac{1}{k*\sigma}*\ln(1 - k*ATN)$ (2)

Both equations allow the determination of k (unitless) and σ (in $m^2\ g^{-1}$) at a wavelength of 880 nm based on ATN and thermal-optical EC surface density (B in $\mu g cm^{-2}$) measurements. Equations (1) and (2) were fitted to the data set as a regression line through the origin with k and σ as model parameters. The parameters k derived from the two approaches are, strictly speaking, not identical but can be taken to be equal to the first order (shown by expanding Eq. (2) in a Taylor series).

The fit was performed by using the non-linear model fit function nls () included in the 'stats' package in R for the non-linear least-square estimates of the parameters of the non-linear model (R Development Core Team, 2008). Once k and σ are determined, the estimation of the surface density B_{calc} via ATN measurements becomes straightforward. Subsequently the surface density B can easily be converted to eBC:

$$eBC\ [\mu g\ m^{-3}] = \frac{B\ [\mu g\ cm^{-2}]*Filter\ Area\ [cm^2]}{Volume\ [m^3]}$$ (3)

3. Results

To compare the performance of the "Virkkula" and "Drinovec" equations, the filter loading parameter k and the mass attenuation cross section σ were evaluated based on the entire data set. In a second step, filters of the different station types were investigated separately to

3

study the influence of the different aerosol composition on k and σ. For interpretation and comparison with literature the more common mass absorption cross section MAC is also calculated, where we take MAC = σ/2.14 (Weingartner et al., 2003) for quartz fiber filters. We want to note that this value of C = 2.14, determined for fresh Palas soot or diesel particles mixed with ammonium sulfate, is not a universal number and other values for C are also reported in literature, e.g. being seasonal specific (Coen et al., 2010). Recently, values around 3.5 were reported for ambient measurements with Aethalometers using quartz filters (Segura et al., 2014; Zanatta et al., 2016).

The significance of the regression coefficients k and σ of the respective model was checked via a t-test, testing the hypothesis that they are different from zero. Thereby a p-value < 0.05 was used as threshold for significance and is indicated by asterisks in the respective tables.

3.1. Comparison of the two different equations to derive B_{calc}

First we compute and compare the respective values for k and σ. Afterwards the performance of the two approaches is validated via a comparison of B obtained by the thermal-optically measurement (referred to $B_{measured}$) and B_{calc} based on the ATN measurements using Eq. (1) and Eq. (2).

3.1.1. Determination and comparison of k and σ

Fits of both approaches (Eq. (1) and Eq. (2)) and the subsequent determination of k and σ were performed using all filters measured in this study (total 299 filters) and filters with ATN < 300 only (total 234 filters). Results are plotted in Fig. 2 and Table 2.

Evaluating all filters the "Virkkula" and "Drinovec" equations yield statistically indistinguishable filter loading parameters k. The mass attenuation cross section σ is calculated slightly lower when the Drinovec equation is applied.

As maximum ATN values reach up to 500 the data set was re-evaluated considering only filters with ATN < 300, to investigate a possible bias caused by dark filters. Using the "Virkkula" equation no statistically relevant changes are obtained for k and σ, when either all filters or only filters with ATN < 300 were evaluated. Applying the "Drinovec" equation both parameters, k and σ increase when the data set is restricted. This indicates a possible dependency on the considered ATN range. Still it should be noted, that the standard error of k increases as well, making the observed change less obvious. Consequently, and due to the limited number of data points, the further calculations are performed using all filters and a possible ATN dependency was not investigated further.

Overall, the comparison of k has to be interpreted cautiously because the observed values are rather small to values given in the literature (Davy et al., 2017; Drinovec et al., 2015). As can be also seen in

Table 2

Results for the filter loading parameter k, the mass attenuation cross section σ and the mass absorption cross section MAC = σ/2.14 (Weingartner et al., 2003) at 880 nm using all filters of all stations. Lowercased values represent the respective standard error, * indicates that a t-test supports the null hypothesis that the coefficients are different from zero using p < 0.05 as threshold for significance.

	k (880 nm)	σ [m² g⁻¹] (880 nm)	MAC [m² g⁻¹] (880 nm)	Number of Filters
„Virkkula equation" all filters	0.00100* ± 0.00021	35.1* ± 1.9	16.4 ± 0.9	299
„Virkkula equation" ATN < 300	0.00098* ± 0.00036	35.8* ± 2.4	16.7 ± 1.1	234
„Drinovec equation" all filters	0.00097* ± 0.00012	32.0* ± 1.1	15.0 ± 0.5	299
„Drinovec equation" ATN < 300	0.00142* ± 0.00029	35.5* ± 1.7	16.6 ± 0.8	234

a theoretical evaluation the two approaches may differ stronger when higher k values are observed.

The influence of k and the ATN range on the two different approaches presented was investigated by the calculation of B at different ATN using k values ranging from 0 to 0.0020 whereas σ was set to 1. The comparison showed that the "Drinovec" equation yields down to 9% lower B_{calc} values (Fig. 3), but for higher ATN and higher k values the "Virkkula" values can fall below the "Drinovec" for several percent (as seen for k = 0.0020).

3.1.2. Validation of the different approaches in respect to the surface density B

Using k and σ derived for all filters (compare Table 2), B_{calc} was calculated for every filter based on the respective ATN measurements applying Eq. (1) and Eq. (2), respectively. B_{calc} was then compared to the thermal-optically determined $B_{measured}$.

To evaluate site specific trends every station was considered separately. This represents an internal validation because filters used for validation were already included in the determination of the respective k and σ values. Table 3 shows R^2 and the slope of the linear regression $B_{measured}$ = a*B_{calc}. The comparison showed almost no differences between the "Virkkula" and the "Drinovec" equation. Thus, conclusions on the performance are valid for both approaches although values in the text refer to the "Virkkula" equation.

The comparison showed a very good correlation for all stations with R^2 in the range of 0.936–0.987. The lowest R^2 was obtained for DB, the station with the highest ATN values. Slopes are ranging from 0.774 to 1.094 and reveal differences between the single station types. Slopes for
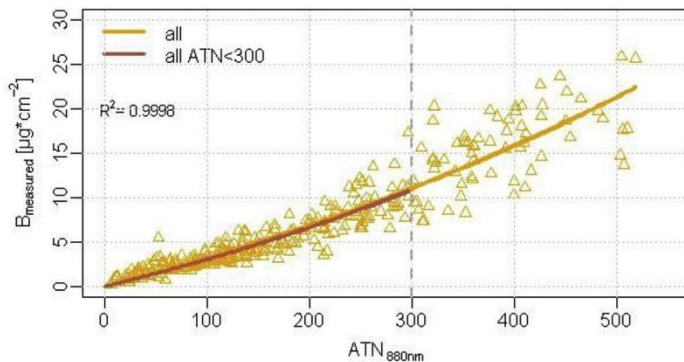

Fig. 2. Calibration curves between ATN at 880 nm and surface density $B_{measured}$ [μgcm⁻²] using all filters of all stations. Regression lines of "Virkkula" and "Drinovec" equations (compare Eq. (1) and Eq. (2)) are very similar so that they overlay each other in the plot, appearing as one single line. The value for R^2 is the same for all regression lines.
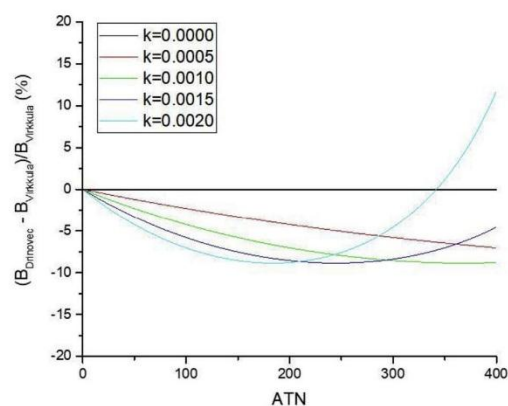
4

Fig. 3. Elemental carbon surface density B calculated from the "Virkkula" and "Drinovec" equations for different values of parameter k The relative difference between the equations showing a down to 9% lower B value for the "Drinovec" equation.

Table 3

Results for the validation using the linear regression $B_{measured} = a*B_{calc}$. Thereby B_{calc} was calculated using the "Virkkula" and "Drinovec" equations given in Eq. (1) and Eq. (2) with the respective k and σ values given in Table 2 if all filters are used. Lowercased values represent the respective standard error.

Station for validation	"Virkkula" equation		"Drinovec" equation		Number of filters for validation
	Slope	R^2	Slope	R^2	
KEND	1.063 ± 0.056	0.952	1.067 ± 0.057	0.951	19
KLG	1.030 ± 0.037	0.965	1.026 ± 0.037	0.965	29
RUD	1.045 ± 0.039	0.966	1.040 ± 0.038	0.966	27
DB	1.046 ± 0.058	0.936	1.043 ± 0.058	0.936	23
ENZ	0.883 ± 0.019	0.987	0.897 ± 0.020	0.986	30
STIX	0.979 ± 0.031	0.972	1.001 ± 0.032	0.971	30
ARN	0.888 ± 0.024	0.986	0.921 ± 0.023	0.986	20
LEI	0.890 ± 0.044	0.955	0.889 ± 0.044	0.956	20
LAVA	1.094 ± 0.041	0.961	1.109 ± 0.043	0.958	30
LIM	0.774 ± 0.032	0.960	0.780 ± 0.031	0.963	25
SBK	0.857 ± 0.025	0.961	0.889 ± 0.027	0.958	46

Table 4

Results for the mass attenuation cross section σ and the mass absorption cross section MAC = σ/2.14 (Weingartner et al., 2003) at 880 nm for the different station types where k was set to zero.* indicates that a *t*-test supports the null hypothesis that the coefficients are different from zero using p < 0.05 as threshold for significance Lowercased values represent the respective standard error.

Stations for computation	Station for validation	k (880 nm)	σ [m² g⁻¹] (880 nm)	MAC [m² g⁻¹] (880 nm)	Number of Filters
URBAN – TRAFFIC					
KLG, RUD, DB	KEND	0	24.3* ± 0.6	11.4 ± 0.3	79
KEND, RUD, DB	KLG	0	24.1* ± 0.6	11.3 ± 0.3	69
KLG, KEND, DB	RUD	0	24.8* ± 0.7	11.6 ± 0.3	71
KLG,KEND, RUD	DB	0	24.6* ± 0.6	11.5 ± 0.3	75
All urban-traffic	–	0	24.4* ± 0.5	11.4 ± 0.2	98
RURAL – BACKGROUND					
ARN, STIX	ENZ	0	31.2* ± 0.7	14.6 ± 0.3	50
ARN, ENZ	STIX	0	32.8* ± 0.5	15.3 ± 0.3	50
ENZ, STIX	ARN	0	31.4* ± 0.6	14.7 ± 0.3	60
All rural-back-ground	–	0	31.8* ± 0.5	14.9 ± 0.2	80
REMOTE					
SBK	SBK	0	33.7* ± 1.4	16.0 ± 0.6	29

urban-traffic stations and LAVA range between 1.030 and 1.094, representing an underestimation of B_{calc} of 3–9%. All other stations were overestimated with slopes ranging from 0.774 to 0.979. The overestimation of B_{calc} was in the range of 2–14%, excluding LIM, which showed a deviation of up to 23%. Different slopes indicate different mass attenuation cross-sections which seem to be related to the station type.

3.2. Evaluation of k and σ for different station types

As shown in previous studies (e.g. Drinovec et al., 2017) k and σ depend on the aerosol type. This and the marked differences between the station types shown before, led us to the station type specific determination of k and σ. We determine k and σ for the "Virkkula" and the "Drinovec" approach separately for three different station types (urban-traffic, rural-background and remote).

To be able to perform an external validation we compute the respective k and σ values several times, always excluding one station which was afterwards used for validation by comparing B_{calc} with $B_{measured}$. This results in a fourfold or threefold external validation for urban-traffic and rural-background stations, respectively. We apply this repeated validation as differences between stations do exist, although they are classified into the same station type. These differences should become visible by this repeated method. The remote station was validated using 17 filters of the same station which were not used for model development (46 filters), simply because no other remote station exists in Austria.

3.2.1. Comparison of k and σ

Results for k and σ of the three different station types are summarized in Table 4, the corresponding fits are plotted in Fig. 4.

Different to the evaluation of the whole data set we observe loading parameters k not significantly different from 0 for both approaches when the station types are considered separately. If k = 0, Eq. (1) and Eq. (2) simplify to B = ATN/σ and only σ is fitted. In case of the "Virkkula" equation, this is obvious by looking at Eq. (1) if k = 0 is inserted. For the "Drinovec" equation given in Eq. (2) this is derived by developing a Taylor series, using only the first element. Data of the first fit, without fixing k to 0, is shown in the supplement (Table S1).

To check whether the result of k = 0 is an effect of the reduced amount of data points, a reduced data set covering the whole ATN range and all station but only 75 filters instead of 299 was evaluated as in section 3.1.1. The calculation again resulted in a k value significantly different from 0 indicating that k = 0 is only obtained when station types are considered separately (see supplement Table S2).
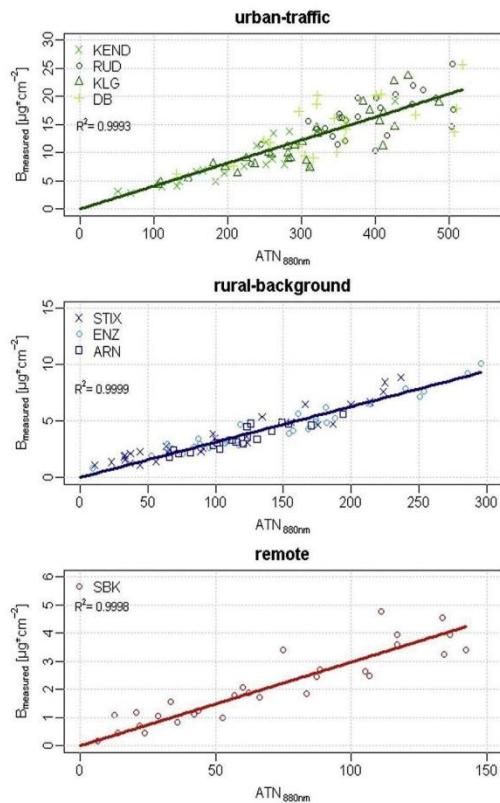
5

Fig. 4. Calibration curves between ATN at 880 nm and $B_{measured}$ in [µgcm^{-2}] for different station types. Graphs show values for filters of all urban-traffic stations (green), all rural-background stations (blue) and the remote station (red) to derive k and σ of the respective station type as described in the text. All station types show a k = 0 and are thus independent of the underlying equation ("Virkkula" or "Drinovec") since both equations simplify to $B_{calc} = ATN/\sigma$. Note the different scales!. (For interpretation of the references to colour in this figure legend, the reader is referred to the Web version of this article.)

Observed σ values are different depending on the station type. Urban-traffic stations show the lowest values, ranging from 24.1 to 24.8 m^2 g^{-1}. If the respective standard error (compare Table 4) is taken into account, values can be treated as equal. Therefore we compute an "urban-traffic σ" of 24.4 m^2 g^{-1} (± 0.5 m^2 g^{-1}), including all urban-traffic stations. We refer to this "urban-traffic σ" for further interpretations or comparisons. Values for the rural-background stations are higher with σ values ranging from 31.2 to 31.8 m^2 g^{-1}. Here the differences between the stations are more pronounced and σ values obtained based on different rural background sites may vary significantly. For comparison reasons also a "rural-background σ", including all rural-background stations was calculated, resulting in a σ of 31.8 m^2 g^{-1} (± 0.5 m^2 g^{-1}). The remote station showed the highest values of σ = 33.7 m^2 g^{-1} (± 1.4 m^2 g^{-1}).

3.2.2. Validation of the different approaches for the different station types

Table 5 shows R^2 and the slope of the linear regression $B_{measured} = a*B_{calc}$ for the respective station types. Results of this validation are displayed as scatterplots whereas conditional quantile

Table 5
Results for the validation using the linear regression $B_{measured} = a*B_{calc}$. Thereby B_{calc} was calculated using the "Virkkula" and "Drinovec" equations given in Eq. (1) and Eq. (2) with the respective k and σ values computed by using all filters of the different station types and given in Table 4. Lowercased values represent the respective standard error.

Stations for computation	Station for validation	Slope	R^2	RMSE [µg cm^{-2}]	Number of filters for validation
URBAN – TRAFFIC					
KLG, RUD, DB (σ = 24.3)	KEND	0.942 ± 0.051	0.949	2.11	19
KEND, RUD, DB (σ = 24.1)	KLG	0.955 ± 0.036	0.961	2.58	29
KLG, KEND, DB (σ = 24.8)	RUD	1.039 ± 0.036	0.970	2.93	27
KLG,KEND, RUD (σ =24.6)	DB	1024 ± 0.051	0.947	3.49	23
RURAL – BACKGROUND					
ARN, STIX (σ =31.2)	ENZ	0.960 ± 0.020	0.987	0.60	30
ARN, ENZ (σ =32.8)	STIX	1.102 ± 0.034	0.973	0.86	30
ENZ, STIX (σ =31.4)	ARN	0.932 ± 0.025	0.987	0.49	20
REMOTE					
SBK (σ = 33.7)	SBK	0.981 ± 0.034	0.982	0.35	17

plots, in analogy to Davy et al. (2017), can be found in the supplement (Figure S1 and S2).

The validation of the urban-traffic stations showed a very good agreement between B_{calc} and $B_{measured}$ with a slope of 0.942–1.039, representing a deviation of 2–6%, and an R^2 of 0.947–0.970. The corresponding scatterplots given in Fig. 5 underline the good agreement. A slight underestimation of B_{calc} for RUD and DB and a slight overestimation for KEND and KLG was observed, pointing to the fact that agreement might get better when a site specific calibration is performed.

The validation of the rural-background stations resulted in a slightly higher deviation, ranging between 4 and 10%, with a slope between 0.921 and 1.102 and a R^2 of 0.973–0.987. Fig. 6 underlines the slight underestimation of B_{calc} for STIX and a slight overestimation for ENZ and ARN. The remote station shows a slope of 0.999 with an R^2 of 0.982 with almost no difference between B_{calc} and $B_{measured}$.

The quality of the fit is also expressed by the RMSE (compare Table 5) which is markedly decreasing from urban (RMSE = 2.11–3.49 µg cm^{-2}) over rural (RMSE = 0.49–0.86 µg cm^{-2}) to remote stations (RMSE = 0.35 µg cm^{-2}).

3.3. Application for additional station types

Based on the result that σ was found to be dependent on the station type, higher deviations between B_{calc} and $B_{measured}$ can be expected, if samples obtained at a different or unknown station types are evaluated using k and σ of the urban-traffic or rural-background station type. We tested this by using three stations (Leibnitz = LEI, Lavamünd = LAVA, Limmersdorf = LIM) which are not classified as urban-traffic or rural-background. LEI is officially classified as "suburban-background" station, whereas LAVA and LIM lack an official classification but can be regarded as "regional background" and "urban background".

Results for validation of the urban-traffic and the rural-background model are given in Table 6. B_{calc} values are subsequently compared with the thermal-optically determined $B_{measured}$.

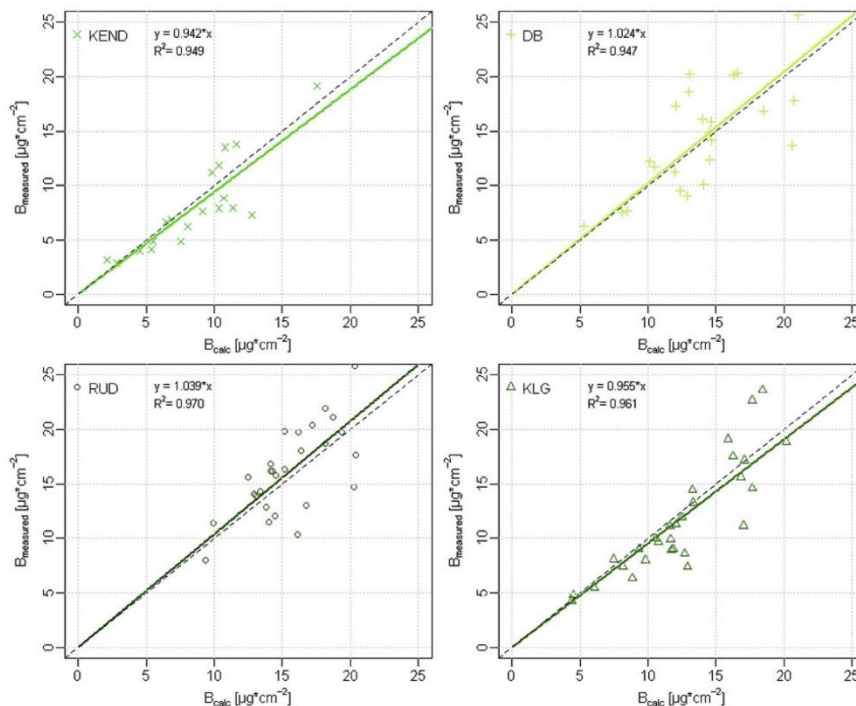Depending on the underlying σ-values of either urban-traffic or

Fig. 5. Scatterplots of B_{calc} vs. $B_{measured}$ of the urban-traffic stations. B_{calc} of KEND and KLG is slightly overestimated whereas B_{calc} for DB and RUD is slightly underestimated. The slope represents a deviation between B_{calc} and $B_{measured}$ between 4 and 6%.

rural-background, varying deviations are observed. If σ of the urban-traffic stations ($σ = 24.4\,m^2\,g^{-1}$) is used, the slope for all 3 stations is always smaller than 1, representing an overestimation of B_{calc}. Values vary between 19% for LEI, 7% for LAVA and 28% for LIM and are thus higher than observed for the stations actually classified as urban-traffic stations. This result is also presented in the left column of the scatterplots of Fig. 7 and Supplementary Figure S3. If σ of the rural-background stations ($σ = 31.8\,m^2\,g^{-1}$) is used, a slope greater than 1, indicating an underestimation of B_{calc}, is observed for LEI (5%) and LAVA (22%). For LIM again an overestimation of B_{calc} is observed with a deviation of 13%. The conditional quantile plots given in the Supplementary material (Figure S3) indicate that low B_{calc} values tend to be overestimated whereas higher ones are underestimated. The RMSE follow the results described.

To estimate a possible effect of the loading parameter k, we used k and σ values derived for urban-traffic and rural-background stations before k was set to 0 (compare Table S1). The use of k does not change the results markedly. Data is presented in the supplementary (section 4 and Table S3).

4. Discussion

Using all filters we found that the "Drinovec" and "Virkkula" equations give comparable results with values of $σ = 32.1\,m^2\,g^{-1}$ ($± 1.1\,m^2\,g^{-1}$) and $σ = 35.3\,m^2\,g^{-1}$ ($± 1.9\,m^2\,g^{-1}$) at 880 nm, respectively. If filters of the different station types are evaluated separately, again no differences between the two approaches occur, but σ values (at 880 nm) are found to be different for the different station

types, ranging between $24.4\,m^2\,g^{-1}$ ($± 0.5\,m^2\,g^{-1}$) for urban-traffic, to $31.8\,m^2\,g^{-1}$ ($± 0.5\,m^2\,g^{-1}$) for rural-background and $σ = 33.7\,m^2\,g^{-1}$ ($± 1.4\,m^2\,g^{-1}$) for remote stations.

These different values might be due to differences in the aerosol composition or differences in the amount of coating of the particles at the respective station. While urban-traffic stations represent mostly traffic related aerosol recently emitted, rural-background filters feature more biomass burning aerosol due to domestic wood burning activities and particles can be expected to be at least slightly aged. Filters from the remote station represent background conditions, featuring predominantly aged aerosol particles. Aging can result in a so-called "lensing effect", meaning a higher absorption per mass, which is reflected in a higher σ compared to the uncoated or fresh aerosol (Bond et al., 2006; Jacobson, 2001). Besides, the OC/EC analysis might underestimate the thermal-optically determined $B_{measured}$ for heavily loaded filters, mostly observed for urban-traffic filters, resulting in a slightly underestimated σ.

A variety of studies are available where σ or corresponding MAC values are stated, but most of them go back to different experimental conditions like a different methodology, a different filter material or wavelength of the measurements. The latest study of Zanatta et al. (2016), investigating rural background sites from southern Scandinavia, central Europe and the Mediterranean using the EUSAAR temperature protocol for the thermal-optical determination of B on quartz fiber filters, found annual geometric mean MAC values of $6.5–17.3\,m^2\,g^{-1}$ at 637 nm, or $9.0–23.9\,m^2\,g^{-1}$ at 880 nm if a 1/λ dependency is used for interpolation. These values are similar to MAC values observed in this study ranging from $11.4\,m^2\,g^{-1}$ to $16.5\,m^2\,g^{-1}$
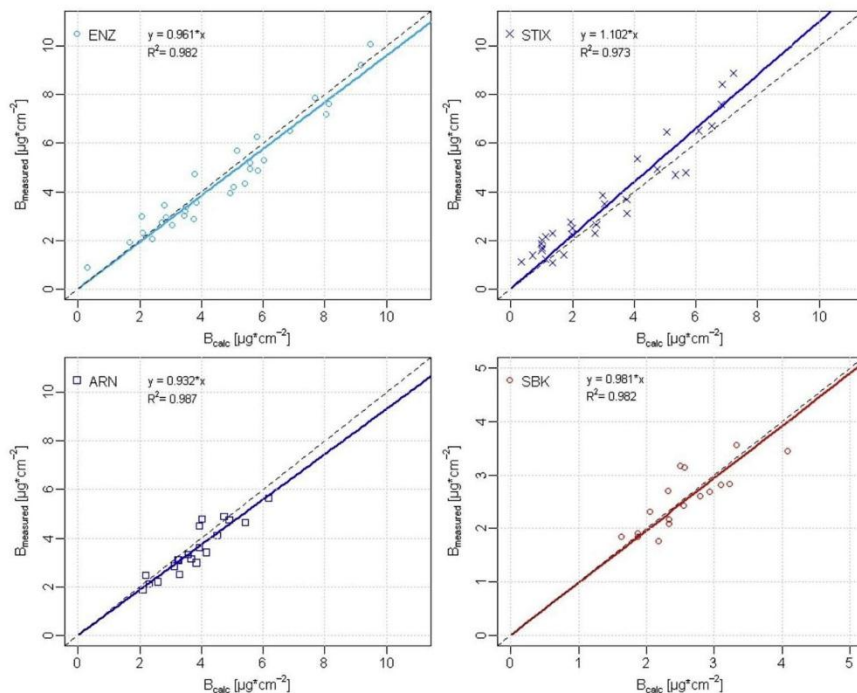
Fig. 6. Scatterplots of B_{calc} vs. $B_{measured}$ of the rural-background (blue) and remote (red) stations. B_{calc} of ENZ and ARN is slightly overestimated whereas B_{calc} for STIX is slightly underestimated. The slope represents a deviation between B_{calc} and $B_{measured}$ between 8 and 10%. For the remote station SBK an almost perfect match was observed. (For interpretation of the references to colour in this figure legend, the reader is referred to the Web version of this article.)

Table 6
Results for the validation of station types other than urban-traffic or rural-background using the linear regression $B_{measured} = a \cdot B_{calc}$. Thereby B_{calc} was calculated using the "Virkkula" and "Drinovec" equations given in Eq. (1) and Eq. (2) with the respective k and σ values computed by using all filters of the different station types and given in Table 4. Lowercased values represent the respective standard error.

Stations for computation	Station for validation	Slope	R^2	RMSE [µg cm^{-2}]	Number of filters for validation
URBAN – TRAFFIC ($\sigma = 24.4$ m^2 g^{-1})					
All urban-traffic	LEI	0.809 ± 0.044	0.946	3.15	20
All urban-traffic	LAVA	0.933 ± 0.033	0.966	1.16	30
All urban-traffic	LIM	0.719 ± 0.037	0.941	3.08	25
RURAL – BACKGROUND ($\sigma = 31.8$ m^2 g^{-1})					
All rural-background	LEI	1.053 ± 0.058	0.946	2.29	20
All rural-background	LAVA	1.215 ± 0.043	0.966	1.48	30
All rural-background	LIM	0.872 ± 0.045	0.941	1.63	25

and using C = 2.14 to convert use the conversion MAC = σ/C based on Weingartner et al. (2003). Drinovec et al. (2015) uses MAC = 7.77 m^2 g^{-1} for the calculation of BC mass concentrations for Aethalometer measurements at 880 nm on a quartz fiber filter band. Davy et al. (2017) found a σ of 72 m^2 g^{-1}, for quartz fiber filters of

urban sites in London. They used the NIOSH temperature protocol for the thermal-optical determination of B. It was shown by Karanasiou et al. (2015) that the EC content is less when the NIOSH protocol is used compared to the EUSAAR protocol suggested by the EN 16909:2017 and used in our study. This might lead to higher values found by Davy et al. (2017) compared to ours. Other studies measured with an incandescent lamp, summarized in Weingartner et al. (2003), show a big scatter of σ values ranging from 5 m^2 g^{-1} in remote areas to 9.3 m^2 g^{-1} at a remote continental site to 14 m^2 g^{-1} at an urban site and 20 m^2 g^{-1} at a near-street site. Gundel et al. (1984) found a σ of 23.9 m^2 g^{-1} for visible light transmission measurements on quartz fiber filters. Considering the scatter of values found in literature our results appear within the expected range. Dutkiewicz et al. (2014) followed a similar approach as presented in this study comparing thermal-optically determined B with attenuation measurements using cellulose filters. They used the TOT NIOSH temperature protocol (Birch and Cary, 1996) for the thermal-optically determination of B and the relationship BC = ATN*σ with σ = 16.6 m^2 g^{-1}, the standard value used in aethalometers since the earliest production of instruments analyzing at 880 nm as stated by the manufacturer, for the calculation of BC out of ATN measurements. Our study is the first determining σ specifically for the different aerosol types and comparing the thermal-optical determination of B using the EUSAAR2 temperature protocol as required by the European standard for OC/EC measurements EN 16909:2017 with attenuation measurements at 880 nm, the standard wavelength used for the determination of eBC. The influence of charring on the determination of EC during thermal-optical analysis might be stronger for wood-smoke containing filters, but the quantification of this effect
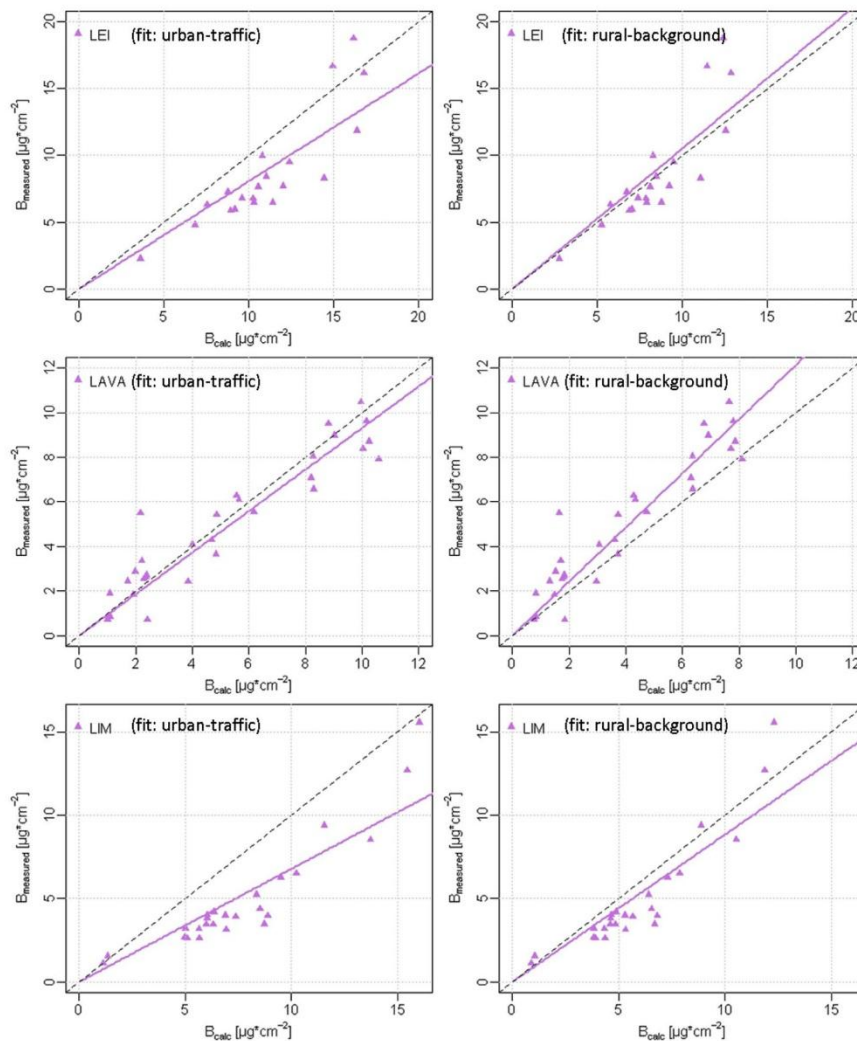
Fig. 7. Scatterplots of B_{calc} vs. $B_{measured}$ of the three stations (LEI, LAVA, LIM) not classified as urban-traffic or rural-background. Plots on the left hand site point to B_{calc} determined using the urban-traffic fit ($\sigma = 24.4$ m^{2}g^{-1}, left column) and plots on the right hand site point to B_{calc} determined using the rural-background fit ($\sigma = 31.8$ m^{2}g^{-1}, right column). Note the different scales!.

proves very elusive.

For k both approaches give statistically indistinguishable results if the all filter (i.e. no restriction to a specific ATN range) are used with values of k = 0.001 (± 0.0001) as well as k = 0.001 (± 0.0002). If filters of the different station types are evaluated separately, again no differences between the two model approaches occur and furthermore k was found to be statistically indifferent from zero, resulting in an independence of the underlying model approach simplifying Eq. (1) and Eq. (2) to B = ATN/σ. In literature a variety of k values can be found, depending on the underlying model (compare Drinovec et al., 2015) as well as on the coating of the sampled particles (Drinovec et al., 2017). Virkkula et al. (2007) found k values at 880 nm ranging from −0.0056

to 0.0054 for three different sites in Finland, using the Magee Scientific Aethalometers AE-16 and AE-31. Davy et al. (2017) found a k = 0.013 (± 0.009) for quartz fiber filters of London urban stations using the Magee Sootscan OT21, the same instrument we have used in this study, with a maximum ATN of about 350. We found lower k values, although we measured up to ATN = 500 or more. Drinovec et al. (2017) report k values for the near IR at 880 nm ranging from 0.001 to 0.008, depending on the seasonality, the particle size and the particle coating. They found that the loading parameter k increases with increasing primary particle size and decreases the more the particles are coated. The filter loading parameter k turned out to be significantly different from zero, only if all filters are evaluated together. The interpretation of

9

these results is quite difficult, but one possible explanation might be the high variation in the ATN range between the different station types. This seems to cause the appearance of a significant k when filters are evaluated together, but is compensated by the differences in σ, if different station types are evaluated separately. If a closer look on the plot for filters from the urban-traffic station is taken, it seems as if a filter loading effect, meaning a non-linear correlation between ATN and $B_{measured}$, is present. Another explanation might be that filters of different seasons were evaluated together to get one k and σ representing all year conditions. As shown by Drinovec et al. (2017) k values experience a seasonality with higher values in winter and lower values in summer due to differences in the coating and in the size of the particles. Our evaluation using filters of all seasons together may compensate the effect of the seasonality, resulting in a non-significant k. It seems that the seasonality of k plays only a minor role if filters of all stations are evaluated together due to the more pronounced influence of the different σ.

The performance of the two approaches, most important if used for the determination of eBC based on ATN measurements, were validated by calculating B from the ATN measurements of filters from one station type using the respective values for k and σ. Comparing the results using k and σ of the entire data set with the results if station type specific values are used, almost identic deviations of 2–6% or 3–6%, respectively, can be found for urban stations. For rural stations the deviation using the overall σ is 12% at the most and drops to 10% at the most if the station type specific values are used. Also for the remote station the deviation can be reduced from 12% to 4% if the station type specific σ is used. Davy et al. (2017) found deviations as low as 2% for one urban station in London. However, the deviations go up to 20% when different filter materials are used.

If stations of a type other than urban-traffic, rural-background or remote are investigated, deviations are higher with values of 10%, 11% and 23%, for LAVA, LEI and LIM respectively, using the overall k and σ. If LEI, classified as suburban-background, is evaluated with σ of the rural-background station the deviation is reduced to 5%. Deviations for LAVA, although classified as regional-background station, are small with only 7% if MAC urban-traffic is used. For LIM no clear answer could be found by using only 25 filters for evaluation. There is a tendency towards the use of σ rural-background but still with deviations of 13%. For this station further filters should be evaluated. According to previous studies (Bauer et al., 2007a, 2007b; Jankowski et al., 2008; Kistler et al., 2013b, 2013a), investigating the source apportionment of exactly the same filters used in this work, LEI and LIM show similar traffic and residential wood burning proportions (both highly absorbing in the IR) than rural stations, matching our results. LAVA could not be attributed to either rural or urban based on the traffic or domestic wood burning proportions, matching somehow our unexpected result that σ urban-traffic gives better results than σ rural-background.

Results reveal, that the application of the proposed method should be verified for each station by comparing the calculated B of some filters with the thermal-optically determined $B_{measured}$. Depending on these evaluations, one has then to decide for every single station which σ to use, either the overall values or the station type specific ones. If all of them show high deviation, we recommend to perform a station type specific or, if the station type cannot be clearly identified, even a site-specific determination of k and σ, representative for the respective aerosol type.

5. Conclusions

The evaluation of quartz fiber filters sampled at different station types in Austria shows that two different filter loading effect models were found to be statistically equal, resulting in of k = 0.001 (± 0.0001) and σ = 32. $m^2 g^{-1}$ ($\pm 1.1 m^2 g^{-1}$) as well as k = 0.001 (± 0.0002) and σ = 35.3 $m^2 g^{-1}$ ($\pm 1.9 m^2 g^{-1}$). A station type specific evaluation shows that k was found to be statistically indifferent

from zero for all station types, representing a linear relationship between $B_{measured}$ and ATN, whereas σ was found to be station type dependent with highest values for the remote station (σ = 33.7 $m^2 g^{-1}$ $+/- 1.4 m^2 g^{-1}$), followed by the rural-background (σ = 31.8 $m^2 g^{-1}$ $+/- 0.5 m^2 g^{-1}$) and the urban-traffic stations (σ = 24.4 $m^2 g^{-1}$ $+/- 0.5 m^2 g^{-1}$). The interpretation of the result that k = 0 for the station type specific evaluation is not straightforward, but might be attributable to the use of filters from different seasons and the wide ATN range covered.

An extensive validation of the two approaches, comparing the surface density B calculated from the ATN measurements using the respective model parameters with the thermal-optically measured B showed that deviations for urban-traffic, rural-background and remote stations were higher if the overall k and σ is used, but is still small with a maximum of 5% (remote), 6% (urban-traffic) or 12% (rural-background). For stations of a different station type than the ones investigated higher deviations up to 23% were found if the overall k and σ values are used. This could be reduced to 13% if the station type specific values of either urban-traffic or rural-background are used. There exists a great potential to apply this method for other station types than urban-traffic and rural-background, but the approach has to be validated for each new station, especially if this station is not distinctly classified. Then deviations of only up to 10% at the most are expected.

The main advantage of this study is to provide a quick, easy and non-destructive method to determine eBC concentrations from either fresh sampled or archived filters by measuring ATN only at the standard wavelength of 880 nm. Hence, eBC can be determined from either fresh or archived filters of different station types routinely sampled within ambient air monitoring networks without time and cost consuming effort to receive a comprehensive monitoring and to obtain long term time-series, going back to times before the existence of on-line instrumentation with high time resolution.

Declaration of interest

Acknowledgements

Appendix A. Supplementary data

Supplementary data related to this article can be found at https://doi.org/10.1016/j.atmosenv.2018.10.017.

References

Bauer, H., Marr, I., Kasper-Giebl, A., Limbeck, A., Caseiro, A., Handler, M., Jankowski, N., Klatzer, B., Kotianova, P., Pouresmaeil, P., 2007a. AQUELLA "Köflach Bestimmung von Immissionsbeiträgen in Feinstaubproben.

Bauer, H., Marr, I., Kasper-Giebl, A., Limbeck, A., Caseiro, A., Handler, M., Jankowski, N., Klatzer, B., Kotianova, P., Pouresmaeil, P., 2007b. AQUELLA "Steiermark Bestimmung von Immissionsbeiträgen in Feinstaubproben.

Bond, T.C., Doherty, S.J., Fahey, D.W., Forster, P.M., Berntsen, T., DeAngelo, B.J., Flanner, M.G., Ghan, S., Kärcher, B., Koch, D., Kinne, S., Kondo, Y., Quinn, P.K., Sarofim, M.C., Schultz, M.G., Schulz, M., Venkataraman, C., Zhang, H., Zhang, S., Bellouin, N., Guttikunda, S.K., Hopke, P.K., Jacobson, M.Z., Kaiser, J.W., Klimont, Z., Lohmann, U., Schwarz, J.P., Shindell, D., Storelvmo, T., Warren, S.G., Zender, C.S.,

M. Greilinger et al.

2013. Bounding the role of black carbon in the climate system: a scientific assessment: black carbon in the climate system. J. Geophys. Res. Atmos. 118, 5380–5552. https://doi.org/10.1002/jgrd.50171.

Bond, T.C., Habib, G., Bergstrom, R.W., 2006. Limitations in the enhancement of visible light absorption due to mixing state. J. Geophys. Res. 111. https://doi.org/10.1029/2006JD007315.

Birch, M.E., Cary, R.A., 1996. Elemental carbon-based method for monitoring occupational exposures to particulate diesel exhaust. Aerosol Sci. Technol. 25, 221–241. https://doi.org/10.1080/02786829608965393.

Cachier, H., Ducret, J., Bremond, M.P., Yoboue, V., Lacaux, J.P., Gaudichet, A., Baudet, J., 1991. Biomass Burning Aerosols in a Savanna Region of the Ivory Coast.

Cavalli, F., Viana, M., Yttri, K.E., Genberg, J., Putaud, J.-P., 2010. Toward a standardised thermal-optical protocol for measuring atmospheric organic and elemental carbon: the EUSAAR protocol. Atmos. Meas. Tech. 3, 79–89.

Coen, M.C., Weingartner, E., Apituley, A., Ceburnis, D., Fierz-Schmidhauser, R., Flentje, H., Henzing, J.S., Jennings, S.G., Moerman, M., Petzold, A., Schmid, O., Baltensperger, U., 2010. Minimizing light absorption measurement artifacts of the Aethalometer: evaluation of five correction algorithms. Atmos. Meas. Tech. 18.

Davy, P.M., Tremper, A.H., Nicolosi, E.M.G., Quincey, P., Fuller, G.W., 2017. Estimating particulate black carbon concentrations using two offline light absorption methods applied to four types of filter media. Atmos. Environ. 152, 24–33. https://doi.org/10.1016/j.atmosenv.2016.12.010.

Drinovec, L., Gregorič, A., Zotter, P., Wolf, R., Bruns, E.A., Prévôt, A.S.H., Petit, J.-E., Favez, O., Sciare, J., Arnold, I.J., Chakrabarty, R.K., Moosmüller, H., Filep, A., Močnik, G., 2017. The filter-loading effect by ambient aerosols in filter absorption photometers depends on the coating of the sampled particles. Atmos. Meas. Tech. 10, 1043–1059. https://doi.org/10.5194/amt-10-1043-2017.

Drinovec, L., Močnik, G., Zotter, P., Prévôt, A.S.H., Ruckstuhl, C., Coz, E., Rupakheti, M., Sciare, J., Müller, T., Wiedensohler, A., Hansen, A.D.A., 2015. The "dual-spot" Aethalometer: an improved measurement of aerosol black carbon with real-time loading compensation. Atmos. Meas. Tech. 8, 1965–1979. https://doi.org/10.5194/amt-8-1965-2015.

Dutkiewicz, V.A., DeJulio, A.M., Ahmed, T., Laing, J., Hopke, P.K., Skeie, R.B., Viisanen, Y., Paatero, J., Husain, L., 2014. Forty-seven years of weekly atmospheric black carbon measurements in the Finnish Arctic: decrease in black carbon with declining emissions: weekly BC measurements in the arctic. J. Geophys. Res. Atmos. 119, 7667–7683. https://doi.org/10.1002/2014JD021790.

EN 16909:2017-06, 2017. Ambient Air – Measurement of Elemental Carbon (EC) and Organic Carbon (OC) Collected on Filters. ICS 1304020.

Gundel, L.A., Dod, R.L., Rosen, H., Novakov, T., 1984. The relationship between optical attenuation and black carbon concentration for ambient and source particles. Sci. Total Environ. 36, 197–202.

IPR Guidance, 2013. Guidance on the Commission Implementing Decision Laying Down Rules for Directives 2004/107/EC and 2008/50/EC of the European Parliament and of the Council as Regards the Reciprocal Exchange of Information and Reporting on Ambient Air. European Commission (Decision 2011/850/EU).

Jacobson, M.Z., 2001. Strong radiative heating due to the mixing state of black carbon in atmospheric aerosols. Nature 409, 695. https://doi.org/10.1038/35055518.

Jankowski, N., Sageder, M., Bauer, H., Marr, I., Kasper-Giebl, A., Limbeck, A., Caseiro, A., Handler, M., Klatzer, B., Kotianova, P., Pouresmaeil, P., Schmidl, C., Ramirez-Santa Cruz, C., Dattler, A., Andrade-Sanchez, J., Puxbaum, H., 2008. "AQUELLA Linz – Oberösterreich" Aerosolquellenanalyse für Linz - Oberösterreich.

Karanasiou, A., Minguillón, M.C., Viana, M., Alastuey, A., Putaud, J.-P., Maenhaut, W., Panteliadis, P., Močnik, G., Favez, O., Kuhlbusch, T.A.J., 2015. Thermal-optical analysis for the measurement of elemental carbon (EC) and organic carbon (OC) in ambient air a literature review. Atmos. Meas. Tech. Discuss. 8, 9649–9712. https://doi.org/10.5194/amtd-8-9649-2015.

Kistler, M., Kasper-Giebl, A., Cetintas, E.C., Ramirez-Santa Cruz, C., Schreiner, E., Sampaio-Cordeiro-Wagner, L., Szidat, S., Zhang, Y., 2013a. PMinter Project - Analysis of Particulate Matter in Leibnitz and Arnfels. Final Rep. Rep. Number CTA-EAC-1113-6.

Kistler, M., Kasper-Giebl, A., Cetintas, E.C., Ramirez-Santa Cruz, C., Schreiner, E., Sampaio-Cordeiro-Wagner, L., Szidat, S., Zhang, Y., Bauer, H., 2013b. PMInter Project - Analysis of Filters and 14C Measurements in Fine Particulate Matter. Final Rep. Rep. Number CTA-EAC-1213-7.

Moosmüller, H., Chakrabarty, R.K., Arnott, W.P., 2009. Aerosol light absorption and its measurement: a review. J. Quant. Spectrosc. Radiat. Transf. 110, 844–878. https://doi.org/10.1016/j.jqsrt.2009.02.035.

Penner, J.E., Chuang, C.C., Grant, K., 1998. Climate forcing by carbonaceous and sulfate aerosols. Clim. Dynam. 14, 839–851. https://doi.org/10.1007/s003820050259.

Petzold, A., Ogren, J.A., Fiebig, M., Laj, P., Li, S.-M., Baltensperger, U., Holzer-Popp, T., Kinne, S., Pappalardo, G., Sugimoto, N., Wehrli, C., Wiedensohler, A., Zhang, X.-Y., 2013. Recommendations for reporting "black carbon" measurements. Atmos. Chem. Phys. 13, 8365–8379. https://doi.org/10.5194/acp-13-8365-2013.

R Development Core Team, 2008. R: a Language and Environment for Statistical Computing. R Foundation for Statistical Computing, Vienna Austria ISBN 3-900051-07-0 URI. HttpwwwR-Proj.

Segura, S., Estellés, V., Titos, G., Lyamani, H., Utrillas, M.P., Zotter, P., Prévôt, A.S.H., Močnik, G., Alados-Arboledas, L., Martínez-Lozano, J.A., 2014. Determination and analysis of in situ spectral aerosol optical properties by a multi-instrumental approach. Atmos. Meas. Tech. 7, 2373–2387. https://doi.org/10.5194/amt-7-2373-2014.

Virkkula, A., Chi, X., Ding, A., Shen, Y., Nie, W., Qi, X., Zheng, L., Huang, X., Xie, Y., Wang, J., Petäjä, T., Kulmala, M., 2015. On the interpretation of the loading correction of the aethalometer. Atmos. Meas. Tech. 8, 4415–4427. https://doi.org/10.5194/amt-8-4415-2015.

Virkkula, A., Mäkelä, T., Hillamo, R., Yli-Tuomi, T., Hirsikko, A., Hämeri, K., Koponen, I.K., 2007. A simple procedure for correcting loading effects of aethalometer data. J. Air Waste Manag. Assoc. 57, 1214–1222. https://doi.org/10.3155/1047-3289.57.10.1214.

Weingartner, E., Saathoff, H., Schnaiter, M., Streit, N., Bitnar, B., Baltensperger, U., 2003. Absorption of light by soot particles: determination of the absorption coefficient by means of aethalometers. J. Aerosol Sci. 34, 1445–1463. https://doi.org/10.1016/S0021-8502(03)00359-8.

Zanatta, M., Gysel, M., Bukowiecki, N., Müller, T., Weingartner, E., Areskoug, H., Fiebig, M., Yttri, K.E., Mihalopoulos, N., Kouvarakis, G., Beddows, D., Harrison, R.M., Cavalli, F., Putaud, J.P., Spindler, G., Wiedensohler, A., Alastuey, A., Pandolfi, M., Sellegri, K., Swietlicki, E., Jaffrezo, J.L., Baltensperger, U., Laj, P., 2016. A European aerosol phenomenology-5: climatology of black carbon optical properties at 9 regional background sites across Europe. Atmos. Environ. 145, 346–364. https://doi.org/10.1016/j.atmosenv.2016.09.035.

Zhang, H., Wang, Z., 2011. Advances in the study of black carbon effects on climate. Adv. Clim. Change Res. 2, 23–30. https://doi.org/10.3724/SP.J.1248.2011.00023.

Supplementary material

This chapter corresponds to the supplementary material of the peer-reviewed publication

Greilinger, M., Drinovec, L., Močnik, G., & Kasper-Giebl, A. (2019). Evaluation of measurements of light transmission for the determination of black carbon on filters from different station types. Atmospheric Environment, 198, 1-11, doi: 10.1016/j.atmosenv.2018.10.017

SUPPLEMENTARY MATERIAL

Evaluation of measurements of light transmission for the determination of Black Carbon on filters from different station types

Marion Greilinger [a,b], Luka Drinovec [c,d], Griša Močnik [c,d], Anne Kasper-Giebl [b]

[a] Zentralanstalt für Meteorologie und Geodynamik (ZAMG),Vienna, 1100, Austria
[b] Technical University of Vienna, Institute for Chemical Technologies and Analytics, Vienna, 1060, Austria
[c] Aerosol d.o.o., Ljubljana, 1000, Slovenia
[d] Jožef Stefan Institute, Ljubljana, 1000, Slovenia

Correspondence:
Marion Greilinger
Marion.greilinger@zamg.ac.at

1. **First evaluation of k and σ for different station types**

Here we give the results of the first evaluation, showing that the null hypothesis of a t-test, testing that the coefficients are different from zero using $p<0.05$ as threshold for significance, could not be rejected. Thus k was set to zero and evaluations for σ were repeated. If k=0, Eq. (1) and Eq. (2) simplify to B= ATN/σ and only σ is fitted

Stations for computation	Station for validation	VIRKKULA k (880 nm)	VIRKKULA σ [m²g⁻¹] (880 nm)	DRINOVEC k (880 nm)	DRINOVEC σ [m²g⁻¹] (880 nm)
URBAN-TRAFFIC					
KLG, RUD, DB	KEND	$-1.7*10^{-5}$ +/- $2.8*10^{-4}$	24.1 * +/- 2.7	$-3.1*10^{-5}$ +/- $5.7*10^{-4}$	24.2 * +/- 2.7
KEND, RUD, DB	KLG	$-1.3*10^{-4}$ +/- $2.5*10^{-4}$	23.0 * +/- 2.4	$-2.6*10^{-4}$ +/- $6.5*10^{-4}$	23.0 * +/- 2.7
KLG, KEND, DB	RUD	$1.8*10^{-5}$ +/- $3.2*10^{-4}$	26.4 * +/- 3.0	$2.9*10^{-4}$ +/- $4.7*10^{-4}$	26.2 * +/- 2.6
KLG,KEND, RUD	DB	$4.2*10^{-4}$ +/- $3.4*10^{-4}$	28.4 * +/- 3.2	$5.6*10^{-4}$ +/- $3.5*10^{-4}$	27.6 * +/- 2.4
All urban-traffic	-	$1.0*10^{-4}$ +/- $2.6*10^{-4}$	25.4 * +/- 2.4	$1.7*10^{-4}$ +/- $4.2*10^{-4}$	25.3 * +/- 2.2
RURAL-BACKGROUND					
ARN, STIX	ENZ	$4.5*10^{-4}$ +/- $5.2*10^{-4}$	33.5 * +/- 2.8	$9.4*10^{-4}$ +/- $6.9*10^{-4}$	33.9 * +/- 2.4
ARN, ENZ	STIX	$3.2*10^{-4}$ +/- $2.8*10^{-4}$	34.7 * +/- 1.8	$6.0*10^{-4}$ +/- $4.0*10^{-4}$	34.8 * +/- 1.6
ENZ, STIX	ARN	$2.0*10^{-5}$ +/- $3.1*10^{-4}$	31.5 * +/- 2.0	$4.6*10^{-5}$ +/- $6.0*10^{-4}$	31.5 * +/- 2.0
All rural-background	-	$1.8*10^{-4}$ +/- $2.7*10^{-4}$	32.9 * +/- 1.7	$3.7*10^{-4}$ +/- $4.6*10^{-4}$	33.0 * +/- 1.6
REMOTE					

SBK	SBK	-1.1×10^{-3} +/- 1.1×10^{-3}	29.5 * +/- 4.1	-4.0×10^{-3} +/- 4.0×10^{-3}	29.2 * +/- 5.1

Table S1: Results for the mass attenuation cross section σ and the mass absorption cross section MAC=σ/2.14 (Weingartner et al., 2003) at 880nm for the different station types. * indicates that a t-test supports the null hypothesis that the coefficients are different from zero using p<0.05 as threshold for significance Lowercased values represent the respective standard error.

2. Reduced data set covering the whole ATN range

To check whether the result of k=0 for the different station types is an effect of the reduced amount of data points, a reduced data set covering the whole ATN range but only 75 filters instead of 299 was evaluated as in section 3.1.1. The 299 filters in total have been arranged in ascending order of the ATN of which every fourth filter has been extracted. Thus, filters of all stations are still represented. The calculation again resulted in a k value significantly different from 0 indicating that k=0 is only obtained when station types are considered separately.

	k (880nm)	σ [m²g⁻¹] (880nm)	Number of Filters
„Virkkula equation" reduced data set	0.00079 * +/-0.00036	34.2 * +/-3.5	75
„Drinovec equation" reduced data set	0.00081 * +/-0.00028	31.7 * +/-2.2	75

Table S2: Results for the filter loading parameter k and the mass attenuation cross section σ at 880nm using a reduced data set of 75 filters of all stations covering the whole ATN range. Lowercased values represent the respective standard error, * indicates that a t-test supports the null hypothesis that the coefficients are different from zero using p<0.05 as threshold for significance.

3. Conditional quantile plots

In analogy to Davy et al. (2017), the conditional medians, using the R function conditionalQuantile() from the 'openair' package (Carslaw and Ropkins, 2012), were plotted. Therefore, the values used for validation were separated in evenly spaced bins, using a bin size of $\sqrt{n}$. The median for each bin is calculated and plotted as a red line to show how the medians vary across all bins. Due to the rather small sample size, it is not possible to calculate the other percentiles like the 25th and 75th or the 10th and 90th percentiles. The plot also shows the histogram of B_{calc} with grey bars and the histogram of the $B_{measured}$ with blue bars. The 1:1 line, based on the observations, is shown as a blue line. This kind of plot shows how well the predictions agree with observations (Carslaw and Ropkins, 2012). The closer the red and the blue lines are, the better B_{calc} values (predictions) match $B_{measured}$ (observations). If the red line is above the blue line, B_{calc} is underestimated and vice versa.

The conditional median plots for the validation of the urban-traffic stations given in Supplementary Figure 1 underline the good correlation. A slight underestimation of B_{calc} for RUD and DB and a slight overestimation for KLG was observed. The plot for KEND (top left) also indicates an underestimation of B_{calc}, showing high deviations of the 1:1 line especially in the third bin due to a big scatter of $B_{measured}$ for samples in this bin. A reanalysis of the thermal-

optically measurement to verify this was not possible because no sample was left.
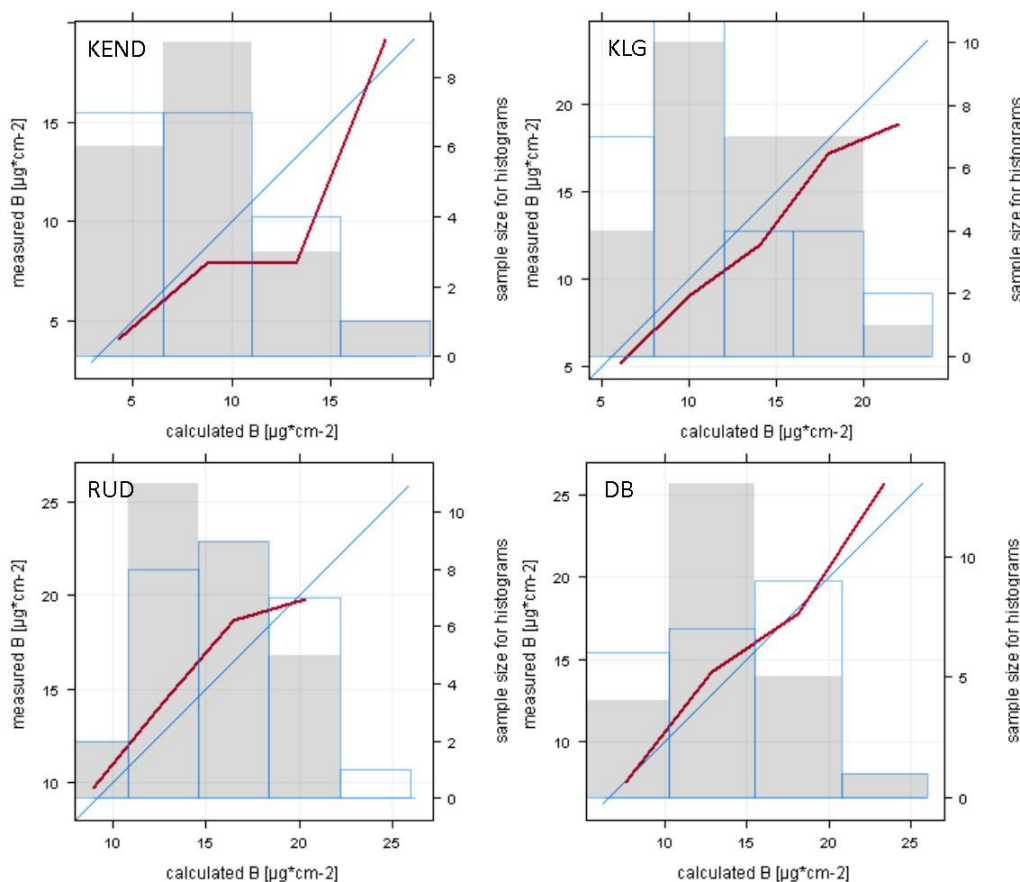

Figure S1: Conditional quantile plot for the validation of the urban-traffic stations always excluding one station for the computation of k and MAC and using the excluded station (given in the left corner of the respective graph) for validation by comparing B_{calc} and $B_{measured}$. The red line represents the median for each bin, the blue 1:1 line shows the perfect model, both referring to the left axis. Grey bars are the histogram of B_{calc} whereas the blue histogram shows $B_{measured}$, both referring to the right axis. Note the different scales!

The validation of the rural-background stations resulted in a slight underestimation of B_{calc} for STIX and a slight overestimation for ENZ and ARN.

The conditional quantile plot for the validation of the remote station (bottom right in Supplementary Figure 2) shows that especially the higher B values are overestimated. This might be due to the fact that there is no $B_{measured}$ in the last bin only a B_{calc}. This leads to an extension of the red line (median) beyond the perfect 1:1 model line (blue).
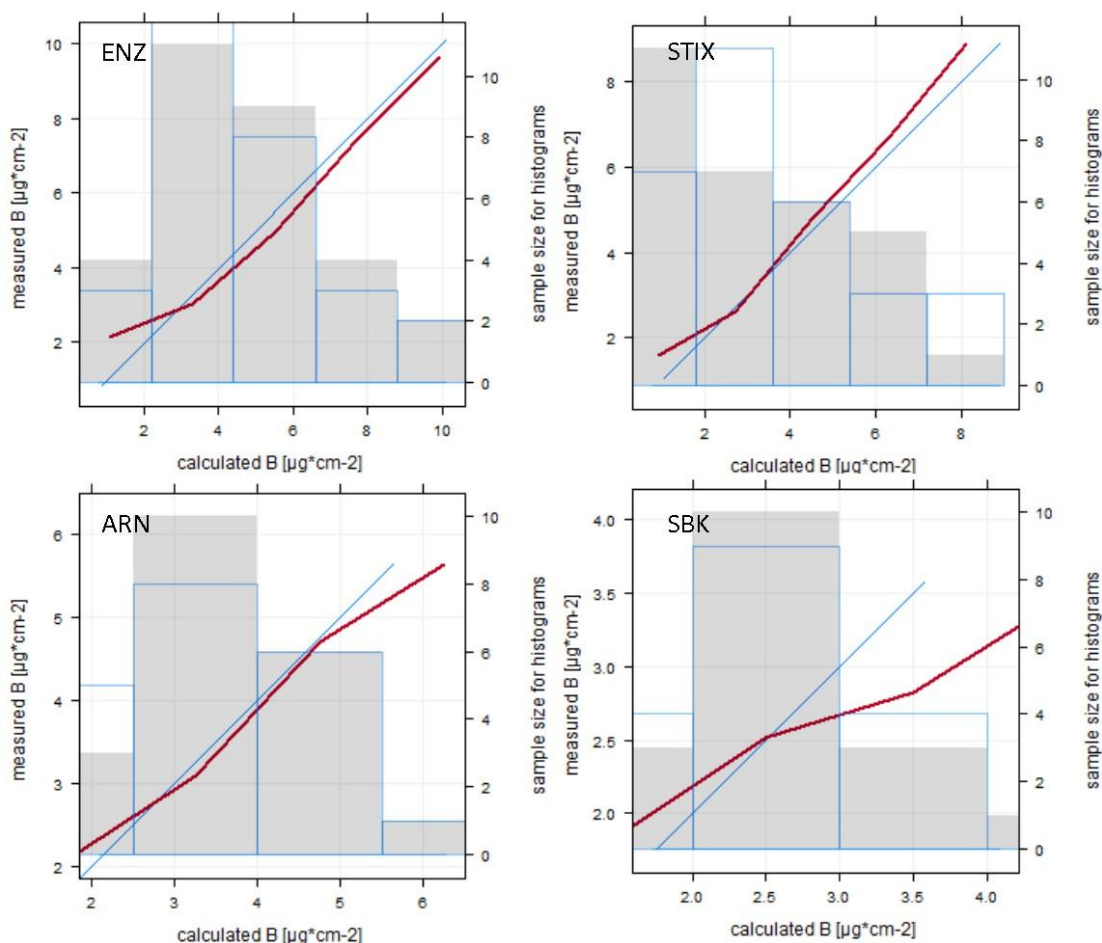
Figure S2: Conditional quantile plot for the validation of the rural-background stations always excluding one station for the computation of k and MAC and using the excluded station (given in the left corner of the respective graph) for validation by comparing B_{calc} and $B_{measured}$. The red line represents the median for each bin, the blue 1:1 line shows the perfect model, both referring to the left axis. Grey bars are the histogram of B_{calc} whereas the blue histogram shows $B_{measured}$, both referring to the right axis. Note the different scales!

If σ of the urban-traffic stations (σ =24.4 m^2g^{-1}) is used, an overestimation of B_{calc} was observed for all three stations. This result is also presented in the left column of the scatterplots in Supplementary Figure 3. If σ of the rural-background stations (σ =31.8 m^2g^{-1}) is used, an underestimation of B_{calc}, is observed for LEI and LAVA. For LIM again an overestimation of B_{calc} is observed. The respective conditional median plot (Supplementary Figure 3 right column, middle) underlines the result for LAVA. The plots for LEI and LIM (Supplementary Figure 3 right column top and bottom) are not as clear, showing an over- or underestimation of B_{calc}, depending on the bin. Lower B_{calc} values tend to be overestimated whereas higher ones are underestimated.
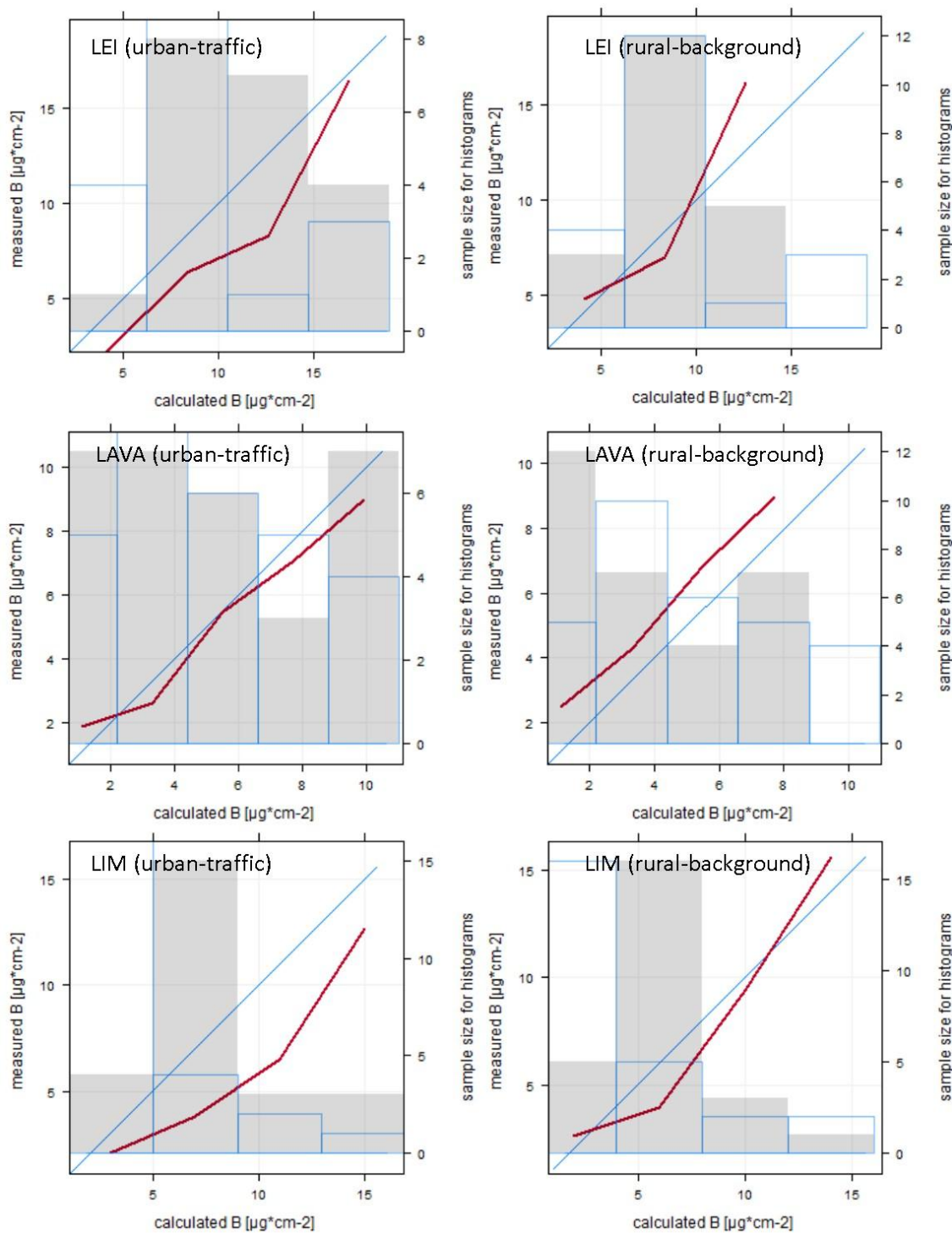
Figure S3: Conditional quantile plot for the validation using three additional stations not representing one of the station types used for the computation of k and MAC by comparing B$_{calc}$ and B$_{measured}$. B$_{calc}$ was once calculated with k and MAC computed using urban-traffic stations and once using rural-background stations. The red line represents the median for each bin, the blue 1:1 line shows the perfect model, both referring to the left axis. Grey bars are the histogram of B$_{calc}$ whereas the blue histogram shows B$_{measured}$, both referring to the right axis. Note the different scales!

4. <u>Discussion on the effect of the loading parameter k</u>

To investigate the effect of the loading parameter k on the evaluation of station types other than urban-traffic or rural-background we calculated the RMSE, the slope and R² using k and sigma values derived by using all urban-traffic and all rural-background stations as presented in Table S1 for the calculation of B$_{calc}$. Since it is not recommended to use k and sigma values

from different fits, we decided to use those values, although the k values were found to be statistically indifferent from zero. Results are presented in Table S3.

Approach		URBAN-TRAFFIC			RURAL-BACKGROUND	
		Virkkula	Drinovec		Virkkula	Drinovec
k	0	0.0001	0.00017	0	0.00018	0.00037
σ [m²g⁻¹]	24.4	25.4	25.3	31.8	32.9	33
LAVA						
RMSE	1.16	1.05	0.96	1.48	1.52	1.52
slope	0.933	1.013	1.011	1.215	1.293	1.293
R2	0.966	0.956	0.956	0.966	0.955	0.955
LEI						
RMSE	3.15	3.05	3.06	2.29	2.20	2.18
slope	0.89	0.816	0.816	1.053	1.032	1.029
R2	0.946	0.947	0.947	0.946	0.949	0.949
LIM						
RMSE	3.08	2.95	2.96	1.63	1.60	1.59
slope	0.719	0.689	0.688	0.827	0.875	0.874
R2	0.941	0.944	0.944	0.941	0.946	0.947

Table S3: Results for the validation of station types other than urban-traffic or rural-background using the linear regression $B_{measured}=a*B_{calc}$. Thereby B_{calc} was calculated using the "Virkkula" and "Drinovec" equations given in Eq. (1) and Eq. (2) with the respective k and σ values computed by using all filters of the different station types and given in Table S1 in comparison to results using k=0 and the respective σ values as given in Table 6.

Results reveal, that the loading correction (k NOT 0) in general does only slightly improve the RMSE. Also the deviation from the 1:1 line, given as the slope, is in most of the cases not improved while R^2 is always comparable high with values >0,9.

Chapter 5
Summary and Conclusion

The importance of the investigation of desert dust contributions to PM concentrations and deposition in Austria is highly relevant due to its impact not only on air quality and the related health issues, but also considering its optical properties related to the direct and indirect effects on radiative forcing, as well as corresponding ecological aspects, e.g. the nutrient supply.

The aim of this thesis was to assess the influence of desert dust on PM concentrations and deposition in Austria. For the first time the long-term influence of desert dust on the ion concentration in wet deposition is explored, to reveal that desert dust deposition is a constant factor influencing terrestrial and aquatic ecosystems in the Alps. On the other hand, the influence of mineral dust on PM_{10} concentrations was investigated to draw conclusions on its impact on PM_{10} limit value exceedance in Austria. Additionally, a method for the identification of desert dust based on its light absorbing properties using filters from air quality monitoring networks is discussed. Aiming at a simple quantification method for mineral dust, an evaluation method for BC could be established in a first step, acting as a basis for further refinement also including mineral dust.

A long-term influence of desert dust on ion concentrations in wet deposition was identified over more than 30 years from 1987 to 2017 for high alpine snow packs. This is the first long-term time series of the investigation of mineral dust in wet deposition in the Alps. Results reveal that especially magnesium and calcium depositions are strongly affected by desert dust input with a 25% and 35% contribution, respectively, on the average annual deposition amount determined for the 30-year period. The contribution of the other investigated ions is well comparable to the deposition amount expected according to the snow water equivalent of affected snow layers. The pH, and hence the acidity, of the samples is markedly influenced, ranging from 5.58 to 7.17 in desert dust affected layers, while the median pH value of all samples is 5.40. It is important to note that the long term decreasing trends which were identified for sulfate and nitrate are not altered if the deposition loads related to the deposition of desert dust would be deducted. This implies that the introduction of sulfur via desert dust deposition is rather small at the investigated site due to its location in the middle of Europe where anthropogenic sources related to SO2 emissions clearly dominate. This seems straightforward, but within the years the dust samples showed highest ionic loads, also for electrolytes, therefore it was checked.

The documentation of the 30-year time series of mineral dust deposited onto a high alpine snow pack in Austria is of great scientific value as it may trigger further research to investigate the impact of the desert dust contribution on ecology, especially in a sensitive environment such as remote alpine snow. Although this study provides a first quantification on the deposition of mineral dust, measurements of minerals and trace elements were not performed. In particular phosphor and iron are essential nutrients for microorganisms and are known to be contained in mineral dust. Not only the biogeochemical cycles of these elements might be affected, also the metabolism, respiration, and productivity of the microbes might be altered, especially if the impact of desert dust on acidity is considered as well. Besides the required chemical investigations, also microbiological studies are of great interest regarding a microbial 'contamination' of sensitive habitats via mineral dust intrusion.

Regarding the influence of mineral dust on measured PM_{10} concentrations an impact was found, but the influence on the exceedances of the daily limit value in a highly polluted urban surrounding is rather small with a maximum of ten days. This is relatively low compared to the allowed amount 25 or 35 days (WMO or IG-L threshold, respectively) exceeding the respective limit values, but still the scales might be tipped in favour of a transgression of that very maximum. Results were obtained via an investigation of two stations, representing a hot spot regarding PM_{10} concentrations in Austria, over a time period of six years (2013 to 2018).

Thereby the applicability of the European Air Quality Directive (2008/50/EC) for the subtraction of the contribution of natural sources from the daily PM_{10} load was evaluated. Different stations and different statistical parameters were evaluated to determine the regional background load (BGL) and subsequently the net dust load (NDL) which can then be subtracted. Results reveal an adapted approach of the EC-methodology, using the +/- 15-day mean average of the PM_{10} at the regional background station Masenberg, together with threshold criteria of BGL > 12µg/m³ and NDL > 10 µg/m³ to identify only desert dust affected days. The results of calculated NDLs were in good agreement with crustal loads determined on filter samples during two desert dust events in 2016.

Within this study only days exceeding the daily limit of 50µg/m³, as set by the European Commission, the World Health Organization (WHO) and the national regulations in the frame of the 'Immissionsschutzgesetz Luft (IG-L)', were examined. This first analysis and the proposed approach allow conclusions on the impact of mineral dust on the limit value exceedance but the impact of desert dust events on the total dust load as well as on annual mean values of PM_{10} concentrations remains unexplored, especially in regions not directly influenced by anthropogenic activities. This would be of special interest regarding the overall impact of mineral dust from natural sources. The proposed approach tends to underestimate the NDL due to the inclusion of all days (also the desert dust affected days) for the computation of the moving 30-day average but a comparison of the NDL with crustal loads chemically measured on filters showed that the NDL is still higher. Thus, using the proposed method also the impact on the mean annual concentrations will be underestimated. To further investigate this discrepancy and two draw conclusions on the annual impact a measurement campaign over at least one year would be worthwhile, to compare the calculated NDL with the chemically measured crustal load. Based on the results obtained, the approach proposed in this work might has to be adapted. Also the representativeness of the proposed station Masenberg for the investigated region should be validated by using e.g. ceilometer measurements to determine the height of the mixing layer, to check whether the higher located stations are decoupled from the lower ones, especially during inversion weather situations, which are very likely around the investigated region.

Besides the need for further research in the region of Graz, the applicability of the proposed approach to other stations needs further investigation too, especially in regions not directly influenced by anthropogenic activities, and thus remains of great importance. By all means, this should be supported by a chemical analysis of the crustal loads, although this is quite time and cost consuming. Thus, a rather easy quantitative assessment of mineral dust on filters sampled within the air quality monitoring networks would be of great interest. Such a new approach was pursued within this work, but unfortunately could not be implemented due to technical limitations of the measurement set up. The idea was to set up a quantification method based on transmissometer measurements of the filters at two wavelengths in the IR and the UV. Based on the obtained values of attenuation at the two wavelengths a source contribution would be possible. Unfortunately, filters sampled at the air quality monitoring stations were overloaded for the measurements in the UV and the applicability of the method could not be further investigated. Still the presented investigation of BC is of great scientific value since the proposed methodology offers the possibility to easily investigate long time series, e.g. from archived filters measured within air quality monitoring networks. Due to the presentation of station type specific factors, such as the filter loading parameter and the mass attenuation cross section, BC concentrations in different environments can be assessed.

In a nutshell, this thesis highlights the influence of desert dust events in Austria. Results show that the impacts on wet deposition in a remote area as well as on air quality in an urban environment are rather small and limited to single events only. Still a remarkable impact can be found for almost every year even if it is limited to a few days only. The findings of this thesis absolutely encourage and endorses further research to investigate the impact on sensitive ecosystems, such as the high alpine regions for which the first quantitative assessments within this study serve as a starting point.

CURRICULUM VITAE

Ing^in. Mag^a. Marion Greilinger (formerly Rothmüller)
Date of birth: 17.09.1984 in Vienna
Telephone: 0650 474 09 41
Email: marion.greilinger@zamg.ac.at

Marital status: Married
Children: 1 daughter, Lea born 23.03.2018

Education

2015-2019	PhD studies in Technical Chemistry at the Technical University of Vienna FFG - Project: *"DUSTFALL – Improvement of particulate matter forecasts in Austria through the detection of Sahara dust falls"*
2007-12	Master´s degree in Meteorology at the University of Vienna *„Temporal trends of ion concentration and deposition in high alpine snow packs from 1983-2011 (Hohe Tauern, Austria)"*
1998–03	Higher Technical School for Chemistry Special focus on technical chemistry and environmental chemistry

Employment History

Since 11/2019	Head of Section 'Climate monitoring and cryosphere' Zentralanstalt für Meteorologie und Geodynamik (ZAMG)
Since 2014	Scientific employee Central Institution for Meteorology and Geodynamics (ZAMG) Section Climate Research in cooperation with the section of Environmental Meteorology
2013 – 15	Office assistant Austrian Polar Research Institute (APRI)
2013 – 14	Maternity leave cover as weather forecaster Zentralanstalt für Meteorologie und Geodynamik (ZAMG)
2003 – 11	Technician University of Natural Resources and Applied Life Science (BOKU) Institute of Applied Microbiology

Skills

Microsoft Office – advanced skills

The R project for statistical computing – intermediate skills

Linux – basic skills

English – advanced skills

Research Interests

Atmospheric chemistry, aerosol chemistry and snow chemistry/ecology

Climatology, chemical composition and environmental effects of Sahara dust events

Climate change

Publications peer-reviewed

Greilinger, M., Zbiral, J., Kasper-Giebl, A. (2019) Desert dust contribution to PM10 loads in Styria (Southern Austria) and impact on exceedance of limit values from 2013-2018. Applied Sciences, 9, 2265, doi: 10.3390/app9112265

Baumann-Stanzer, K., **Greilinger, M.,** Kasper-Giebl, A., Flandorfer, C., Hiede, C., Lotteraner, C., Ortner, M., Vergeiner, J., Schauer, G., Piringer, M. (2019) Evaluation of WRF-Chem Model Forecasts of a Prolonged Saharan Dust Episode over the Eastern Alps, Journal of Aerosol and Air Quality Research, DOI: 10.4209/aaqr.2018.03.0116

Greilinger, M., Drinovec, L., Močnik, G., & Kasper-Giebl, A. (2019). Evaluation of measurements of light transmission for the determination of black carbon on filters from different station types. Atmospheric Environment, 198, 1-11.

Greilinger, M., Baumann-Stanzer, K., Skomorowski, P., Schauer, G., Schöner, W., & Kasper-Giebl, A. (2018). Contribution of Saharan dust to ion deposition loads of high alpine snow packs in Austria (1987-2017). Frontiers in Earth Science, 6, 126.

Rauser, F., **et al. (M. Greilinger)**, "Earth System Science Frontiers-an ECS perspective." Bulletin of the American Meteorological Society 2016 (2016).

Greilinger, M., Schöner, W., Winiwarter, W., & Kasper-Giebl, A. (2016). Temporal changes of inorganic ion deposition in the seasonal snow cover for the Austrian Alps (1983–2014). Atmospheric Environment, 132, 141-152.

Stadlmayr G., Mecklenbräuker A., **Rothmüller M.**, Maurer M., Sauer M., Mattanovich D., Gasser B. (2010): Identification and characterisation of novel Pichia pastoris promoters for heterologous protein production, Journal of Biotechnology, Volume 150, Issue 4, 2010, 519–529

Conference proceedings - Talks

Greilinger, M., Binder, D., Felbauer, L., Hynek, B., Neureiter, A., Schöner, W. (2019): Gletscher im Klimawandel – Ergebnisse des glaziologischen Monitorings im Bereich des Hohen Sonnblicks und der Pasterze, 8. Österreichischer Meteorologentag, Salzburg, Austria

Ofner, J., Eitenberger, E., Friedbacher, G., Brenner, F., Hutter, H.,Schauer, G., Kistler, M., **Greilinger, M.,** Lohninger, H., Lendl, B., Kasper-Giebl, A. (2017): Single Particle Analysis by Combined Chemical Imaging to Study Episodic Air Pollution Events in Vienna, EGU General Assembly, Vol. 19, p. 16457, Vienna, Austria

Greilinger, M., Kau, D., Schauer, G., Kasper-Giebl, A. (2017): Impact of Saharan dust on deposition loads at a remote high alpine monitoring site in Austria, VAO-Symposium, Bolzano, Italy

Rothmüller, M., Bartsch, A., Flandorfer, C., Hirtl, M., Kasper-Giebl, A., Močnik, G., Schauer, G., Simic, S., Spangl, W. (2016): DUSTFALL-Impact of SDEs on air quality forecasts in Austria; Method for the quantification of SD on filters, 2nd International conference on atmospheric dust (DUST2016), Castellaneta Marina, Italy

Scheifinger, H., Kahrer, A., Zuvela-Aloise, M., **Rothmüller, M.**, Matulla, C., Moyses, A., and Egartner, A. (2016): Potentielle Wintermortalität im gegenwärtigen und zukünftigen Klima Europas von Helicoverpa armigera (Baumwollkapselwurm), Trogoderma granarium (Khapra Käfer) und Tuta absoluta (Tomatenminiermotte), DACH 2016, Berlin, Germany

Rothmüller M., Kasper-Giebl A., Schöner W., Winiwarter W. (2015): Temporal trends of the ionic composition in the wintertime snow cover of two high alpine sampling sites over three decades (1983 – 2014), VAO-Symposium, Salzburg, Austria

Rothmüller M., Bartsch A., Kasper-Giebl A., Schöner W., Schreiner E. (2015): Temporal trends of the ionic composition in the wintertime snow cover of two high alpine sampling sites over three decades (1983 – 2014), IUGG – 26th General Assembly, Prague, Czech Republic

Conference proceedings - Poster

Firmkranz J., **Greilinger M.**, Schauer G., Kasper-Giebl A. (2018): Ion composition of precipitation samples collected in an high alpine environment (Sonnblick Observatory, 3106 m a.s.l.), EGU General Assembly, Vol. 20, p. 14842, Vienna, Austria

Kasper-Giebl, A., **Greilinger, M.**, Kistler, M., Gurezcny, H., Redl, P., & Schauer, G. (2018): Time series of measurements of light absorbing aerosol particles at the Sonnblick Observatory, EGU General Assembly, Vol. 20, p. 13190, Vienna, Austria

Greilinger M., Schauer G., Kasper-Giebl A. (2017): Monitoring of Saharan Dust –Influence on aerosol composition and snow chemistry, 2.-3.November 2017, 6th International Symposium for Research in Protected Areas, Salzburg, Austria

Baumann-Stanzer, K., Flandorfer, C., Lotteraner, C., Piringer, M., **Greilinger, M.,** Kasper-Giebl, A., Schauer, G. (2017): Long-range transport to summits north, south and at the Eastern Alpine divide – an outstanding Sahara dust event, 18-23.06.17, International Conference on Alpine Meteorology (ICAM), Reykjavik, Iceland

Greilinger, M., Drinovec, L., Mocnik, G., Kasper-Giebl, A. (2017): Quantification of Black Carbon on filters of different station types in Austria via transmissiometer measurements, 27.08.-01.09.2017, European Aerosol Conference (EAC), Zurich, Switzerland

Ofner, J., Eitenberger, E., Friedbacher, G., Schauer, G., **Greilinger, M.,** Lohninger, H., Lendl, B., Kasper-Giebl, A. (2017): Physico-chemical transformation of Saharan dust particles by the city of Vienna – A combined imaging approach, 27.08.-01.09.2017, European Aerosol Conference (EAC), Zurich, Switzerland

Greilinger, M., Kau, D., Schauer, G., Kasper-Giebl, A. (2017): Identification of mineral dust layers in high alpine snow packs, 23.-28.04.2017, EGU General Assembly, Vienna, Austria

Greilinger, M., Flandorfer, C., Hirtl, M., Lotteraner, C., Piringer, M., Schauer, G., Baumann-Stantzer, K., Kasper-Giebl, A. (2017): Saharan dust under observation – From modelling and tracing towards in-situ measurements, VAO-Symposium, 28.-31.03.2017, Bolzano, Italy

Rothmüller M., Bartsch A., Baumann-Stanzer K., Flandorfer C., Hirtl M., Kasper-Giebl A., Močnik G., Piringer M., Schauer G., Simic S., Spangl W. (2015): DUSTFALL – Impact of Sahara Dust on air quality forecasts in Austria, 6. Österreichischer Meteorologentag, Vienna, Austria

Baumann-Stanzer K., Stenzel S., Schauer G., Kasper-Giebl A., **Rothmüller M.**, Scheifinger H., Flandorfer C. (2015): Meteorological Analysis of the Sahara Dust Transport to Sonnblick in April 2014, Virtual Alpine Observatory Symposium, Salzburg, Austria

Rothmüller M., Bartsch A., Baumann-Stanzer K., Flandorfer C., Hirtl M., Kasper-Giebl A., Močnik G.,

Piringer M., Schauer G., Simic S., Spangl W. (2015): DUSTFALL – Impact of Sahara Dust on air quality forecasts in austria, Virtual Alpine Observatory Symposium, Salzburg, Austria

Bartsch A., **Rothmüller M.**, Binder D., Hynek B., Kaiser A., Kasper-Giebl A., Koch R., Niedermoser B., Olefs M., Reisenhofer S., Riedl C., Schauer G., Scheifinger H., Schöner W., Staudinger M. (2015): LTER Sonnblick (Hohe Tauern), LTER Austria Konferenz, Vienna, Austria

Bartsch A., **Rothmüller M.**, Binder D., Hynek B., Kaiser A., Kasper-Giebl A., Koch R., Niedermoser B., Olefs M., Reisenhofer S., Riedl C., Schauer G., Scheifinger H., Schöner W., Staudinger M. (2015): LTER Sonnblick (Hohe Tauern) – Monitoring Atmosphere & Cryosphere, LTER Austria Konferenz, Vienna Austria